RESEARCH ON DETERMINATION OF DIFFUSION COEFFICIENTS

NATIONAL AERONAUTICS AND SPACE ADMINISTRATION
GEORGE C. MARSHALL SPACE FLIGHT CENTER
HUNTSVILLE, ALABAMA

PREPARED UNDER CONTRACT NO. NAS8-11000
BY ARTHUR D. LITTLE, INC., CAMBRIDGE, MASSACHUSETTS
BY THE FOLLOWING AUTHORS:

J. C. BURKE
S. W. BODMAN
R. W. MOORE
R. C. REID
J. L. LUNDHOLM
A. H. RAWDON

JULY 1964

TABLE OF CONTENTS

TABLE OF CONTENTS (CONTINUED)

TABLE OF CONTENTS (CONTINUED)

TABLE OF CONTENTS (CONTINUED)

LIST OF TABLES

LIST OF FIGURES

LIST OF FIGURES (CONTINUED)

LIST OF FIGURES (CONTINUED)

I. SUMMARY

A. PURPOSE

The purpose of this study has been to define the mechanisms of oxygen and hydrogen propellant evaporation into a helium pressurant gas and to develop techniques for computing propellant evaporation suitable for flight vehicle design analysis.

B. SCOPE

Propellant transfer to the ullage occurs by convective and diffusional mass transfer mechanisms. These processes were modeled analytically and the important independent variables of geometry, diffuser design, wall convective flow, ullage mixing, etc., were considered. A solution of the molecular diffusion equations was obtained to permit calculation of diffusion rates and concentration gradients. The boundary condition of liquid surface temperature was studied in some detail and correlating relations developed for both general and specific cases.

C. CONCLUSIONS

1. A molecular diffusion model appears to be a useful analytical tool for computing diffusion in a non-convective ullage situation. The exact importance of convection effects which may result from ullage gas natural circulation and pressurant gas inlet flow cannot be defined on an analytical basis. However, it appears that in many instances, these effects may be small, and the molecular diffusion solution valid.

2. Analytical studies of the ullage natural convection flow patterns indicated that even when conditions were chosen so as to maximize this natural convection flow, the resulting diffusion rates were in the same range as that predicted as molecular diffusion, for times of about 30 seconds. We conclude that, except for long times, the more important mechanism for surface mass transfer is pure diffusion.

3. Convective mixing by the pressurant inlet gas flow is likely to be very strong during initial pressurization and will probably result in complete mixing of the initial propellant vapor and the helium pressurant. However, during expulsion, when the liquid is remote from pressurant gas inlet, a reasonable diffuser configuration will minimize mixing at the liquid interface.

4. Liquid surface temperatures and gradients near the surface are very important to the evaporation process. In adiabatic systems, surface temperature is controlled by liquid gas interactions, and, in the non-convective case, may be estimated by a conduction-diffusion solution which predicts a surface temperature that is invariant with time. Ambient heat leak results in a time dependent surface temperature which may be estimated with a transient conduction solution.

5. Under high heat leak conditions, free boiling at the liquid surface is a possibility. We have presented a method for computing free boiling evaporation--and have found it to be relatively small for the conditions considered in this report.

6. Propellant evaporation may also occur from the liquid film left on the tank walls during drawing. However, our studies indicate that except for very small tanks and high draining rates, the evaporation contributed by this film is negligible.

7. For the conditions considered in the report, the quantity of propellant evaporation appears extremely small as a fraction of total propellant but may be significant in terms of ullage gas mass. Because of its lower volumetric heat capacity and the steepness of its vapor pressure curve, the percentage of propellant evaporated is generally much larger for hydrogen than for oxygen. However, because of the higher density of the oxygen vapor, mass of evaporated propellant vapor may be comparable for the two fluids.

D. RECOMMENDATIONS

We feel that the usefulness of the analytical procedures for computing propellant evaporation presented in this report could be greatly improved by experimental studies to verify or modify certain assumptions in the analysis. Detailed recommendations are included in Section X of this report.

II. INTRODUCTION

The diffusion of oxygen and hydrogen propellant vapors into a helium pressurant gas is an important design consideration in many space vehicle applications. The mixing of the propellant vapor with the helium pressurant will have a strong bearing on both the helium pressurant gas requirements and the gas residual weight at burn out. Accordingly, knowledge of propellant evaporation is of concern both for the evaluation for various types of pressurization systems and in the optimization and control of a particular pressurization system. The propellant-pressurant interface reactions associated with evaporation may also influence the shape of the liquid temperature stratification. Fairly precise knowledge of the liquid temperature gradients is frequently necessary to establish the trade-offs in tank pressure and liquid residuals established by turbo pump NPSH requirements. Very frequently the design of cryogenics propellant systems is handicapped by the lack of analytical techniques for estimating the extent of propellant evaporation and its effects on system performance.

The program described in this report has been an attempt to define the propellant evaporation process as well as possible from an analytical basis. This work has included consideration of the true molecular diffusion process--including limits imposed by surface kinetics--as well as other elements of interfacial mass transfer such as surface convection induced by ullage gas natural circulation flow and pressurant gas diffuser impingement. In addition, considerable study has been devoted to methods of computing liquid surface temperatures and gradients in the vicinity of the surface since this information is vital to computing the diffusional and/or free boiling evaporation at the surface.

III. DISCUSSION OF MECHANISM OF PROPELLANT VAPOR DIFFUSION

In flight vehicle propellant tanks, mass transfer of hydrogen or oxygen vapors into the helium pressurant gas is dependent upon the combined effects of molecular diffusion and convective mass transfer at the vapor liquid interface. The mass transfer resulting from these surface interactions is, in turn influenced by the liquid surface temperature, which in most cases, will differ substantially from the bulk liquid temperature due to stratification. In certain cases of high ambient heat leak, the surface temperature may rise high enough to cause free boiling which will result in a layer of pure vapor immediately above the liquid in addition to the vapor migrating into the helium pressurant gas by diffusional or surface convective effects. In applying the term diffusion to the over-all propellant evaporation process, we must recognize that it is, in effect, a defined term including effects due to ullage convection and liquid temperature gradients as well as molecular diffusion.

For the case of molecular diffusion, with a known liquid surface temperature, the diffusion of propellant vapor into the helium pressure obeys fairly straightforward theory for which the appropriate equations can be developed and for which the diffusion coefficients may be estimated with reasonable accuracy. However, molecular diffusion theory is not in itself a complete solution to the problem since ullage convective effects may augment the evaporation due to molecular diffusion. Of even more importance, is the fact that knowledge of liquid temperature gradients is necessary in order to establish the boundary conditions for the molecular diffusion solution.

Convective mass and heat transfer at the vapor-liquid interface, might be expected to have some influence on the mass transfer of oxygen and hydrogen into the helium pressure gas. In a gross sense, the ullage is convectively stable, since the warm pressurant gas is introduced above the cold liquid. However, we would expect that the cold walls will tend to set up convective gradients within the ullage, particularly during liquid expulsion. Likewise, any disturbances induced by the flow from the inlet gas diffuser will tend to augment convection. These convection currents will induce flow along the liquid surface which may cause high heat and mass transfer coefficients at the liquid surface.

The liquid surface temperature is very important in governing the rate of mass transfer into the helium pressurant. In most cases, stratification in the liquid will result in the liquid surface being appreciably higher than the bulk liquid temperature. This temperature stratification results both from the preferential distribution of external heat input to the liquid at the liquid surface due to the rising boundary layer flow along the tank wall, and also from the vapor heat transfer at the liquid-gas interface. Stratification may be an important consideration since a 1°F rise in surface temperature is equivalent to a 1 psi rise in saturation pressure for oxygen, or about 3 psi for hydrogen. Also, if the heat input to the tank and the stratification is severe enough, the possibility of free boiling exists which would cause much more evaporation than might be predicted from surface mass transfer rates.

IV. SURVEY OF CURRENT LITERATURE ON PROPELLANT EVAPORATION

We have found little direct information in the literature which permits direct evaluation of propellant evaporation. However, considerable semi-quantitative information exists which gives us some clues as to the mechanism and magnitude of propellant evaporation. In addition, fairly considerable amount of information is available on the general subject of tank pressurization and on liquid temperature gradients.

A. INTERFACIAL MASS TRANSFER FOR HELIUM PRESSURIZATION OF HYDROGEN, OXYGEN, AND NITROGEN

1. Investigations and Ranges of Conditions Studied

We are aware of the work of three investigators of tank pressurization studies whose results include data on interfacial mass transfer with helium pressurization. In brief, their studies were:

NASA-Lewis Research Center: (3, 6)* Performed tests on liquid hydrogen transfer using both gaseous hydrogen and gaseous helium pressurant. The tests were run in a 220-gallon insulated tank. The parameters studied were pressure and expulsion time.

NASA-Marshall Space Flight Center: (4, 5) Two different test series were performed. The first were liquid nitrogen pressurization tests in an insulated 16-gallon tank. The second series was performed in large Jupiter-size tanks (uninsulated). Liquid oxygen was transferred with gaseous oxygen pressurant, and gaseous nitrogen or helium as the prepressurant.

The Lockheed-Georgia Company: (1, 2, 7) In a 500-gallon insulated tank, Lockheed has studied the transfer of liquid hydrogen using both hydrogen and helium as pressurant. They studied the parameters of expulsion time, slosh, and inlet temperature. Another test series was run in a 12-gallon insulated tank. Both liquid hydrogen and oxygen were transferred using helium or their own vapor as pressurant.

---

*Underlined numbers in parenthesis refer to References at end of main body of report.

2. Discussion of Problems Involved in Measuring Interfacial Mass Transfer

All of the above investigators attempted to measure the mass transfer occurring at the liquid-vapor interface. As this phenomenon is quite difficult to measure directly, indirect means were used--generally a mass balance technique in which mass transfer was taken as the difference between the change in ullage gas mass and the net pressurant gas addition to the tank. An inherent difficulty in determining mass transfer data with a mass balance calculation is that the mass transfer term is computed by the subtraction of quantities which are frequently much larger than the mass transfer term itself. Hence, small percentage errors in the entering mass and final ullage mass may result in large percentage errors in the interfacial mass transfer. This problem is especially acute when the ullage gas is a two-component system. In addition, the mass balance method merely results in a net mass tranfer term and does not differentiate between gas-liquid interfacial mass transfer and other sources of mass transfer such as evaporation of the liquid film on the tank walls.

3. Test Results

a. Helium Pressurized Transfer of Liquid Hydrogen

In large tank tests both NASA-Lewis[6] and the Lockheed-Georgia Company[7] agree that a negligible amount of interfacial mass transfer takes place. There is evidence, however, that a small quantity of evaporation was taking place during these tests. NASA-Lewis[3] reports that there was a lowering of the liquid hydrogen surface temperature below that which would be anticipated due to thermal stratification. In fact, in some cases, the surface temperature was lower than the bulk temperature. This is an indication that the surface was being cooled by evaporation into the almost 100% helium-filled ullage space.

In their small tank tests data, Lockheed[1] did not show measurements of the interfacial mass transfer. However, they do state that helium in the ullage space had the effect of inhibiting condensation when the tank was prepressurized with helium, and hydrogen was used as the transfer pressurant.

b. Helium Pressurized Transfer of Liquid Oxygen and Liquid Nitrogen

The Lockheed-Georgia Company is the only investigator which reports the helium-pressurized transfer of liquid oxygen.[1] They do not show any interfacial mass transfer results, but they do note that a parameter which they call a collapse factor increases substantially over that obtained during oxygen-pressurized transfer. (Collapse factor is defined as the actual pressurant requirement divided by the idealized requirement if the pressurant gas were not allowed to cool or condense.) The high collapse factor for helium is evidence that the cooldown of helium gas results in a greater loss in specific volume than does the combined cooldown and condensation process for oxygen gas and that the hydrogen evaporation quantity is apparently not a large factor in this case.

In other tests, Lockheed-Georgia shows that when helium is used as a prepressurant during gaseous nitrogen transfer of liquid nitrogen, the measured condensation rate is decreased by a factor of 75%.[1] An explanation of this is that the helium is acting as a noncondensable gas creating a stagnant film through which the nitrogen must diffuse.

When liquid nitrogen is transferred solely with helium pressurant gas, NASA-Marshall reports that there is evaporation of nitrogen.[4] Our calculations (presented in Section VI) indicate that the experimental results are compatible with molecular diffusion.

B. LIQUID TEMPERATURE GRADIENTS

A good deal of experimental data on liquid temperature gradients is available in the literature.[8, 9, 10, 11, 12, 13, 14] Data are available for both self-pressurization tests, and tests in which the tank is externally pressurized at some predetermined level with helium. One common experimental problem has been the direct measurement of surface temperatures. Direct measurement of the liquid surface temperature is difficult because the temperature gradient is generally quite steep in the vicinity of the surface and it is generally impossible to know the precise location of the liquid surface. In self-pressurization tests, this problem can be circumvented rather neatly by measuring the ullage pressure and taking the liquid surface temperature to the saturation at ullage pressure. Because of this problem, it has been frequently difficult to determine what, if any, influence addition of a helium pressurant gas has on the liquid surface temperature history.

Techniques for calculating liquid temperature gradients have been proposed by Martin, [14] Arthur D. Little, Inc., [15] and Lockheed-Georgia. [10] The Martin technique assumes all tank heat input is absorbed by a thermal layer at the liquid surface which results from boundary layer flow along the walls of the tank. This model has the advantage of simplicity of calculation and involves no experimental inputs. In some instances, at least, the agreement between calculated experimental surface temperatures is quite good even though gradients predicted by the model do not agree very well with the experimental gradients. The Arthur D. Little, Inc., model is based on conduction theory. The gradients generated by this model are in accordance with a constant heat flux entering the liquid at the liquid vapor surface. The surface heat flux, which is less than the total heat flux entering the tank, is determined by an empirical correlation of test data. This model also has been reasonably successful in predicting liquid surface temperatures--although, in general, for lower tank heat inputs than those to which the Martin model has been applied. The Lockheed-Georgia analysis is much more sophisticated than either the Martin or Arthur D. Little, Inc., model and includes both conductive and convective effects. However, this model is rather difficult to apply and it contains certain empirical constants which must be evaluated by comparison with test data.

C. PRESSURIZATION ANALYTICAL METHODS DEALING WITH INTERFACIAL MASS TRANSFER

Many investigators have analyzed the interfacial mass transfer of a liquid cryogen under its own vapor. These analytical methods have utilized a wide variety of calculation techniques and/or assumptions with respect to the mass transfer processes occurring at the walls and liquid interface. Some investigators have assumed no heat or mass transfer at the liquid-vapor interface. Others have used a heat transfer coefficient at the interface. One investigator included his mass transfer term from experimental data, and still another is attempting to use the method due to Knuth, that of using a convective analysis which makes use of equivalent thermal conductivities and the Fourier conduction equation. A rather complete review of the work in this area is contained in Reference 16.

It is of interest to examine a comparison of the use of different calculational methods in attempting to predict the pressurant requirements in the pressurized transfer of liquid hydrogen. Methods due to Arthur D. Little, Inc., [18, 19] the Lockheed-Georgia Company, [1] and NASA-Lewis [3] all have been able to predict pressurant requirements for both helium and hydrogen pressurized transfer of liquid hydrogen. This is an indication, albeit not strong, that the two processes are similar, and supports the conclusion that the interfacial mass transfer in both cases is essentially the same and probably very small.

One interesting approach has been the application of energy convection equations to the vapor and liquid near the interface to estimate the interfacial mass transfer.[17] This analysis results in a limiting vapor temperature separating evaporation and condensation when oxygen is pressurized with its own vapor. Pressurant gas temperatures above this limiting value will result in evaporation, lower temperatures, condensation. Typical values of limiting temperatures are 1250°R for GO_2/LO_2 and 96°R for GH_2/LH_2.

D. RESULTS

From this literature survey, the following can be stated:

1. Since the interfacial mass transfer is difficult to measure directly, indirect means of obtaining data have been used. By their very nature, these means lump all the experimental and calculational errors in the interfacial mass transfer term. Thus, there is virtually no accurate quantitative data on the interfacial mass transfer from a liquid cryogen into a helium pressurized ullage space.

2. There is a considerable amount of semi-quantitative evidence that when liquid hydrogen is pressurized with helium the interfacial mass transfer is very small and presumably in the range of molecular diffusion. This is only one mass transfer test result on the helium pressurized transfer of liquid nitrogen with helium. This result shows that there was evaporation of nitrogen into the helium-filled ullage space, roughly in accordance with molecular diffusion. In addition, the effectiveness of a helium prepressurant in reducing condensation indicates a stagnant diffusion layer adjacent to the liquid surface. Therefore, these results tend to indicate that propellant evaporation may be limited by molecular diffusion.

3. A considerable amount of data on liquid temperature gradients is available. However, several rather conflicting, analytical models have been proposed and the physical mechanism of liquid stratification has not been well defined.

V. THERMODYNAMIC OR LIMITING CASE ANALYSIS

A. GENERAL APPROACH

The analysis described in this section circumvents treatment of the kinetics of heat and mass exchange by assuming that a fraction of liquid, initially in a storage volume, mixes with a fraction of the gas, in the volume at the completion of transfer, so that thermal and phase equilibrium are established between the two. With this approach, we seek to examine conditions that might occur in transfer operations, as limited by energy and mass balances. A simplified version of the approach has previously been described.(20)

With the model used, gradients of composition and temperature in the ullage and the liquid are represented by step changes. In an actual transfer process, the kinetics of heat and mass exchange, that are not dealt with here, would determine distributions of composition and temperature in gas and liquid and, in effect, the interacting fractions in our model.

The analysis leads to determination of the amount of fuel vaporized during transfer, the amount of pressurant gas required to fill the ullage space, and the gas composition in the mixed portion of the ullage as functions of transfer pressure, pressurant gas temperature, and the fractions of interacting liquid and gas.

B. ANALYSIS

Consider the conditions before and after transfer in the arrangement of Figure 1. We will assume that: 1) The initial ullage volume is negligible and all of the liquid is transferred. 2) Displacement gas comes from an infinitely large reservoir at constant temperature and pressure. 3) The liquid in "b" is pressurized to the transfer pressure and the transfer takes place with the pressure remaining constant in both "b" and "c." 4) A volume fraction, X, of the liquid initially in tank "b" mixes with a volume fraction, Y, of the gas finally in tank "b" so that thermal equilibrium between the mixed ullage gas and the mixed liquid, and phase equilibrium between the fuel vapor in the mixed portion of the ullage and the mixed liquid, are achieved.

For the system comprising M_{pm} and XM_{fb1}, conservation of energy requires that

$$M_{pm} U_{pm} + M_{fb2} U_{fb2} + FXM_{fb1} U_{fc2} - XM_{fb1} U_{fb1} - M_{pm} U_{pa} =$$

$$Q - \frac{1}{J}\left[P(1-X)\,V + PF\,X\,M_{fb1}\,\nu_{fc2} - P_a\,M_{pm}\,\nu_a - P(1-Y)V\right] \qquad (1)$$

Conservation of mass yields

$$XM_{fb1} = M_{fb2} + F\,X\,M_{fb1} \qquad (2)$$

The Gibbs-Dalton Law applied to the gas in the volume YV is

$$P = P_f + P_p \qquad (3)$$

and assuming the pressurant in YV to be a perfect gas

$$M_{pm} = \frac{P_p}{R_p T_y} \cdot Y\,V \qquad (4)$$

We further note that

$$M_{fb1} = \rho_{fb1}\,V \qquad (5)$$

$$M_{fb2} = \rho_{fb2} \cdot YV \qquad (6)$$

and assume that

$$\nu_{fc2} = \nu_{fb1} \qquad (7)$$

Relations (1) through (7) may be combined, eliminating F and P_p and solving for P to yield

$$P = J \left[\frac{\frac{P_f}{R_p T_y}\left(H_a - U_{pm}\right) + \rho_{fb2}\left(U_{fb2} - U_{fc2}\right) + \frac{X}{Y}\rho_{fb1}\left(U_{fc2} - U_{fb1}\right) - \frac{Q}{YV}}{\frac{H_a - U_{pm}}{\frac{R_p}{J} \cdot T_y} - \left(1 - \frac{\rho_{fb2}}{\rho_{fb1}}\right)} \right] \quad (8)$$

From our phase equilibrium assumption P_f, ρ_{fb2}, U_{fb2}, U_{fc2}, and ρ_{fc2} are determined by T_y. Hence, P can be calculated from Equation (8) for any T_y. Then

$$P_p = P - P_f \quad (9)$$

and since

$$M_p = M_{pm} + M_{pu} = \frac{P_p}{R_p T_y} \cdot YV + \frac{P}{R_p T_a}(1 - Y)\, V$$

The mass of pressurizing gas per unit storage volume is given by

$$\frac{M_p}{V} = Y \cdot \frac{P_p}{R_p T_y} + (1 - Y)\,\frac{P}{R_p T_a} \quad (10)$$

Finally, the fraction of fuel vaporized, ϵ, is given by

$$\epsilon = \frac{\rho_{fb2} \cdot YV}{\rho_{fb1} V} = Y \cdot \frac{\rho_{fb2}}{\rho_{fb1}} \quad (11)$$

With the model used in this analysis, ϵ cannot be greater than X, by definition. When ϵ is equal to X all the mixed liquid is just vaporized. Thus,

$$\epsilon \leq X$$

or using Equation (11) for θ,

$$Y \cdot \frac{\rho_{fb2}}{\rho_{fb1}} \leq X$$

and

$$\frac{X}{Y} \geq \frac{\rho_{fb2}}{\rho_{fb1}} \qquad (12)$$

Equation (12) places a limitation on values of X and Y that are consistent with the analytical model for any particular transfer pressure (i.e., ρ_{fb2}). The procedure for calculating θ and $\frac{M_p}{V}$, the quantities of interest, for a given X and Y was as follows. Choose a value of T_y and determine the fuel properties at Time 2; calculate P from Equation (8), P_p from Equation (9), $\frac{M_P}{V}$ from Equation (10) and ϵ from Equation (11). Calculations of this nature for various values of T_y, have been used to determine ϵ and $\frac{M_p}{V}$ as functions of P for given X and Y.

C. PROPELLANT EVAPORIZATION AND PRESSURANT GAS REQUIREMENTS FOR ADIABATIC TRANSFER

1. Liquid Hydrogen Transfer

The percent of liquid hydrogen vaporized during transfer, ϵ, and the helium gas requirements, $\frac{M_p}{V}$, have been calculated for helium pressurized transfers under adiabatic conditions, over a range of transfer pressures and for several combinations of values of X and Y.

The liquid hydrogen was assumed initially saturated at 36°R. Figure 2 shows the percent of liquid that is vaporized, assuming that the helium gas input temperature is 530°R. The three curves, excluding the two for X=1, are perhaps most representative of real transfer processes, because considerable stratification usually takes place in the liquid. As one would expect the percent of liquid hydrogen vaporized increases with transfer pressure. The curve for X = .02 stops at P = 39.7 psia; at that point $\epsilon = X$, i.e., all the mixed liquid has been vaporized.

The proportions of hydrogen vapor and helium in the mixed portion of the ullage are indicated by Figure 3. The Figure shows that, for X less than about 0.1, the volume fraction of hydrogen in the mixed ullage is very high and nearly constant, regardless of the precise values of X and Y, and almost independent of transfer pressure. For these cases of small X, only a fraction of the heat given by the helium as it cools to near liquid hydrogen temperature is absorbed as sensible heat by the liquid. The controlling energy balance is between the cooling helium and the vaporizing liquid hydrogen. The heat release of the helium per unit mass and the heat absorbed by the hydrogen per unit mass are both fixed by the final temperature, which never departs widely from the initial liquid temperature. Thus, the energy balance implies a nearly fixed mass ratio, and, hence, volume ratio, of hydrogen and helium in the mixed ullage, almost independent of X, Y and transfer pressure.

For small X, where the volume fraction of hydrogen in the mixed portion of the ullage is nearly independent of Y, and the transfer pressure, the mass of fuel vaporized is approximately proportional to Y and the transfer pressure, as may be seen in Figure 2.

At a transfer pressure of about 16.5 psia, the curves in Figure 3 for various values of X and Y intersect. At that pressure, the final mixed liquid temperature exactly equals the initial liquid temperature. No heat is absorbed by the mixed liquid remaining after transfer, so the value of X does not influence the heat balance. Y also cancels out of the heat balance. The mixed gas temperature is the same as the initial liquid temperature, i.e., fixed; the heat balance fixes the final mass ratio. The pressure ratio is determined by the mass ratio and, because the partial pressure of hydrogen is fixed at the saturation value corresponding to the initial liquid temperature, the transfer pressure for this unique condition is fixed.

The helium gas requirements are shown in Figure 4. As would be expected, the mass of gas required increases with transfer pressure for all values of X and Y. For transfer pressures higher than 16.5 psia, which are of most interest, the helium required increases with both X and Y, i.e., with the amount of mixing. When X = 0, no mixing occurs between liquid and pressurant gas,

and the helium gas remains at its input temperature. Therefore, its density and the mass of gas required are a minimum. For small values of X, as described above, the influence of the liquid fraction on the energy balance and thus on the mass of pressurant gas required, is not strong. Furthermore, the volume fraction of hydrogen and helium in the mixed portion of ullage are nearly independent of transfer pressure. Consequently, for a given value of Y, the mass of helium required will be essentially proportional to transfer pressure, as Figure 4 shows. The effect of Y on the helium required, as shown by the curves for X = 0.1; Y = 0.5, and 1.0, is weaker than one might expect. Even though the helium in the mixed portion of the ullage is at a much lower temperature, hence, higher density, Figure 3 has shown that the fraction of hydrogen in the mixed portion is high, and the partial pressure of helium correspondingly low. Hence, replacing unmixed helium volume with the mixture of helium and hydrogen does not greatly increase the total amount of helium required.

The effect of helium input temperature on percent liquid hydrogen vaporized is shown in Figure 5, for the case X = 1, Y = 1. Two curves are shown, one for an inlet temperature of 530 R, the other for 350 R. As is evident, the warmer gas can vaporize a greater amount of liquid hydrogen for a given transfer pressure. Both Figures 2 and 3 were drawn for helium input temperature of 530°R. Similar plots for a temperature of 350°R would be expected to show the same general influence of X and Y. However, we would expect the volume fraction of hydrogen in the mixed portion of the ullage for given X and Y to be lower than shown in Figure 3, since the energy content of the incoming helium and its ability to vaporize hydrogen would be significantly reduced.

2. Liquid Oxygen Transfer

In the calculations for liquid oxygen, the liquid was assumed initially saturated at 162°R. The percent of liquid oxygen vaporized during transfer is shown in Figure 6, again for a helium input temperature of 530°R. The amount vaporized is relatively insensitive to both pressure and X, being mainly dependent on Y. Figure 7 shows the partial pressure of oxygen in the mixed portion of the ullage. Over much of the transfer pressure range, say from 25 to 50 psia transfer pressures, the oxygen pressure deviates little from the saturation pressure corresponding to the initial liquid temperature. The large volumetric heat capacity and latent heat of the liquid keep the mixed liquid temperature near its initial temperature, and the partial pressure of fuel vapor in the mixed ullage near 15 psia. At a transfer pressure of 38 psia, the mixed liquid temperature exactly equals the initial liquid temperature, as with hydrogen at 16.5 psia. The pressure at which this condition occurs, and the partial pressure of oxygen in the mixed portion of the ullage for this condition are both independent of X and Y.

At transfer pressures below 38 psia the mixed liquid temperature after transfer would be lower than the initial value, as cooling by evaporation of fuel into the ullage would overbalance the heat input to the liquid from the helium.

The presence of warm helium gas during transfer has only a limited influence on the behavior of the liquid oxygen. At low transfer pressures the process resembles that for a wet accumulator, wherein a saturated liquid is permitted to drain from a fixed volume, while flashing of the liquid remaining in the volume maintains a diminishing pressure in the ullage. Even at as high a transfer pressure as 50 psia, the heat content of the helium gas, when absorbed by only a small portion of the liquid, for example, X = .003, would raise the pressure in the ullage just 3 psia above the value corresponding to the initial liquid temperature.

Figure 8 shows the helium gas requirements. The helium required increases with pressure. It is cooled to near the initial liquid temperature almost independent of X, so the total mass required at a given pressure is principally dependent on Y. The curve for X = 0 represents the case where no mixing occurs between helium and liquid oxygen. The helium would remain at its input temperature and a minimum amount is required. Mixing with only a small portion of the liquid can cause a substantial increase in the gas required. For example, at 50 psia transfer pressure, mixing with a fraction of liquid of only .003, increases the helium required per unit volume from .035 pounds per cubic feet to .052 pounds per cubic feet, an increase of about 50 percent. This results from the large volumetric heat capacity and latent heat of the liquid oxygen.

The effect of helium input temperature on liquid oxygen vaporized is shown in Figure 9. The effect of reducing the input temperature from 530 R to 350 R on the amount of liquid oxygen vaporized is minor, consistent with the limited influence of the warm helium on the oxygen transfer process, as discussed above.

D. AMBIENT HEAT LEAK EFFECTS

Heat leak into propellant tank can cause additional vaporization of liquid over and above that predicted by the gas liquid interaction discussed previously. In this section, we have evaluated reasonable limits with a range of ambient heat leaks to be anticipated for liquid hydrogen and liquid oxygen tanks and consider the influence which this might have on the previous results.

1. Propellant Tank Heat Leak Range

Although it is desirable that analytical methods be applicable to as large a range of heat leak as possible, it is probable that some facets of our work may ultimately depend on semi-empirical correlations or analytical methods having a limited range of validity. Also, numerical examples will be of most value if applied to representative heat flux conditions. Therefore, it is desirable to define the heat leak ranges of most interest. To this end we have briefly reviewed the heat leak ranges typical of liquid oxygen and liquid hydrogen tankage on first and second stage vehicles.

It is generally accepted that liquid hydrogen tankage must be insulated; whereas liquid oxygen tanks need not be insulated. The need for insulation on hydrogen tanks results from both the low volumetric sensible and latent heat of hydrogen and also the high heat fluxes of uninsulated tanks of liquid hydrogen. For instance, if we assume that a rise in bulk liquid saturation pressure of 1 psi per minute is an allowable limit for the heat input to a closed 20 foot diameter tank of liquid hydrogen, the maximum allowable side heat leak is 700 Btu/hr/ft^2. Ambient heat transfer to uninsulated surfaces at liquid hydrogen temperatures is of the order of 5000 Btu/hr/ft^2. Therefore, insulation is indicated for liquid hydrogen tanks. On the other hand, a 20-foot diameter liquid oxygen tank can tolerate a heat leak of 10,000 Btu/hr/ft^2 for the same allowable saturation pressure rise of 1 psi per minute. Ambient heat transfer to uninsulated tanks of liquid oxygen is unlikely to exceed 5000 Btu/hr/ft^2 under severe ground heat leak conditions such as a 50 knot wind and 50% relative humidity. We have not studied aerodynamic heating rates to any extent, however, some prior studies conducted in conjunction with an airframe manufacturer on a large first stage vehicle indicated maximum aerodynamic heating rates of about 5000 Btu/hr/ft^2. Higher velocity vehicles would have higher maximum aerodynamic heating rates. However, for our present studies, we will assume that aerodynamic heating rates will not be substantially over 5000 Btu/hr/ft^2 for a major portion of the flight. Therefore, it appears unnecessary to insulate liquid oxygen tanks.

For liquid hydrogen tanks insulated with the equivalent of 1/2 inch of styrofoam, we would expect a heat leak of about 200 Btu/hr/ft^2. Based on the criteria above, we feel that a maximum heat leak should not exceed about 700 Btu/hr/ft^2. Therefore, we would consider a heat leak range of 100 to 1000 Btu/hr/ft^2 to be adequate for liquid hydrogen tanks.

Under fairly low ground heat leak conditions (no wind, 50% relative humidity) we would expect the ambient heat leak to liquid oxygen tanks to be about 500 Btu/hr/ft^2. As previously stated, we would not expect aerodynamic heating rates to be substantially above 5000 Btu/hr/ft^2. Therefore, we feel a range of 500 to 5000 Btu/hr/ft^2 is reasonable for liquid oxygen tankage.

2. Incorporation of Heat Leak into Basic Analytical Method

Heat leak into the fuel tank during transfer can cause additional vaporization of liquid. Equation (8) shows the effect of the heat leak from external to the tank into the system consisting of M_{pm} and XM_{fbl}. Heat added to the system, a positive Q, would decrease P for a given T_y. For the given T_y, P_f is fixed, P would be less and the ration $P_{f/P}$ would be increased. Thus, the fraction of fuel in the ullage gas after transfer, which is proportional to $P_{f/P}$, would be larger.

We have considered recomputing the previous results for a range of heat addition terms. However, we have felt that the significance of this calculation would not merit the rather large effort required. Therefore, we have used an alternate approach of comparing the ambient heat input with the heat input which would result from cooldown of the helium pressurant gas.

3. Comparison of Ambient Heat Addition with Heat Liberated by Cooldown of Helium Pressurant Gas

The heat per unit volume resulting from ambient heat leak can be compared with the heat per unit volume liberated by helium cooldown as an indication of the relative importance of these two heat sources. In this development, we shall use some rather broad assumptions, but we feel the results will at least have qualitative significance.

For the purpose of this comparison we will take the volumetric specific heat of the helium gas to be .03 Btu/cu ft °F. This volumetric specific heat is obtained as the product of the density and specific heat of the pressurant gas at a temperature of 460°R and a pressure of two atmospheres. In fact, the density of the helium gas will tend to increase as it cools down which acts to increase the mean volumetric specific heat, but on the other hand, not all the helium will cool down, so perhaps the assumption that the helium gas cools down at the initial volumetric specific heat is not too far from the actual fact. To compute the total heat liberated by the helium, we assume that the helium pressurant gas will cool to the atmospheric boiling point of the propellant. Therefore, the total cooldown heat per unit volume for helium above hydrogen is 13 Btu/ft^3; and for helium above oxygen, 9 Btu/ft^3.

In computing the total ambient heat addition, we will assume a tank diameter of 20 feet and a heat addition time of 10 minutes. For a heat flux of 1000 Btu/hr/ft^2 the heat addition per unit volume will be 20 Btu/cu ft. At other values of ambient heat flux the heat addition term is ratioed linearly. Now, making use of the ranges of ambient heat leak defined in Section 1 above, we would expect the total heat addition per unit volume will range from 2 to 20 Btu/ft^3 for hydrogen and from 10 to 100 Btu/ft^3 for oxygen.

The numerical values developed in the preceding two paragraphs are presented in Table V-1 below.

TABLE 1

COMPARISON OF AMBIENT HEAT LEAK AND HELIUM COOLDOWN HEAT QUANTITIES

Heat Source	Heat Addition Btu/ft^3	
	Hydrogen	Oxygen
Ambient Heat Leak	2-20	10-100
Helium Cooldown	13	9

Although the results presented in the table above are rather qualitative, a rather interesting difference between hydrogen and oxygen is apparent. In the case of hydrogen, the heat addition associated with helium cooldown is about in the middle of the range of heat addition due to ambient heat leak. Therefore, for the low end of the ambient heat leak range we would expect liquid hydrogen surface temperature and evaporation to be controlled primarily by liquid-ullage gas interaction and only at the high end of the ambient heat leak range would we expect the heat leak to be important. With oxygen, on the other hand, even the lower values of ambient heat leak are equivalent to the heat addition associated with helium cooldown.

Since our previous work has shown that the interaction between the helium and the hydrogen is apparently sufficient to elevate the hydrogen surface temperature to near saturation, we might expect surface temperatures in liquid hydrogen tanks to fall in the range of near saturation for low values of heat leak and at saturation for higher values of heat leak. Stated alternately, we might not expect ambient heat leak to influence liquid hydrogen surface temperature very much since the surface temperature in the absence of heat leak is frequently close to saturation, but at higher values of heat leak free boiling may result. In the case of oxygen, since previous adiabatic studies have shown helium cooldown to have little influence on surface temperature, and since the heat range in general falls above that resulting from helium cooldown, we would expect the liquid oxygen surface temperature to be solely controlled by external heat leak.

E. DISCUSSION OF RESULTS

The analysis described is based on only energy and mass balances. It cannot be used to predict how much mixing will occur between liquid fuel and the pressurant gas. Nevertheless, by assuming that certain fractions of liquid and pressurant gas interact, some interesting results have been obtained. In a liquid hydrogen transfer, the volume fraction of hydrogen gas in the mixed portion of the ullage, for small values of X, is essentially independent of the transfer pressure and of Y. Thus, when the liquid is highly stratified the mass of hydrogen vaporized is nearly proportional to the transfer pressure and to the fraction of final ullage volume containing well mixed hydrogen and helium. Low transfer pressures and prevention of mixing of gases in the ullage volume could contribute significantly to reducing fuel vaporization.

In a liquid oxygen transfer, the partial pressure of oxygen in the mixed portion of the ullage tends to remain at a value near the saturation pressure corresponding to the initial liquid temperature (about 15 psia in our calculations). As with hydrogen, the mass of liquid oxygen vaporized is nearly proportional to Y, the fraction of mixed ullage volume. However, in contrast to hydrogen, the mass of liquid oxygen vaporized is only weakly dependent on the transfer pressure.

The considerable differences between hydrogen and oxygen stem from the widely differing thermal properties of the two. Their properties, that are of most significance in an energy balance, are shown in Table V-2 below. Both the volumetric specific heat and latent heat are much higher for liquid oxygen. As a result, the heat exchange between warm helium and liquid hydrogen is relatively more important than with oxygen. Mixing in the ullage gas is important in both liquid hydrogen and liquid oxygen transfers, though for somewhat different reasons. With liquid hydrogen the mixing carried hydrogen vapors into the ullage volume and supplies enough energy to cause considerable liquid vaporization. With liquid oxygen the mixing merely carries fuel vapor at a pressure near 15 psia, into the ullage.

TABLE 2

THERMAL PROPERTIES OF LIQUID HYDROGEN AND LIQUID OXYGEN SATURATED @ 1 ATM

Property	Hydrogen	Oxygen
Liquid Density, ρ_L - $\frac{LB}{ft^3}$	4.4	71
Liquid Specific Heat, C_L - $\frac{Btu}{LB-°F}$	2.2	0.5
Latent Heat, λ - $\frac{Btu}{LB}$	194	90
Volumetric Liquid Specific Heat, $\rho_L C_L$ - $\frac{Btu}{ft^3-°F}$	9.7	35
Volumetric Latent Heat, $\rho_L \lambda$ - $\frac{Btu}{ft^3}$	850	6400

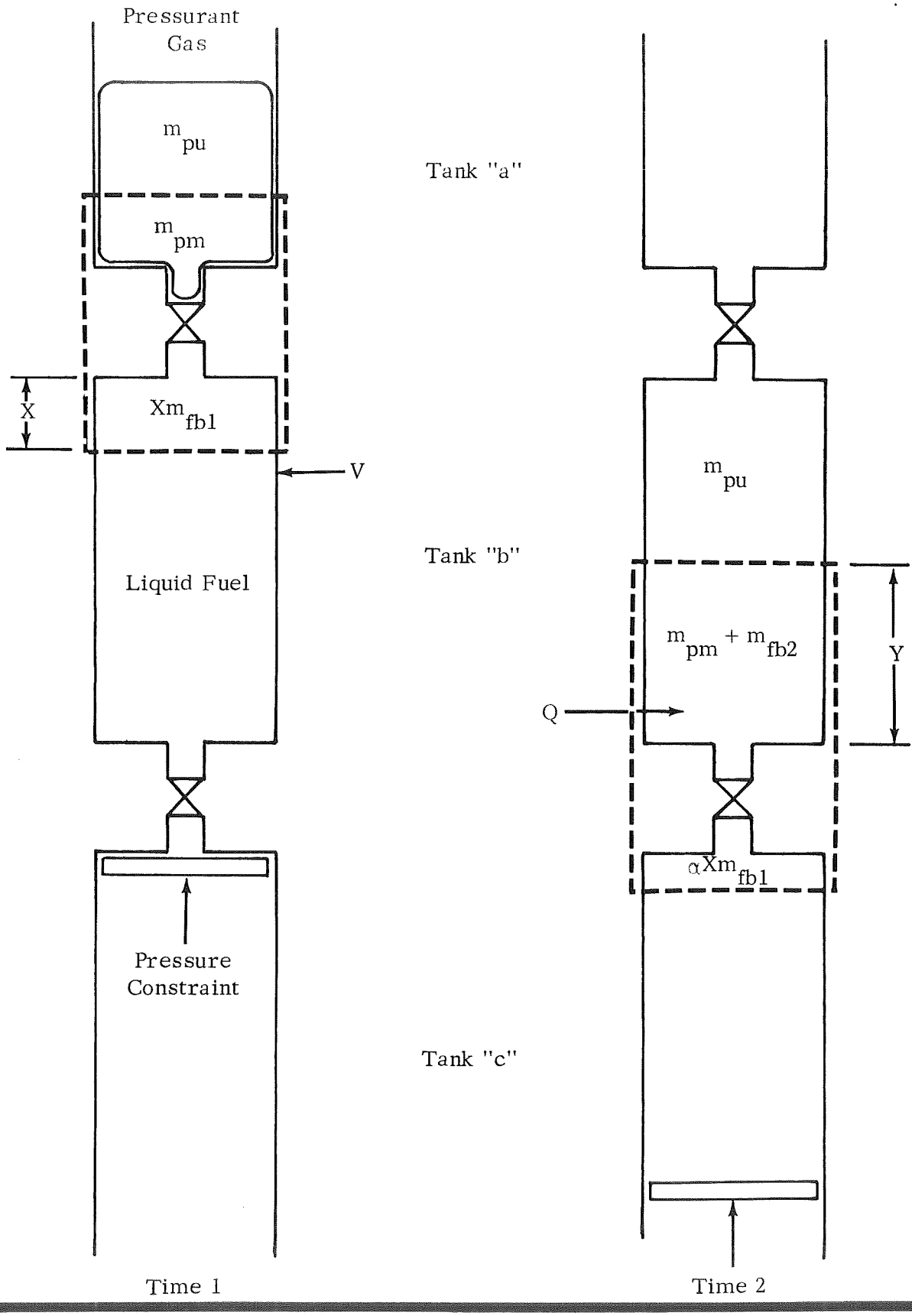

FIGURE 1 GAS PRESSURIZED TRANSFER MODEL FOR THERMODYNAMIC ANALYSIS

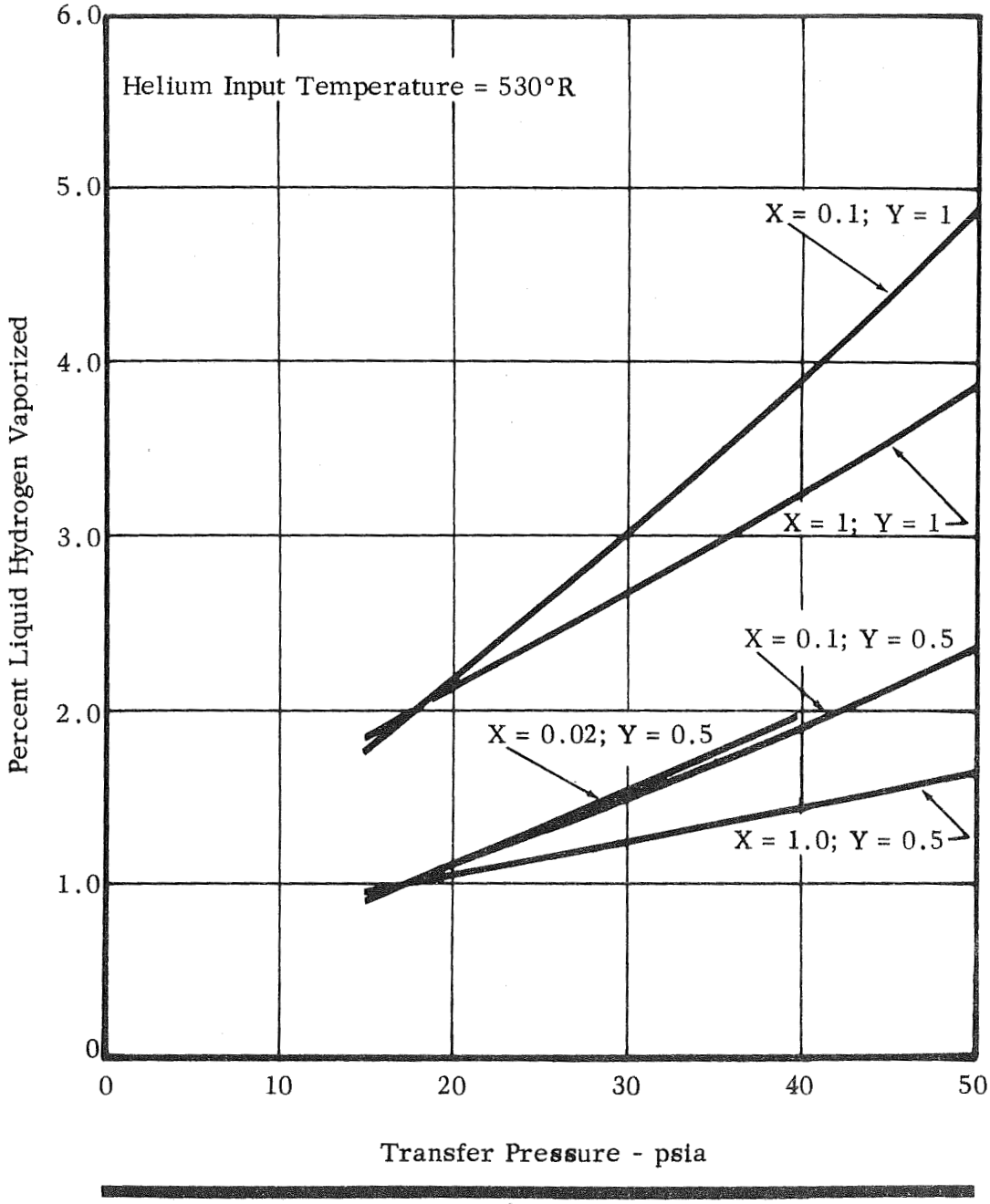

FIGURE 2 LIQUID HYDROGEN VAPORIZED DURING TRANSFER

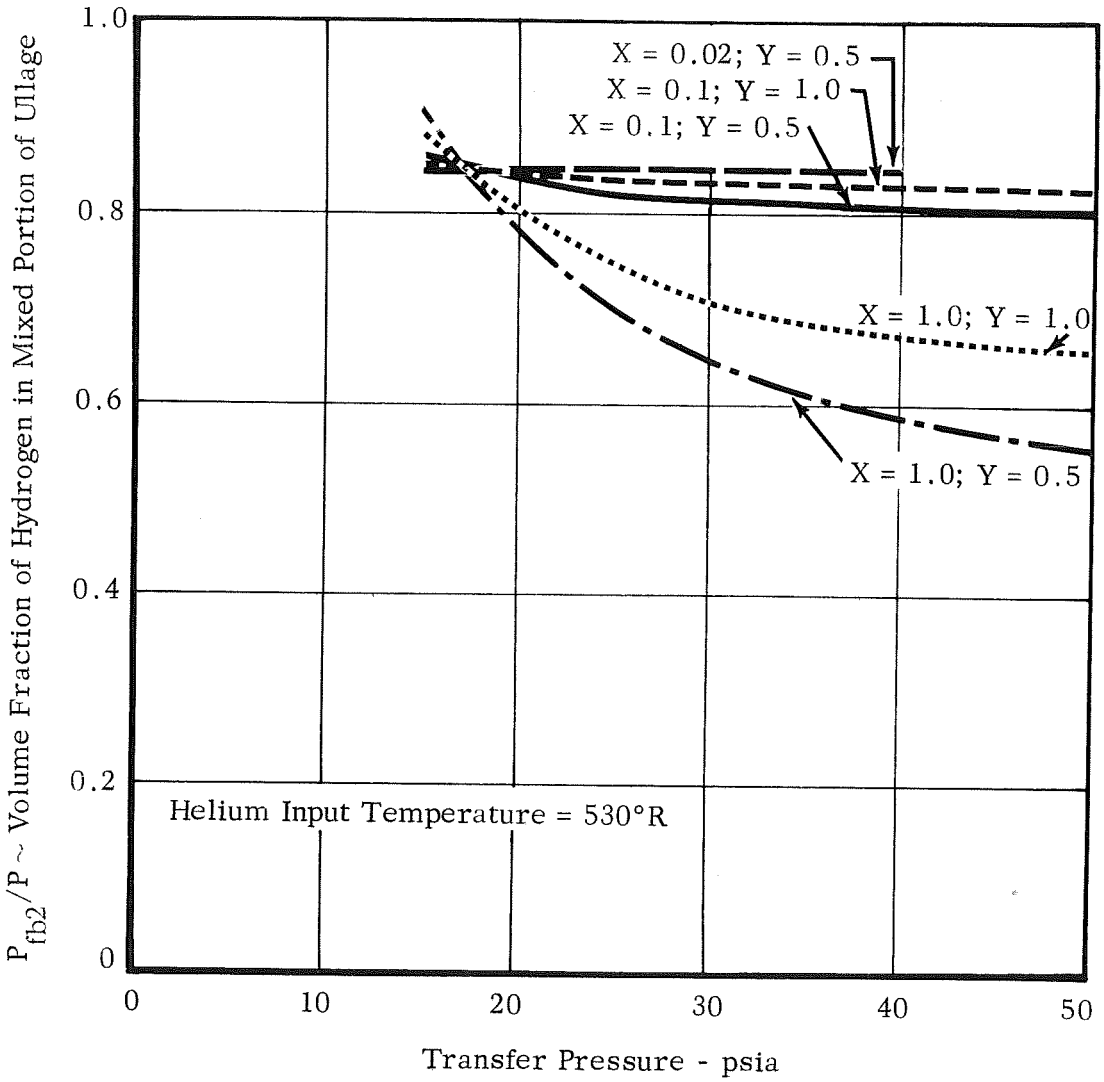

FIGURE 3 VOLUME FRACTION OF HYDROGEN IN MIXED PORTION OF ULLAGE

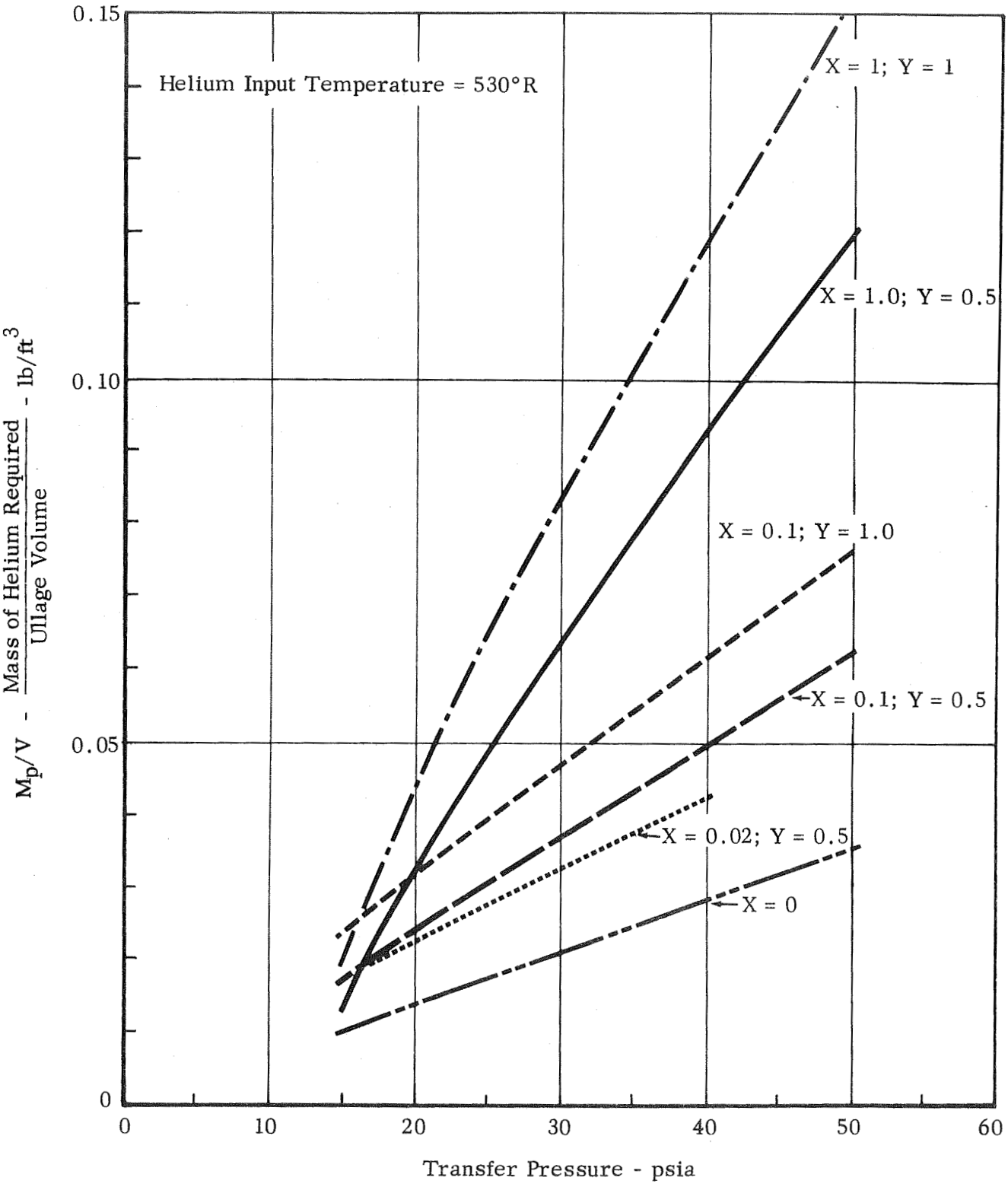

FIGURE 4 GASEOUS HELIUM REQUIREMENTS--TRANSFER OF LIQUID HYDROGEN

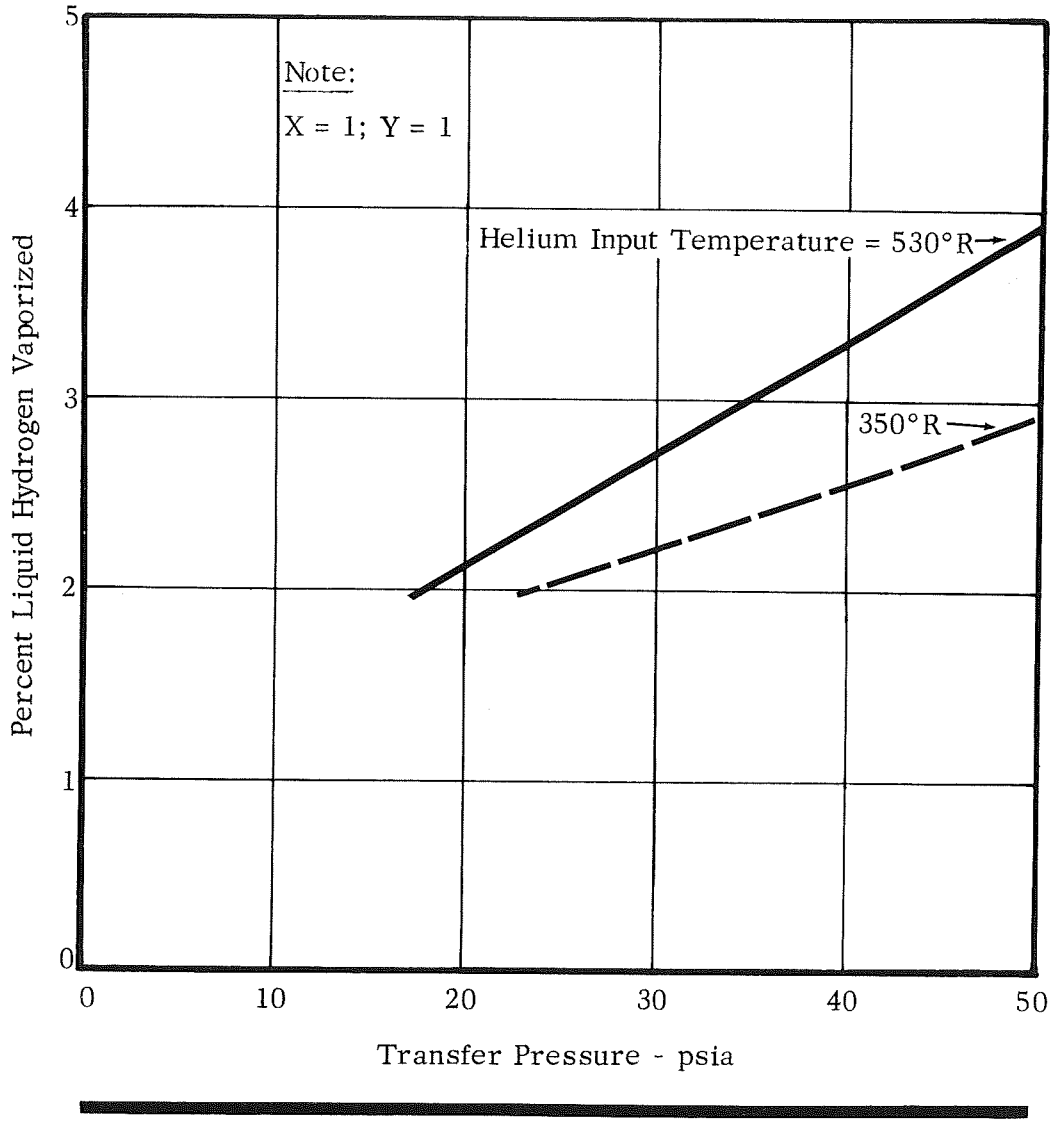

FIGURE 5 EFFECT OF HELIUM INPUT TEMPERATURE ON LIQUID HYDROGEN VAPORIZATION

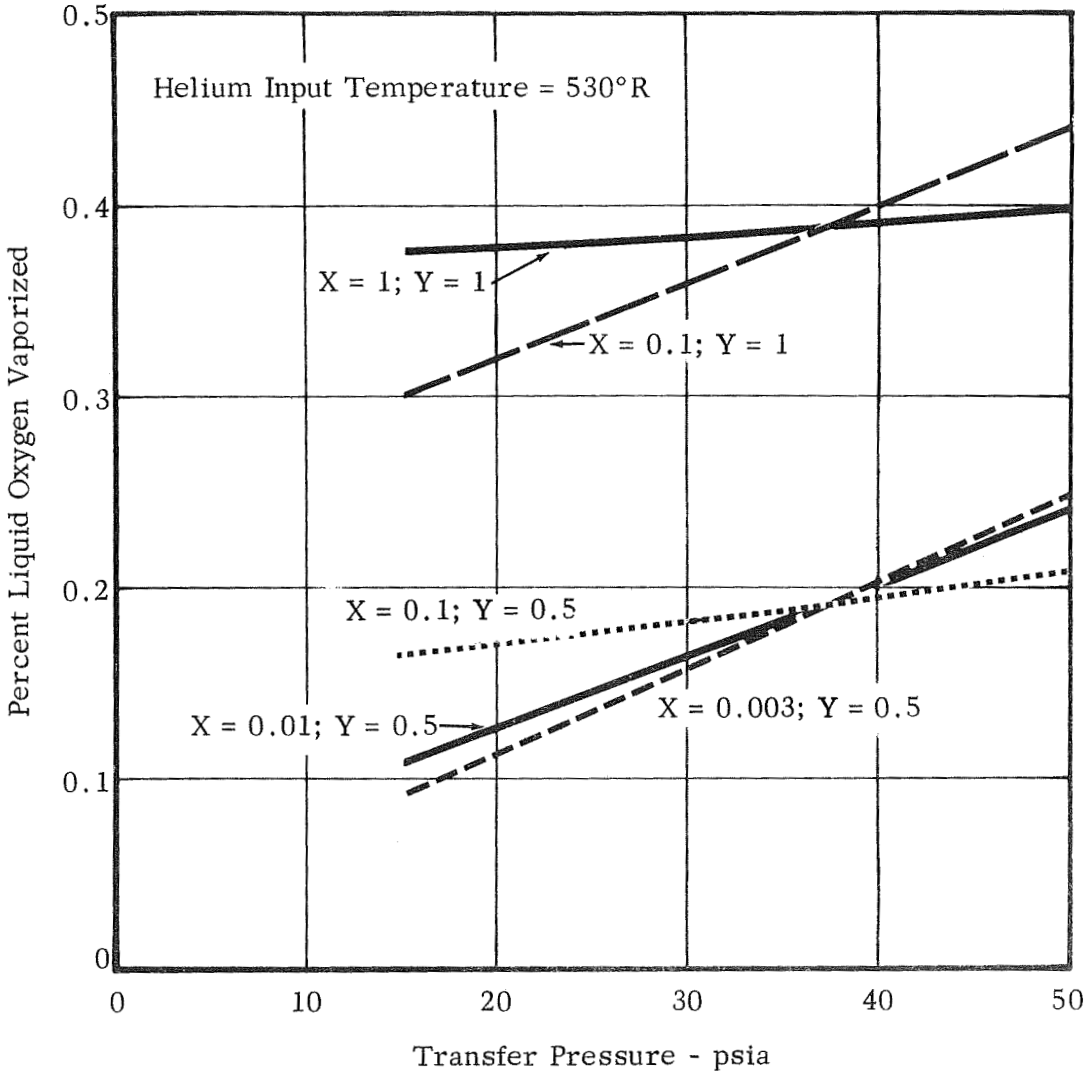

FIGURE 6 PERCENT LIQUID OXYGEN VAPORIZED DURING TRANSFER

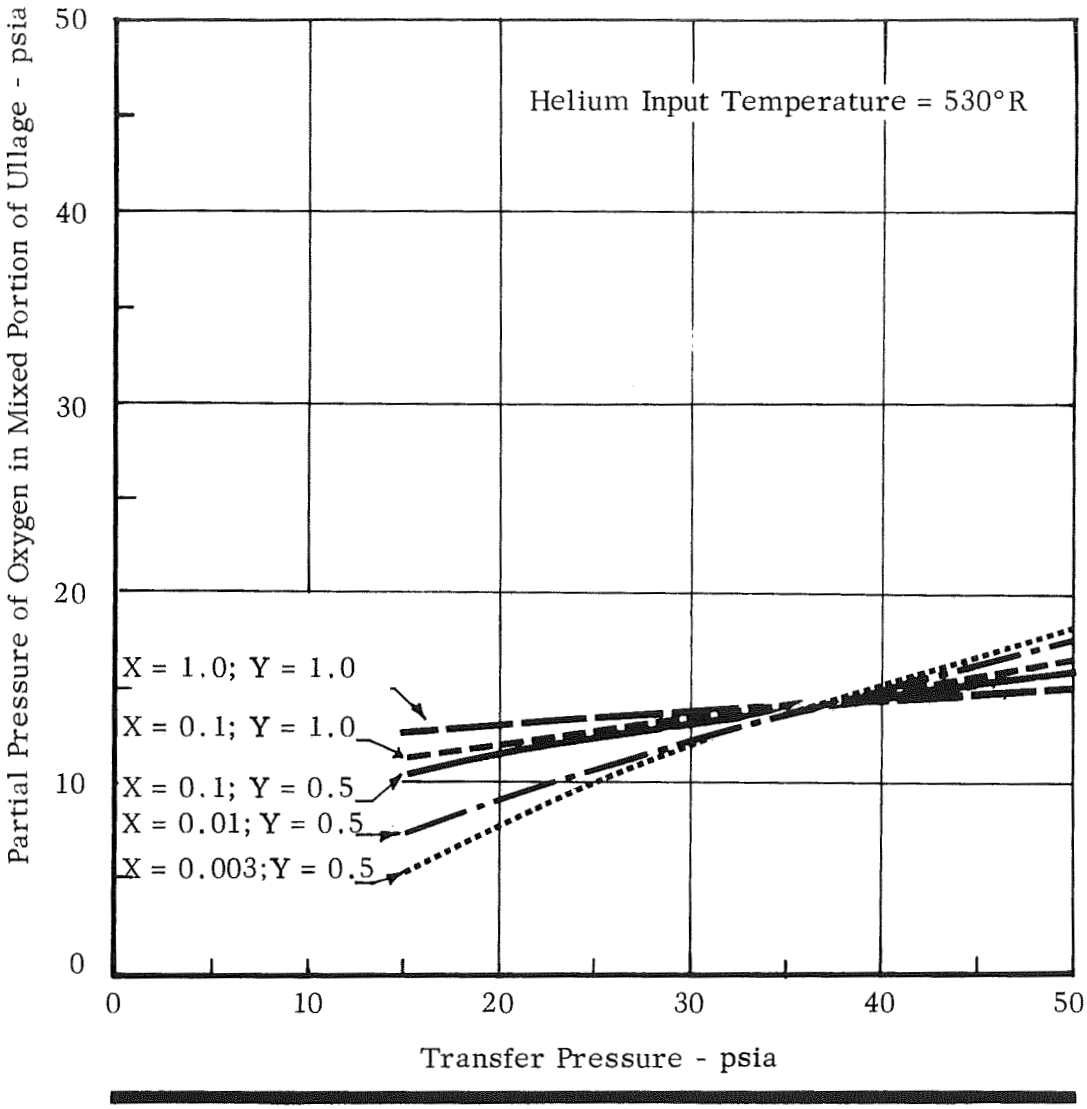

FIGURE 7 PARTIAL PRESSURE OF OXYGEN IN MIXED PORTION OF ULLAGE

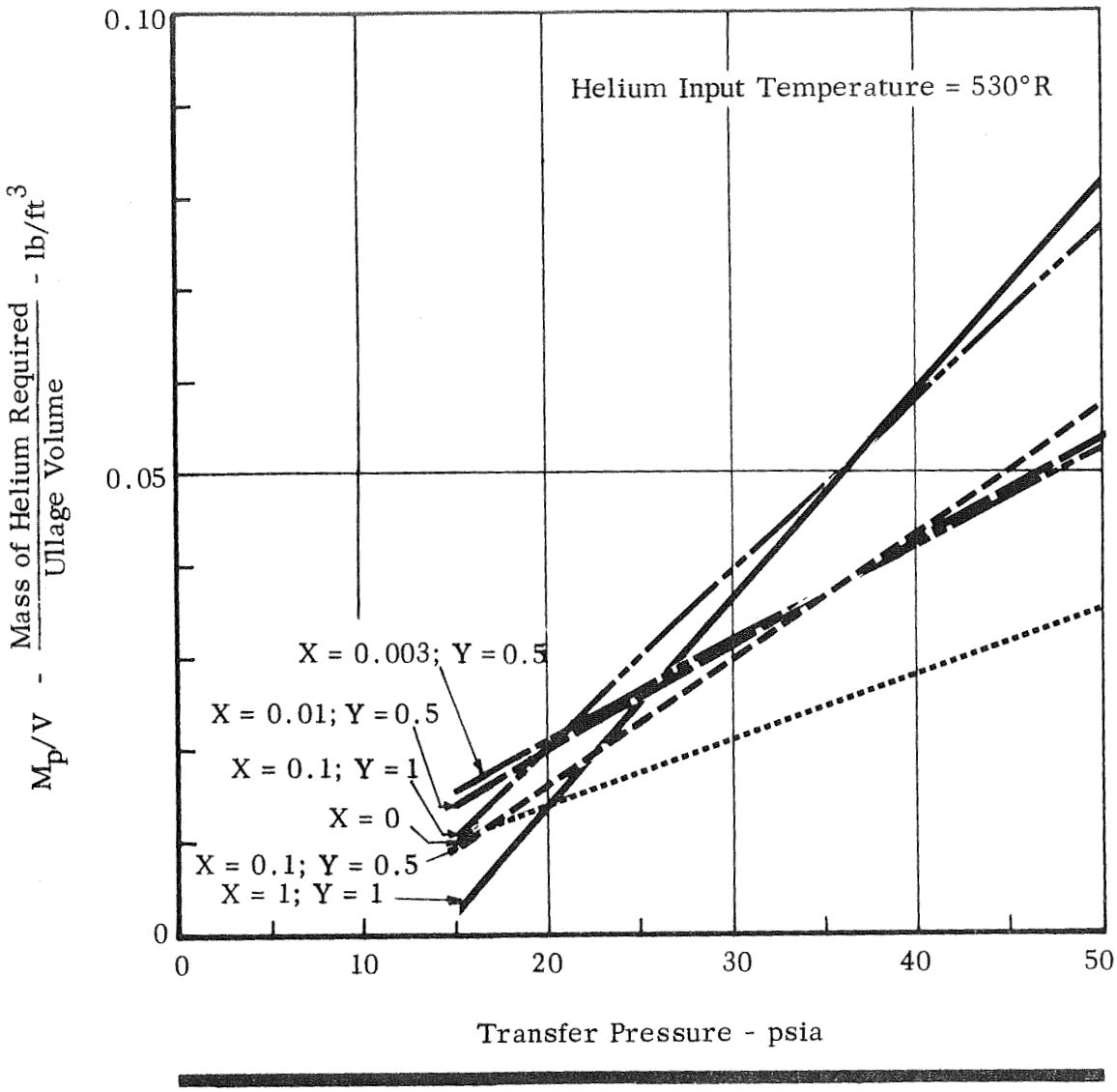

FIGURE 8 GASEOUS HELIUM REQUIREMENTS - TRANSFER OF LIQUID OXYGEN

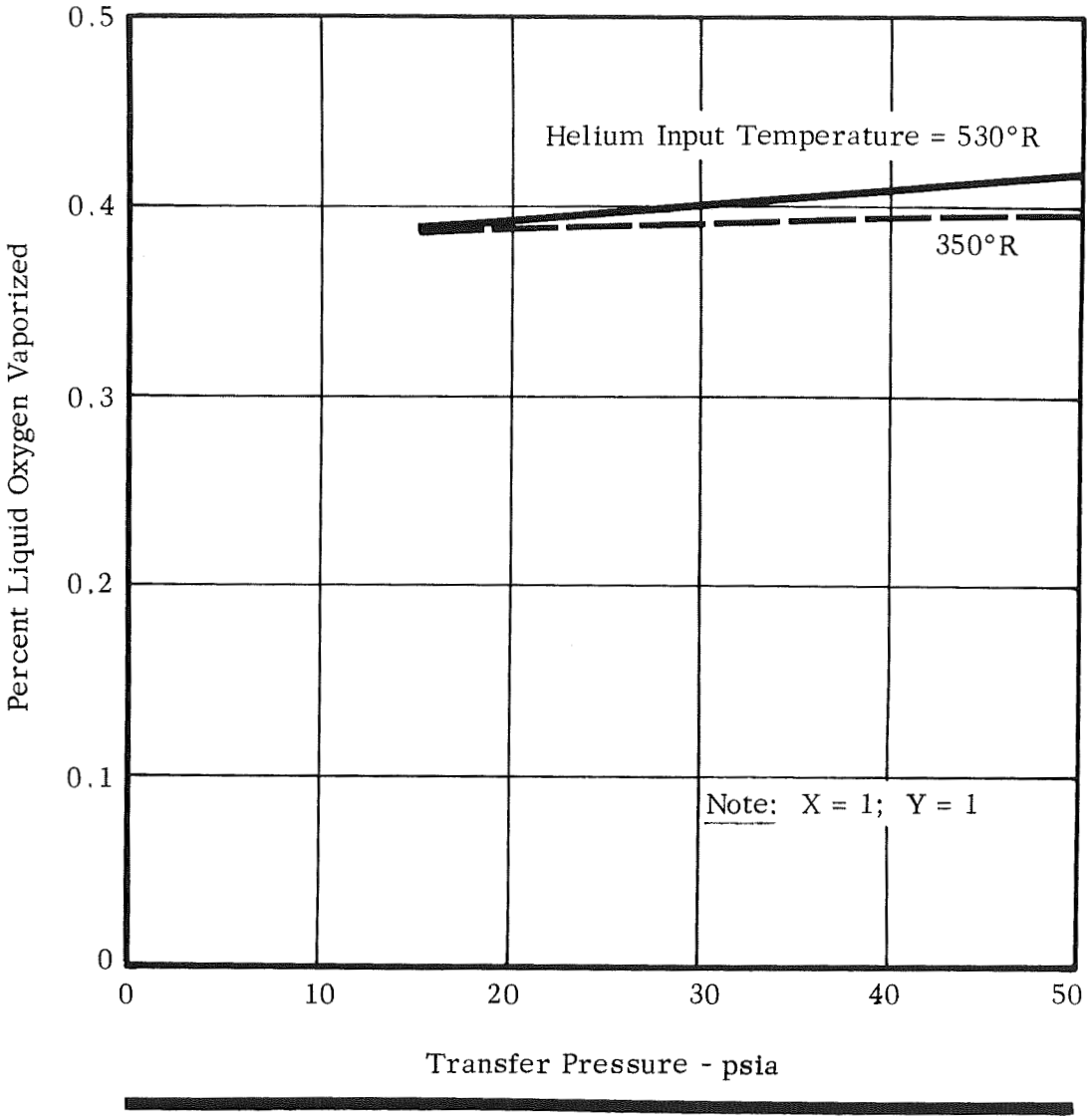

FIGURE 9 EFFECT OF HELIUM INPUT TEMPERATURE ON LIQUID OXYGEN VAPORIZATION

VI. INTERFACIAL MASS TRANSFER AT LIQUID SURFACE IN THE ABSENCE OF FREE BOILING

A. GENERAL APPROACH

Experimental data which are presently available indicate that the mass transfer rate from the surface of a liquid cryogen is controlled by a molecular diffusion mechanism. In order to make available a quantitative model for the interfacial mass transfer process, the partial differential equations for the diffusion of an evaporating cryogen through inert pressurant are formulated and then integrated. By converting the integrated results into dimensionless form a general correlation is presented which allows the calculation of the rate of liquid evaporation once the conditions at the liquid surface and the ullage concentration at infinity have been specified. Methods of determining the liquid surface temperature are considered in Section VII of this report.

After a discussion of the diffusion mechanism, the effect of free convection in the helium ullage is investigated. Since only minor differences are found between the results of the diffusion and free-convective models, it is felt that reliable means for the calculation of interfacial mass transfer have been determined.

Both the diffusion and convection models assume that the flow pattern of the ullage gas is unaffected by the flow of pressurant gas into the ullage. In order to check the validity of this assumption, a theoretical analysis is provided which predicts the penetration length of a jet issuing into a stagnant ullage.

Finally, the results of all theoretical calculations are compared with available experimental data and a final basis is formulated for the calculation of interfacial mass transfer rates.

B. MOLECULAR DIFFUSION

There is considerable experimental evidence that the rate of evaporation of a liquid cryogen into an ullage filled with an insoluble pressurant is limited by the molecular diffusion of the vaporized cryogen into the ullage. Thus it is hypothesized that a stagnant layer of gas is built up on the liquid surface and that this layer constitutes the main resistance to mass transfer. This section presents a method for calculating the amount of evaporated liquid and concentration gradients in the ullage as functions of time assuming that molecular diffusion is controlling and that convective effects are unimportant.

A mathematical difficulty is encountered in applying the molecular diffusion equations when the cryogen vapor pressure on the liquid surface approaches the total pressure of the system, i.e., at the onset of free boiling. Under these conditions it is shown that the results of the kinetic theory may be applied to determine the surface temperature, thus avoiding any such mathematical difficulties.

In order to apply the results of these calculations to the problem at hand, a method is presented for the calculation of the molecular diffusivities of oxygen and hydrogen in helium. Finally, calculations are made for typical hydrogen-helium and oxygen-helium systems.

1. General Development of Classical Molecular Diffusion Theory

a. Mathematical Development of Diffusion Equations

The system being considered, shown schematically in Figure (10), consists of a cylindrical storage tank containing a liquid cryogen which is being expelled by an insoluble pressurant. It is assumed that the area of the liquid surface remains constant throughout the operation and that there are no radial gradients in either temperature or composition.

If x is the distance from the liquid surface, the following differential material balance may be written on component A, the vaporized cryogen in the gas phase:

$$- \frac{\partial N_A}{\partial x} = \frac{\partial C_A}{\partial t} \tag{13}$$

But the flux of A may be expressed as the sum of two terms whereby

$$N_A = - D \frac{\partial C_A}{\partial x} + N_T y_A$$

or

$$N_A = - D \frac{\partial C_A}{\partial x} + C_A u_m \tag{14}$$

The first term on the right-hand side of this equation equals the molal flux of A relative to an imaginary plane of no-net-molal-flux. The second term accounts for the motion of this imaginary plane with respect to the liquid surface; it is this term which destroys any analogy between this problem and any of the standard heat transfer problems.

Substituting Equation (14) into Equation (10) and assuming D and C_T to be independent of both time and distance, the following is obtained:

$$D \frac{\partial^2 y_A}{\partial x^2} - \frac{\partial}{\partial x} (u_m y_A) = \frac{\partial y_A}{\partial \theta} \qquad (15)$$

As it was assumed that C_T is a function of neither x nor θ, it is shown in Appendix A that u_m is independent of x at any given time and that Equation (15) may be reduced to the Stefan-Maxwell equation:

$$D \frac{\partial^2 y_A}{\partial x^2} - u_m \frac{\partial y_A}{\partial x} = \frac{\partial y_A}{\partial \theta} \qquad (16)$$

with boundary conditions:

$$y_A = y_{Ao} \text{ at } x = 0, \text{ all } \theta \qquad (17a)$$

$$y_A = y_{A\infty} \text{ at } \theta = 0, \text{ all } x \qquad (17b)$$

$$y_A = y_{A\infty} \text{ at } x = \infty, \text{ all } \theta \qquad (17c)$$

These boundary conditions are based on the assumptions that (a) the concentration of A at the surface remains constant throughout the operation, (b) that the ullage space is filled initially with a gas of uniform composition, and (c) that the dimensions of the ullage are large compared to the distance that the vaporized cryogen penetrates into the ullage.

The numerical values of y_{Ao} and $y_{A\infty}$ will depend upon what mechanism is postulated for the formation of the stagnant gas layer above the liquid surface. The various possible mechanisms and values of y_{Ao} and $y_{A\infty}$ will be discussed after the general differential equation has been solved.

In order to solve Equation (16), it is necessary to define a new independent variable, $\xi = x/2\sqrt{D\theta}$. By substituting this variable into Equation (16), the following equation results:

$$\frac{d^2 y_A}{d\xi^2} + 2\left(\xi - \sqrt{\frac{\theta}{D}}\, u_m\right)\frac{d y_A}{d\xi} = 0 \qquad (18)$$

Using the fact that N_T is equal to N_{Ao} and is independent of s for the case under consideration, it is shown (Appendix A) that:

$$\left[\frac{-1}{2(1 - y_{Ao})}\left(\frac{d y_A}{d\xi}\right)_{\xi = 0}\right] = u_m\sqrt{\frac{\theta}{D}} = \phi \qquad (19)$$

where the parameter ϕ is independent of both x and θ. Equation (18) may then be written as

$$\frac{d^2 y_A}{d\xi^2} + 2(\xi - \phi)\frac{dy_A}{d\xi} = o \qquad (20)$$

with boundary conditions

$$y_A = y_{Ao} \quad \text{for} \quad \xi = o \qquad (21a)$$

$$y_A = y_A \quad \text{for} \quad \xi = \infty \qquad (21b)$$

Equation (20) may be integrated directly to yield

$$Y_A = \frac{1 - \text{erf}(\xi - \phi)}{1 + \text{erf}\,\phi} \qquad (22)$$

where

$$Y_A = \frac{y_A - y_{A\infty}}{y_{Ao} - y_{A\infty}}$$

Combination of Equations (19) and (22) results in

$$\frac{y_{Ao} - y_{A\infty}}{1 - y_{Ao}} = \sqrt{\pi}\,(1 + \text{erf}\,\phi)\,\phi\exp(\phi^2) \qquad (23)$$

A complete derivation of Equations (22) and (23) is given in Appendix A. The work of Arnold [21] and Byrd [22] may be consulted for further treatment of this and other related diffusion problems.

b. Determination of Concentration Profiles

In order to determine concentration profiles for the penetration of the vaporized propellant into the ullage, Equation (22) may be solved for specified values of Y_A. Since Equation (23) relates ϕ to $(y_{A_o} - y_{A_\infty}) / (1 - y_{A_o})$, the quantity ξ_{Y_A} may be plotted versus $(y_{A_o} - y_{A_\infty}) / (1 - y_{A_o})$ for various values of Y_A. This has been done in Figure 11 and this plot allows the direct calculation of concentration profiles at any time for any specified pair of y_{A_o} and y_{A_∞}. The quantity $(y_{A_o} - y_{A_\infty}) / (1 - y_{A_o})$ may be computed from the selected values of y_{A_o} and y_{A_∞}; then the values of ξ_{Y_A} may be read from Figure 11 for each value of Y_A shown on the graph. Now by multiplying each value of ξ_{Y_A} by $2\sqrt{D\theta}$ the penetration distance corresponding to each value of Y_A may be calculated. Since the values of Y_A at $x = o$ and $x = \infty$ are already known, the complete composition profile may be determined at any time for any set of boundary conditions.

c. Determination of Total Amount Vaporized

The mass of propellant lost per unit of surface area is given by:

$$W_A = M_A \int_o^\theta N_{Ao}\, d\theta = M_A C_T \int_o^\theta u_m\, d\theta$$

Making use of Equation (19)

$$W_A = 2 C_T M_A \phi \sqrt{D\theta} \qquad (24)$$

The parameter ϕ may now be eliminated between Equations (23) and (24) and the quantity $W_A / C_T M_A \sqrt{D\theta}$ may be plotted as a single-valued function of the variable $(y_{Ao} - y_{A\infty})/(1 - y_{Ao})$. This plot is shown in Figure 12 and allows calculation of the mass evaporated as a function of time for any pair of y_{Ao} and $y_{A\infty}$, values.

The parameter $W_A C_T M_A \sqrt{D\theta}$ has special significance when converted to an effective diffusion length. To accomplish the conversion we note that, for ideal gas behavior, the product $C_T M_A$ is equivalent to the propellant vapor density evaluated at the ullage pressure and some defined temperature, which will be discussed below. To further explain this point we may recall that C_T is defined as total moles per unit volume and, for perfect gas behavior, is solely a function of the propellant vapor (M_A), one obtains a mass per unit volume or density. Therefore, we may define a term $L_1 \equiv \frac{W_A}{C_T M_A}$ which is the thickness of an equivalent layer of pure vapor and from the prior development, $L_1 / \sqrt{D\theta} = 2\phi$, is a single valued function of the variable $(y_{A_o} - y_{A_\infty})/(1 - y_{A_o})$.

In order for this difference in length to be useful, we must specify the temperature associated with the diffusion process. First the diffusion is generally confined to a gas layer adjacent to the surface. Secondly, the temperature effect is weak, since the temperature dependent factor $C_T \sqrt{D}$ is proportional to $T^{.25}$.

Therefore, for simplicity, we have decided to use the propellant saturation temperature at ullage pressure as the temperature associated with the diffusion process. At this point, we may now consider the length L_1 to represent an equivalent thickness of pure vapor saturated at ullage pressure. This equivalent thickness is a convenient way of expressing the total mass of diffused vapor. The mass diffused can be taken as the product of (L_1) x (Surface Area) (saturated density). The volume percentage of diffused propellant may be interpreted in two ways:

(1) If we consider the actual physical situation, of the propellant lying in the cold region adjacent to the liquid surface, the volumetric fraction for a cylindrical tank is merely L_1 divided by total ullage height.

(2) If we think in terms of a hypothetical mixed situation, where the propellant vapor is assumed to be distributed throughout the ullage, the actual propellant vapor volumetric fraction of (1) above is multiplied by the ratio of mean ullage temperature to liquid saturation temperature.

d. Applicability of the Diffusion Model

In making use of Figures 11 and 12 to calculate diffusion rates and concentration profiles, the values of y_{A_o} and y_{A_∞} must first be specified. However, if y_{A_o} is allowed to approach unity, Equation (23) and Figure 11 show that ϕ must increase to infinity. Equation (24) shows that this limit leads to the unreasonable results of an infinite vaporization rate.

Thus, before any calculations are carried out, Section VI-B-2 is presented to clear up the mathematical difficulties involved when large values of y_{Ao} are to be considered; i.e., when the liquid surface temperature is (nearly) equal to saturation at ullage pressure.

2. Kinetic Theory Application to Saturation Liquid Surfaces

As pointed out in the previous section, the factor ϕ increases to infinity as y_{Ao} approaches unity. Under these conditions, the liquid is approaching a state of free boiling and the foregoing diffusion analysis is not sufficiently comprehensive to treat this problem.

In order to avoid these mathematical difficulties, it is proposed that the principles of kinetic theory be brought to bear on the problem. With the aid of kinetic theory, it may be shown y_{Ao} approaches an upper limit established by the rate at which liquid can evaporate from the surface.

In order to consider the evaporation process more closely, consider the section of the cryogen liquid surface as shown schematically in Figure 10. It is to be assumed that there exists a quiescent liquid surface at temperature T_o and vapor pressure P_{A_o}. As the liquid vapor pressure is allowed to approach the total system pressure, the resistance to the liquid vaporization process becomes an appreciable portion of the total resistance to mass transfer. Now the problem must be solved by combining the law governing the rate of evaporation from a liquid surface with the equations already developed for diffusion in the gas phase.

Since the resistance to the evaporation process is now important, the partial pressure of component A just above the liquid surface, P_{A_o}, will be slightly less than P_{A_o}. The results of kinetic theory may be applied under these circumstances to show that the rate of evaporation is given by:

$$N_A = \Gamma \left(2\pi M_A R T_o\right)^{-\frac{1}{2}} \left(P_{A_o} - P^{+}_{A_o}\right) \qquad (25)$$

Where Γ, the sticking coefficient of molecules at the liquid surface is taken as unity for the present analysis.

Also, Equation (24) may be differentiated with respect to time to yield

$$\frac{d}{d\theta}\left(\frac{W_A}{M_A}\right) = N_A = C_T \phi (D/\theta)^{\frac{1}{2}}$$

Now these two equations may be combined as

$$P^{+}_{A_o} = P_{A_o} - \gamma\phi$$

where

$$\gamma = \frac{1}{\Gamma} (2\pi M_A R T_o)^{-\frac{1}{2}} C_T (D/\theta)^{\frac{1}{2}}$$

Also using the same procedure, the defining equation for ϕ, Equation (23), may be written

$$\sqrt{\pi}\ (1 + \text{erf}\ \phi)\ \phi\ e^{\phi^2} = \frac{P_{A_o} - P_A - \gamma\phi}{P - P_{A_o} + \gamma\phi}$$

and for the case where $P_{A_o} = P$,

$$\phi + \sqrt{\pi}\ (1 + \text{erf}\ \phi)\ \phi^2\ e^{\phi^2} = \frac{P_{A_o} - P_A}{\gamma} \qquad (26)$$

Since the term $\left(P_{A_o} - P_A\right) / \gamma$ may be easily defined for any given problem, the above equation may be used to find an upper value for ϕ in the case where the l liquid nears the free boiling range. For example, calculations performed over a range of saturation pressures from 1 to 3 atmospheres and times from 10^2 sec to 10^4 sec for hydrogen and oxygen indicate that $\left(P_{A_o} - P_A\right) / \gamma$ falls in the range of 3×10^5 to 3×10^7, and consequently, from Equation (26), ϕ falls in the range of 3.0 to 3.6. An average value of $\phi = 3.3$ (or from Equation (23) $\left(\frac{y_{A_o} - y_{A_\infty}}{1 - y_{A_o}}\right) = 10^7$) may be used for the cases of liquids nearing free boiling, and the results should be consistent with both the results for diffusion in the gas phase and the predictions of the kinetic theory of liquid evaporation.

3. Molecular Diffusivities of Hydrogen and Oxygen in Helium

In order to make use of the results of the diffusion analysis it is of course necessary to know the molecular diffusivities of the species in question. Values of these quantities are calculated by standard methods and are compared to available experimental data.

a. Experimental Data

Although methods are available for calculating molecular diffusion coefficients, experimental data are useful as an independent check on the analytical results. The need for an experimental check is most important in the case of helium-hydrogen mixtures at low temperatures, since quantum effects might be expected to be significant in this region.

For helium-hydrogen mixtures, three references were located.[24, 25, 26] All measurements were made at one atmosphere; the temperature range covered was from 52°K to 293°K. This data is identified in Figure 13.

Similar data on helium-oxygen mixtures were unavailable.

b. Theoretical Estimation of Diffusion Coefficients

At low pressures where the gas mixture does not deviate appreciably from an ideal gas, theory is sufficiently advanced to allow one to calculate binary gas diffusion coefficients.

For molecules for which we have either viscosity or P-V-T data it has been possible to determine the Lennard-Jones potential parameters. Such parameters may be used directly in the theoretical first-approximation formulae for binary diffusion coefficients. Hydrogen, helium and oxygen are in this class.

For reasonably low pressure gases, the diffusion coefficients may be calculated as follows:

$$D_{12} = \frac{2.628 \times 10^{-3}\, T^{3/2}\, M^{*1/2}}{P\, \sigma_{12}^{2}\, \Omega^{(1,1)}(T_{12}^{*})} \qquad (27)$$

Reid and Sherwood[26] and Hirschfelder, Curtiss and Bird[27] show rather extensive comparisons between experimental values of D_{12} and those calculated by Equation (27). Agreement is surprisingly good, i.e., less than 10 percent. Equation (27) was thus used to calculate

$$D_{O_2} - He \text{ and } D_{H_2} - He$$

over a wide temperature range. The plots are shown in Figure 13. D increases with temperature and the temperature effect is felt predominantly in the $T^{3/2}$ term. $\Omega^{(1,1)}(T_{12}^*)$ is a weak function of temperature and varies from somewhat less than one to somewhat greater than one. Bird[28] gives a good physical interpretation of this collision integral function. For hard sphere molecules that do not interact, $\Omega^{(1,1)}$ is unity; for interacting molecules at low temperatures, molecular energies are low and collisions sluggish with longer effective collision times; $\Omega^{(1,1)}$ is greater than unity and D_{12} decreases. At high temperatures molecular energies are large and upon collision of molecules some interpenetration occurs, the result of which essentially decreases the time of a collision; D_{12} increases and $\Omega^{(1,1)}$ is less than unity.

Pressure affects D_{12} inversely in the simple case, thus Figure 13 shows, for example,

$$D_{10 \text{ ATM}} = (1/10)\, D_{1 \text{ ATM}}, \text{ etc.}$$

c. Discussion of Quantum Effects

Bird[28] states that for binary systems involving He or H_2 below 50°C, Equation (27) should be corrected for quantum effects. Such corrections are very difficult to obtain and at the present time introduce large uncertainties. It is proposed here that the quantum corrections are of minor importance and may be neglected. The evidence for this statement is as follows:

1) On Figure 13, the experimental data available appear to agree with predicted values of $D_{He\text{-}H_2}$ within experimental accuracy.

2) Comparisons of self-diffusion coefficients of H_2-H_2 and O_2-O_2 at 20.6°K and 77.7°K respectively, calculated from Equation (27) and from experimental data agree well. (See Table 8.4-13 of Ref. 27.) These temperature ranges coincide with values of T* of as low as 0.6. In the present estimation, the lowest value of T* used is 1.09 (H_2-He at 20°K).

d. Conclusion

Although experimental data for diffusion coefficients of $He-H_2$ and $He-O_2$ are scarce and of somewhat doubtful accuracy, predicted values from Equation (27) are believed accurate to 10-15 percent. The recommended values are shown in Figure 13. Quantum effects are not believed to be significant in these cases.

4. Typical Results for Hydrogen and Oxygen Systems

In the discussion above the basic equations for molecular diffusion have been developed for classical diffusion theory, and curves presented to allow for a determination of concentration profiles and quantity vaporized in terms of boundary conditions for the molecular diffusion process, and the diffusivities of the phases involved. Kinetic theory has been used to resolve the rather anomalous situation where classical diffusion theory tends to predict an infinite rate of evaporation as the vapor fraction adjacent to the surface approaches unity. Data for the molecular diffusion coefficients of hydrogen and oxygen diffusing into a helium gas have been developed and presented graphically. In this section we will illustrate application of these methods and calculate actual evaporation quantities.

It must be noted that the classical diffusion model is applicable to calculation of diffusion rates resulting from fixed surface and ullage concentrations. Specification of these boundary conditions required independent information about the situation in the propellant tank, and subsequent portions of this report will be devoted to means of determining these boundary conditions, particularly the liquid surface temperature . At this point we will merely attempt to establish reasonable maximum and minimum concentrations for the ullage and liquid surface. For the liquid surface the maximum partial pressure would occur if the liquid surface was almost saturated at ullage pressure. As will be discussed in more detail in Section VII, we might expect this situation to occur in liquid hydrogen tanks or in liquid oxygen tanks subjected to high heat leak. As the other limit we might expect the liquid surface to be saturated at one atmosphere. We might expect this condition to be typical of low heat-leak liquid oxygen tanks. For the ullage gas we might expect an initial maximum concentration of one atmosphere, and an initial minimum concentration of zero. We might anticipate the concentration of one atmosphere to be typical of the situation existing at the end of initial pressurization with a normal diffuser configuration which would allow good mixing in the ullage. We might consider the case of zero concentration in the ullage to be representative of the ullage concentration during transfer when the propellant vapor originally present in the ullage is diluted to a large extent by the increase in ullage volume. These combinations of liquid surface and ullage concentration result in four possible cases which are presented in Table 3. It may be noted that the fourth case in which the liquid surface of the ullage concentrations are both equal to one atmosphere is a trivial case since the diffusion rates would be identically equal to zero for this situation.

TABLE 3

CASES TO BE INVESTIGATED IN THE DIFFUSION ANALYSIS

Case No.	Evaporating Cryogen Partial Pressure, Atm: Liquid Surface	Evaporating Cryogen Partial Pressure, Atm: Ullage	y_{A_o}	y_{A_∞}	$\frac{y_{A_o} - y_{A_\infty}}{1-y_{A_o}}$
I	P	0	1.0	0	∞
II	1.0	0	1/P	0	$\frac{1}{P-1}$
III	P	1.0	1.0	1/P	∞
IV	1.0	1.0	1/P	1/P	0

Notes:

1. Liquid Surface Partial Pressure
   a. The condition where $P_{A_o} = P$ corresponds to a high heat leak to the liquid surface, thus bringing the surface vapor pressure up to the total system pressure.
   b. The condition where $P_{A_o} = 1.0$ represents the case of very low heat leak to the surface.
2. Ullage Partial Pressure
   a. The condition of $P_{A_\infty} = 1.0$ corresponds to the case of good mixing in the ullage during initial pressurization.
   b. The condition of $P_{A_\infty} = 0$ is typical of the situation during transfer.

In Figure 14 we have presented a plot of dimensionless penetration length as the function of total ullage pressure for the three combinations of liquid surface partial pressure and ullage partial pressure of interest. From this plot it may be noted that cases I and III are identical since when the liquid surface partial pressure approaches the ullage pressure diffusion is limited entirely by surface kinetics and, as such, is uninfluenced by the partial pressure in the ullage space. Also, for these two cases the dimensionless penetration length is independent of ullage pressure. For case II in which the liquid surface is assumed to be saturated at one atmosphere and concentration in the ullage is taken to be zero, dimensionless penetration length drops off with pressure. In this case the major effect seems to be that the quantity diffusing is constant. However, as the ullage pressure increases this becomes a smaller percentage of ullage mass and, therefor, the dimensionless penetration length is reduced.

Figure 15 presents a plot of penetration length as a function of time for cases I and III for hydrogen and oxygen diffusing into helium. For cases I and III in which the evaporation is primarily limited by surface kinetics, the dimensionless penetration length is independent of ullage pressure as discussed in the above paragraph. It may be noted from this plot (which really indicates a maximum evaporation due to diffusion) that the penetration lengths are quite small and when combined with reasonable tank heights will indicate very small volumetric percentages of propellant diffusion.

C. INFLUENCE OF ULLAGE GAS FREE CONVECTION ON INTERFACIAL MASS TRANSFER

In this section an analysis is carried out to determine the effects of convective flow patterns existing in a helium ullage bounded by cold tank walls and a cold liquid surface. This study indicates that boundary layer flow down the tank walls will result in a stagnant gas layer adjacent to the liquid surface. Boundary layer flow calculations show that the growth of this stagnant gas layer on the liquid surface is much more rapid than the rate of penetration of propellant vapor into the ullage due to molecular diffusion. Therefore, it is felt that the assumption of a stagnant ullage is valid for the purposes of molecular diffusion calculations.

It would be expected that the stagnant layer adjacent to the liquid surface would be convectively stable, and that the "new gas" flowing down the tank wall would deposit on top of the gas which had preceded it. However, as a model to illustrate the maximum effects due to convective mass transfer it is assumed that the boundary layer flowing down the tank walls continually undercuts the stagnant layer and flows adjacent to the liquid surface. By comparing both this result and those of the molecular diffusion calculations with experimental data, some light should be shed on the mechanism of mass transfer at the liquid surface.

1. Calculation of Gas Flow Rate Down the Tank Walls

When an inert pressurant such as helium is fed to a tank originally containing a liquid cryogen at one atmosphere pressure, it is anticipated that natural convection currents will be set up in the ullage space. The gas near the cold walls will be chilled and will tend to flow down the walls in a film as shown in Figure 16A.

The rate of gas flow down the walls is to be calculated in order to estimate the rate of growth of the stagnant gas layer which rests on the liquid surface. It is to be assumed that all the gas which flows down the walls in the convective film remains on the liquid surface and adds to the volume of the stagnant gas layer. The thickness of the stagnant gas layer is extremely important because it has been postulated that this layer represents the main resistance to mass transfer at the liquid surface.

It is assumed that the thickness of the gas film, δ, is small compared to the tank diameter, d; thus the problem may be treated as natural convection on a vertical flat plate. It has been shown elsewhere [29] that the solution to this natural convection problem is given by

$$u = \frac{27}{4} u_{max} \frac{y}{\delta} \left(1 - \frac{y}{\delta}\right)^2 \tag{28}$$

where

$$u_{max} = 0.766\, \nu\, (0.952 + Pr)^{-\frac{1}{2}} \left(\frac{g\, \beta_f\, \Delta T}{\nu^2}\right)^{\frac{1}{2}} x'^{\frac{1}{2}} \tag{29}$$

and

$$\delta / x' = 3.93\, Pr^{-\frac{1}{2}} (0.952 + Pr)^{\frac{1}{4}}\, Gr_{x'}^{-\frac{1}{4}} \tag{30}$$

The heat transfer coefficient at any x' is given by

$$h = 2\, k / \delta \tag{31}$$

and by integrating over x' from 0 to L_2, it is easily shown that the average heat transfer coefficient is

$$\bar{h} = 4/3\, h_{(x' = L_2)} \tag{32}$$

In order to obtain the flow rate of gas down the walls, Equation(28) may be integrated at a fixed value of x' from y = 0 to y = δ. Thus:

$$u_{ave} = \frac{1}{\delta} \int_0^{\delta} u\, dy = \frac{27}{4} \left(\frac{1}{12}\right) u_{max}$$

$$u_{ave} = 27/48\, u_{max} \tag{33}$$

In order to make use of these equations, it is necessary to obtain the properties of helium at the temperatures in question. An average film temperature is used in order to simplify the calculations; this film temperature is given by

$$T_f = \tfrac{1}{2} (T_{ave} + T_w) = \tfrac{1}{2} \left[\tfrac{1}{2} (T_i + T_o) + Tw \right]$$

and since $T_o \cong T_w$

$$T_f = \tfrac{1}{4} T_i + 3/4\, T_o \tag{34}$$

From the results of the diffusion calculations, it is anticipated that a stagnant gas layer six inches thick would offer enough resistance to mass transfer as to make molecular diffusion through the layer the controlling mechanism. By solving Equations (29)and (30) at $x' = L_2$ and then using Equation (33), the flow rate of gas into the stagnant layer may be calculated. It is then easily shown that the time for the formation of a six-inch layer of gas is given by:

$$(\theta)_{(\Delta = 6 \text{ inches})} = \frac{d}{8\ g\ \mu_{av,\, x' = L_2}} \tag{35}$$

Numerical values from these equations (29, 30, 33 and 35) are easily obtained. Assuming (1) an ullage pressure of 50 psia, (2) an inlet helium gas temperature of 530°R and bulk liquid and wall temperatures of 37°R for hydrogen and 160°R for oxygen, and (3) a T_f from Equation (34) but the ΔT (in Equations (29) and (30) as the arithmetic average between T_i and T_o, and choosing kinematic viscosities and Prandth numbers of helium for the film temperatures corresponding to the hydrogen and oxygen cases as 4.87×10^{-5} and 11.7×10^{-5} ft^2/sec and 0.76 and 0.70, the numerical values shown in Table 4 are obtained.

TABLE 4

ULLAGE GAS BOUNDARY LAYER FLOW DOWN WALLS WITH GROWTH OF STAGNANT VAPOR BLANKET ON LIQUID SURFACE

L, ft	d, ft	$(u_{ave})_{x' = L_2}$, fps		$(\delta)_{x' = L_2}$, ft		(Time Required to Form 6-inch Layer on Liquid Surface-Sec)	
		LH_2	LOX	LH_2	LOX	LH_2	LOX
0.50	2.0	1.63	2.02	0.0113	0.0219	13.6	10.0
1.0	4.0	2.32	2.85	0.0134	0.0260	16.0	12.0
2.0	8.0	3.26	4.03	0.0160	0.0310	19.2	14.2
10	20	7.35	9.0	0.0238	0.0462	14.3	10.7
20	20	10.4	12.7	0.0284	0.0550	8.5	6.4

The few values shown in Table 4 may be extended in a simple manner with the following ratios:

$$\left(\frac{\mu_1}{\mu_2}\right)_{\text{av } x' = L} = \left[\frac{(L2)_1}{(L2)_2}\right]^{\frac{1}{2}}$$

$$\left(\frac{\delta_1}{\delta_2}\right)_{x' = L} = \left[\frac{(L2)_1}{(L2)_2}\right]^{\frac{1}{4}}$$

$$\left(\frac{\theta_1}{\theta_2}\right)_{\Delta = 6 \text{ in.}} = \frac{d_1}{d_2} = \left[\frac{(L2)_1}{(L2)_2}\right]^{\frac{3}{4}}$$

The results of Table 4 make it clear that a stagnant gas layer of sufficient thickness to act as a barrier to diffusion is formed very rapidly. Since a pressurized-hold-time of 3-5 minutes has been specified for this problem, the stagnant gas layer should be stabilized long before the expulsion process is started.

By using Equations (31) and (32), average heat transfer coefficients in the range of 4-9 Btu/hr/ft^2 °F are calculated. These results may be used in later analyses which take the heat leak into account.

The principal purpose of this analysis has been fulfilled; it has been shown that the stagnant gas layer is formed essentially instantaneously when compared to the times required for the pressurization, hold, and expulsion phases of the process.

2. Mass Transfer Coefficients at the Liquid Surface

In the first phase of this analysis, it was assumed that the gas which flows down the walls of the tank, settles in a gas layer or blanket on the liquid surface. This assumption is quite reasonable, since the gas blanket is convectively stable at the bottom of the ullage space. It is interesting to speculate as to what would happen if the gas flowing down the sides of the tank possessed enough momentum to pass through or "undercut" the stagnant layer and flow out across the liquid surface.

Such a situation would result in a flow pattern as shown in Figure 16B. If it is assumed that the gas film from the wall becomes well mixed as it turns the corner and flows horizontally, a laminar boundary layer of thickness $\delta = 0$ at $y = 0$ will be formed on the liquid surface. This model should result in the maximum heat and mass transfer rates at the liquid surface if it is assumed that an efficient diffuser is employed and that the helium does not "jet" down onto the liquid surface.

The above model is readily analyzed by applying the relations for flow over a flat plate. It is to be assumed that the stream velocity of the gas over the liquid surface is equal to the average velocity of the gas flowing down the walls, $(u_{av_{x'=L_2}})$ as calculated in the preceding section. Actually the area for flow will tend to decrease and δ will increase as y increases because the liquid surface is actually circular; however, the one dimensional problem will be treated in order to obtain maximum values of the heat and mass transfer coefficients.

Reynolds numbers must first be calculated in order to determine what type of flow is to be expected. Using the same helium properties as in previous computations, all values of $(Re)_{y = d/2}$ are found to be less than the critical value of 5×10^5.[29] Thus, all the boundary layers to be treated here may be considered as laminar. The film thickness of such a laminar boundary layer is given by [29].

$$\delta/y = \frac{4.64}{Re_y^{\frac{1}{2}}} \qquad (36)$$

Using Equation (36) film thicknesses are calculated for the same six cases as considered before; the results are given in Table 5.

TABLE 5

ULLAGE GAS BOUNDARY LAYER FLOW DOWN WALLS WITH SWEEPING OF LIQUID SURFACE

L_2, ft	d, ft	$u_{ave_{x'=L_2}}$, fps		$(Re)_{y=d/2}$		$(\delta)_{y=d/2}$, ft	
		LH_2	LOX	LH_2	LOX	LH_2	LOX
0.5	2.0	1.63	2.02	33,500	9,780	0.0252	0.047
1.0	4.0	2.32	2.85	95,200	27,400	0.0302	0.056
2.0	8.0	3.26	4.03	268,000	77,500	0.0365	0.067
10	20	7.35	9.0	1,510,000	424,000	0.0380	0.070
20	20	10.4	12.7	2,130,000	614,000	0.0320	0.059

For other combinations of L_2 and d,

$$\left(\frac{Re_1}{Re_2}\right)_{y = d/2} = \frac{d_1}{d_2} \left[\frac{(L2)_2}{(L2)_1}\right]^{\frac{1}{2}}$$

and

$$\left(\frac{\delta_1}{\delta_2}\right)_{y = d/2} = \left(\frac{d_1}{d_2}\right)^{\frac{1}{2}} \left[\frac{(L2)_2}{(L2)_1}\right]^{\frac{1}{4}}$$

The heat transfer coefficient at any position x is given by (29):

$$Nu_x = \frac{h_y\, y}{\lambda} = 0.332\, Pr^{\frac{1}{3}}\, Re_y^{\frac{1}{2}} \qquad (37)$$

and the average heat transfer coefficient up to any value y by (29)

$$\bar{h} = 2h_y \qquad (38)$$

Now the mass transfer coefficient is defined by the following equation

$$N_A = k_g(P_{A_1} - P_{A_2}) \qquad (39)$$

where (31):

$$k_g = \frac{DP}{RT\, \delta\, p_{He_m}} \qquad (40)$$

The DP product for both the systems considered here are obtained from the Section VI-B-3.

In the diffusion calculations to be presented in Section VI-E, the best check with experimental data is obtained when it is assumed that the liquid surface is heated up until the vapor pressure of the liquid approaches the total pressure of the system. If the vapor pressure is taken exactly as the total pressure, p_{He_m} becomes infinite and the analysis breaks down. However calculations show that p_{He_m} is not greatly affected by varying the liquid vapor pressure from 90 to 99 percent of the total system pressure. For illustrative purposes, let the liquid vapor pressure be 95 percent of the total pressure or 47.5 psia. If it is assumed that the partial pressure of the vaporized liquid in the bulk is essentially zero, then p_{He_m} is easily calculated to be (50-2.5) / ln (50/2.5) = 15.8 psia.

Since δ is parabolic in y, an average value of δ for use in Equation (40) may be defined as:

$$\delta_{ave} = \frac{2}{3} \left(\delta\right)_{y\,=\,d/2} \tag{41}$$

Making use of the foregoing assumptions and Equations (39) - (41), mass transfer coefficients for oxygen and hydrogen in a helium boundary layer may be computed. These results, combined with those from Equations (37) and (38) are shown in Table 6.

TABLE 6

SURFACE HEAT AND MASS TRANSFER WHEN BOUNDARY LAYER FLOW SWEEPS LIQUID SURFACE

L, ft	d, ft	h $\left(\frac{\text{Btu}}{\text{hr-ft}^2\,^\circ\text{F hr}}\right)$		kg $\left(\frac{\text{lb mole}}{\text{sec-ft}^2\text{-atm}}\right)$		$\dot{W}_A$ $\left(\frac{\text{lb}}{\text{sec-ft}^2 \times 10^4}\right)$	
		LH_2	LOX	LH_2	LOX	LH_2	LOX
0.5	2.0	4.44	3.12	$10. \times 10^{-5}$	3.72×10^{-5}	6.45	38.2
1.0	4.0	3.74	2.62	8.32	3.06	5.35	31.4
2.0	8.0	3.14	2.20	6.87	2.60	4.42	26.8
10	20	2.98	2.08	6.60	2.46	4.24	25.4
20	20	3.55	2.50	7.86	2.96	5.02	30.5

In Table 6, Equation (39) was used to determine the mass flux at the surface from the assumed partial pressure difference of 3.22 atm, as

$$W_A = k_g M_A \quad (3.22) \qquad (42)$$

Mass fluxes computed by the above method have, in many cases, been found to be in good agreement with both molecular diffusion calculations and experimental data. This surprising agreement will be discussed more fully in Section VI-E. To determine $\bar{h}$ and k^g for other values of L_2 and d,

$$\left(\frac{\bar{h}_1}{\bar{h}_2}\right) = \left(\frac{d_2}{d_1}\right)^{\frac{1}{2}} \left[\frac{(L2)_1}{(L2)_2}\right]^{\frac{1}{4}} = \left(\frac{kg_1}{kg_2}\right)$$

D. INLET GAS FLOW DURING PRESSURIZATION AND ITS EFFECT ON GAS MIXING

The pressurization of liquid cryogens with gas raises the problem of what effect do inlet gas diffusers have on the mixedness or turbulence in the gas phase. On one hand, if no turbulence results, then gas-liquid interactions can be treated by diffusion theory, at least in the gas phase. The other extreme occurs when large diameter inlet jets are employed and extreme turbulence is generated. In the latter case it has been too often demonstrated that when a large diameter jet is directed toward the liquid surface it is almost impossible to pressurize a liquid cryogen with its own vapor due to the high mass and heat transfer rates between gas and liquid. Even in the case of helium pressurization, gross mixing is not desirable as the helium is rapidly cooled and the cryogen is evaporated.

Unfortunately, it is very difficult to obtain a rigorous mathematical solution to the problem. The theoretical literature is immense (32) but there are only a few reliable experimental studies for the case of interest here. Our approach to the problem has been to present a rather simplified, but usually satisfactory, analysis from momentum transfer theory, although more exact treatments from vorticity transfer theory are available.(33) We also limit ourselves to the case of an axially symmetric circular turbulent jet issuing into a large gas phase which is not in bulk motion. This case seems most applicable to the usual diffuser design; treatment of circular laminar jets and laminar or turbulent plane jets are available.(34)

1. Qualitative Picture of Jet Flow

A circular jet issuing into a rest gas might be conveniently viewed as shown below.

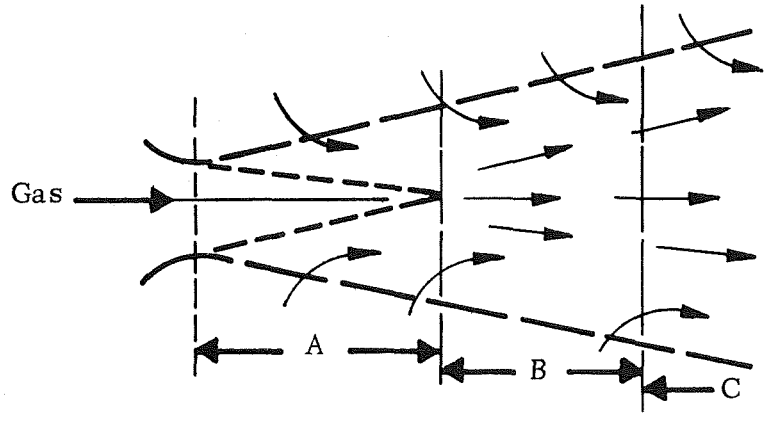

Near the inlet jet there is a core of potential flow in which the velocity is constant and equal to the inlet jet velocity. This core ends at A but between the inlet and A fluid sucked into the jet expands the boundaries; the dashed line represents the limit where the axial velocity is zero. There is mixing in the zone surrounding the potential flow core.

In region B, mixing takes place in the entire jet and the average (and center-line) velocity decreases as the jet broadens. Region B is very difficult to represent mathematically. In region C, the velocity profiles and axial gradients tend toward an asymptotic value. In this region, the classical solution of Tollmien appears valid.(35) This solution predicts that the ratio of u_z (at some radial distance r) to u_z (center-line velocity) is a unique function of (r/r^o) where r^o is the radial width (i.e., $uz/uz_{\mathbb{L}} = f(r/r^o)$.

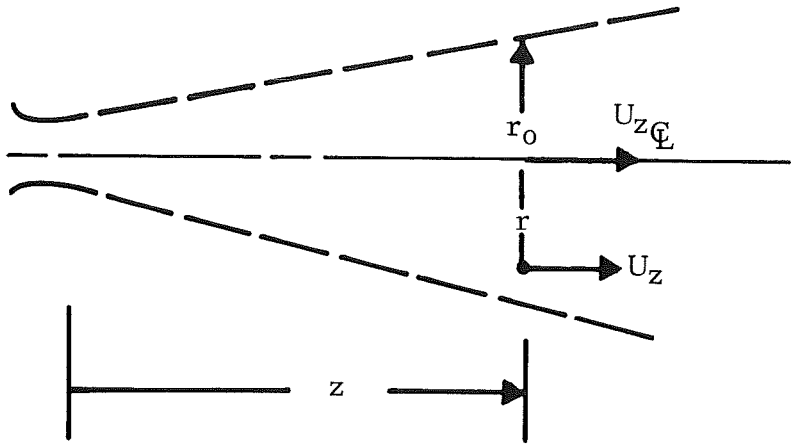

Also, it is very important to note that Tollmien's solution predicts that $u_{z_{\mathbb{C}}}$ is inversely proportional to z, thus, the center-line velocity damps out as 1/z.* We would be satisfied to determine quantitatively what the constant B would be in Equation (43),

$$u_{z\mathbb{C}} = B/z \tag{43}$$

since the penetration length of the center-line velocity into the bulk fluid would indicate, qualitatively at least, what mixing effect the jet was causing. We need one $u_{z_{\mathbb{C}}}$-z reference point to obtain the value of B. It will be shown later that B is obtained from experimental data.

---

*This proportionality may be different for different jet types, e.g., for a turbulent plane jet $u_{z\mathbb{C}} \propto 1/z^{\frac{1}{2}}$, while for a laminar circular jet $u_{z_{\mathbb{C}}} \propto 1/z$ and for a laminar plane jet $u_{z_{\mathbb{C}}} \propto 1/z^{\frac{1}{3}}$. (34)

2. Velocity Relationships for Jet

Let u_z = velocity in axial direction

u_r = velocity in radial direction

z = axial distance

r = radial distance

ℓ = Prandtl's Mixing Length

It is assumed that there is no pressure gradient parallel to the axis of flow thus the momentum of the jet plus gas entrained is constant, i.e., at any z

$$2\pi \int_0^{r^o} u_z^2 \, r \, dr = \text{const} = 2\pi E_1^2 \tag{44}$$

where r^o is the outer boundary of $u_z = 0$ and E_1 is a constant.

At a point sufficiently far from the jet that the gradients have stabilized, then the equations of continuity and momentum may be combined to give,

$$u_z \frac{\partial u_z}{\partial z} + u_r \frac{\partial u_z}{\partial r} = \frac{1}{r} \frac{\partial}{\partial r} \left[-(1/r^2)\left(\frac{\partial u_z}{\partial r}\right)^2 \right] \tag{45}$$

This equation may be solved (33) to yield:

$$u_z = \frac{a_o}{z} f(\eta/b^{\frac{1}{3}}) \tag{46}$$

$$\eta \equiv (r/z), \; a_o = \text{const}, \; \ell^2 = bz^2$$

It can be shown that $u_{z_\ell} \alpha 1/z$ and $\ell \alpha r^o \alpha z$ and the boundary conditions give

$u_z = 0$ at $r = r^o$ so: (47)

$$r^o/Z = 3.4\, b^{\frac{1}{3}} \tag{48}$$

thus

$$u_z = \frac{a_o}{z} f(3.4\, r/r^o) \tag{49}$$

and

$$u_{z_\ell} \alpha 1/z \tag{50}$$

3. Development of Quantitative Information on Decay in Jet Center-Line Velocity

The development of Equation (49) shows that at reasonable distances downstream from the jet inlet (i.e., in Region C) that the axial velocity depends only on $1/z$ and r/r^o, where $r^o \alpha z$. Suppose that the maximum velocity, u_z at the center-line, is desired, then $(u_z)_{\mathfrak{L}} = a_o/z$ and this is the same relation as Equation (43). To get B or a_o, we need experimental data or an analysis of the region near the jet inlet. Both are provided by Kuethe.(36) In essence, Kuethe studied the velocity profiles in a small air jet at distances near the jet inlet. His theory is only approximate but appears to yield consistent checks with experiment once a single empirical constant was determined.

The work of Kuethe has shown that the net center-line velocity, in Region C, is inversely proportional to the number of jet diameters from the jet discharge. Therefore, the ratio $(u_z/u_{z_o})_{\mathfrak{L}}$ = Constant/N_D where N_D is the number of jet diameters. On log-log paper the relationship plate a straight line with a slope of -1.

Data obtained by Kuethe in the transition region B provides a means of connecting the potential flow region, in which the center-line velocity is constant, with region C in which the slope of the center-line velocity as a function number of jet diameters is known. Kuethe's data indicates that the potential core region ends at about 1.76 jet diameters. At about 9 jet diameters, the experimental curve of center-line velocity against jet diameters, when plotted on log-log paper is approximately tangent to the -1 slope predicted by theory. The experimental point at 9 jet diameters can, therefore, serve as an anchor point for the theoretical slope of -1 which is valid for Region C. Evaluating the proportionality constant at this experimental point where $u_o = 9$ and $(u_z/u_{z_o})_{\mathfrak{L}} = 7.6$, there results the following relationship for region C.

$$(u_z/u_{z_o})_{\mathfrak{L}} = 6.85/N_D$$

Figure 17 was drawn utilizing all the available information and Kuethe's experimental data. Only the center-line velocity is shown as a fraction of the inlet velocity. The axial distance is measured in jet diameters. For example, if the inlet hole of a jet diffuser were 0.01-inch, then Figure 17 would predict that to decrease the center-line axial velocity to 1 percent of the inlet velocity, some 800 diameters or 8-inch would be required.

4. Momentum Model for Predicting Center-Line Velocity in Region C

Probably Figure 17 should be interpreted only as an approximation since we are assuming that Kuethe's empirical constants are generally applicable. One confirmation that this treatment might be general, is the fact that with the same constant one can show that the value of (dr^o/dz) from Kueth's data agrees closely with unrelated experiments quoted by Schlicting.[34] Also, it is interesting to note that the relationship shown in Figure 17 may be obtained in yet another way. Making use of the fact that the momentum of the jet is conserved, one may write Equation (44) as:

$$\pi \rho \int_o^\infty u_z^2 \cdot dr^2 = \dot{m} \tag{51}$$

where ρ = fluid density

u_z = velocity in the axial direction at some value r,z

r = radius

$\dot{m}$ = momentum flux

The limit o-∞ indicates the integration is to be carried out over the entire width of the jet. To eliminate the integral, define a profile shape factor,

$$K_2 \equiv \int_o^\infty (u_z/u_{z_\ell})^2 \, d(r/r^*)^2 \tag{52}$$

where r^* = radius where the velocity is 0.5 the center-line velocity. The value of such a definition lies in the fact that turbulent jets are "self-preserving,",i.e., they maintain their generalized profile over the entire jet length. Thus K_2 is a constant for all turbulent, circular jets and a value of 0.78 is generally accepted.[37] Combining Equations (51) and (52),

$$\pi K_2 \rho u_{z_\ell}^2 r^{*2} = \dot{m} \tag{53}$$

It may also be shown that for such jets:

$$r^* = c \tag{54}$$

where c is a non-dimensional constant and for circular turbulent jets = 0.085.[37]

Combining Equations (53) with (54):

$$\pi K_2 \rho u_{z_\ell}^2 c^2 z^2 = \dot{m} = \text{constant} \tag{55}$$

Note that Equation (55) predicts $u_{z_{\mathfrak{C}}} \propto 1/z$ as found previously. To obtain a value of $\dot{m}$ consider the jet inlet. Assume that the velocity of the jet is about u', independent of the radius across the jet nozzle, then with the radius of the jet = r', Equation (51) yields:

$$\dot{m} = \pi \rho \int_0^{r'} u'^2 \, dr^2 = \pi \rho \, r'^2 \, u_o^2 \tag{56}$$

From Equation (55),

$$\frac{u_{z_{\mathfrak{C}}}}{u'} = \frac{r'}{cz} \sqrt{1/K_2} = \frac{r'}{0.085z} \sqrt{1/.78} = \frac{1.13}{0.085} \frac{r'}{z}$$

now let z be expressed as N_D, the number of jet diameters, i.e.:

$$z = ZN_D r' \tag{57}$$

then:

$$\frac{u_{z_{\mathfrak{C}}}}{u'} = 6.8/N_D \tag{58}$$

Equation (58) indicates that the fractional decrease in center-line velocity is given by $6.8/N_D$, an equation very close to that plotted in Figure 17.

Note that the properties of the fluid are unimportant in this case where the inlet and rest gas are the same. The mixing and velocity-damping are governed almost completely by eddy viscosities rather than intrinsic viscosities and thus the turbulence phenomena are of extreme importance.

Finally, no mention of the values of u_z other than at the center-line was made. If $u_{z_{\mathfrak{C}}}$ is known, Schlicting[34] presents equations to obtain u_z at other values of r. The $u_{z_{\mathfrak{C}}}$ value is of the greatest interest as it indicates the maximum mixing effect at any value of z.

5. Practical Significance in Terms of Ullage Gas Mixing

The studies presented above indicate at downstream distances greater than about 7 jet diameters, the center-line velocity of a gas jet discharging into a stagnant gas decays inversely proportional to axial distance. This analysis by no means defines the total problem connected with the diffuser impingement, since it does not treat effects such as interference between adjacent jets and the influence of deflecting the stream with baffles. Such considerations may be very important but they are generally specific to particular designs and their general treatment would result in an extremely complex analysis. The single jet analysis does allow us to arrive at some very general conclusions with respect to diffuser jet impingement.

First of all, it appears obvious that the inlet pipe should never be directly toward the liquid surface. For almost any reasonable inlet pipe size and velocity, the velocity decay of a single jet is much too slow to decelerate the flow before it reaches the liquid surface. Therefore, it appears that it is always advisable to direct the inlet gas against a baffle plate of some type. Should conditions require that the entry flow be pointed toward the liquid, then the diffuser flow should be split up into a number of small jets. Also, the diffuser should be designed that, insofar as practical, the inlet flow is evenly distributed over the tank cross-section area.

In order to obtain some specific values of jet surface velocities using the single jet analysis, we have considered the case of a 6-inch inlet pipe with a flow velocity of 100 ft per second discharging against a baffle plate positioned at 1, 2, or 5 inches in front of the inlet of the pipe. We have considered both a simple baffle arrangement, in which the side-wise flow discharge is unimpeded (and in which we consider the baffle separation distance to approximate the jet diameter), and also a porous pipe arrangement in which the side-wise flow passes through a screen having a 50 percent open area and a pore diameter of .01 inch. We have considered a distance of 10 inches between discharge and liquid surface to be typical of initial pressurization, and a distance of 100 inches to be typical for transfer. The resulting velocities approaching the liquid surface are tabulated in Table 7.

TABLE 7

ESTIMATES OF DIFFUSER JET VELOCITIES APPROACHING LIQUID SURFACE

Opening	Baffle Separation (inches)	Velocity Approaching Surface ft/sec	
		Initial Pressurization	Expulsion
Free	1	102	7
	2	75	9
	5	30	7
Screen, 50% Open and .01 in. pores	1	2.4	.3
	2	1.2	.15
	5	.48	.06

The surface velocities tabulated above are rough approximations. The neglect of the velocity loss which will be associated with turning the flow from a horizontal to a vertical direction results in the calculated surface velocity, being higher than the actual velocity. However, these numbers do give a rough indication of the range of velocities approaching the surface. We would generally expect jet velocity velocities substantially in excess of about a tenth-of-a-foot-per-second to be high enough to cause substantial mixing. The value of .1 -foot-per-second is chosen as being typical of the average gas velocity which might exist if the pressure and gas flow were distributed uniformly throughout the total tank cross-section area--and is roughly comparable to the liquid level velocities which might be expected during transfer. Using a jet velocity of a tenth-of-a-foot-per-second as a criterion for mixing, we would expect that substantial mixing would occur during initial pressurization even with careful diffuser design. During expulsion it would appear that mixing might be minimized by careful diffuser design, but unless care is taken to minimize diffuser jet velocities, mixing might also be a problem during expulsion. As a general rule of thumb, we feel it may be reasonable to adopt the philosophy that during initial pressurization complete mixing will occur in the ullage. However, during expulsion, mixing due to jet impingement will be unimportant.

E. EXPERIMENTAL DATA ON INTERFACIAL MASS TRANSFER

Despite the great number of experimental investigations in this area, very little reliable experimental data on interfacial mass transfer is available. Most data have been obtained by measuring the variation in the mass of ullage gas with time; thus, the amount of evaporated liquid is found by taking the difference between two large numbers. Any small errors in measuring the mass of the gas in the ullage are reflected as large errors in the final result.

Nein and Head[4] have provided one of the very few sets of data which may be used in evaluating the applicability of the molecular diffusion model. Their data were obtained from tests using helium at 50 psia and 460°R to pressurize a tank containing liquid nitrogen originally at one atmosphere; the results are reported as rate of evaporation versus time.

It is instructive to compare the experimental results of Nein and Head with the diffusion and convection analyses presented in this section of the report. First of all, the diffusion calculation is carried out in a manner analogous to that used in Section VI-B-4. Computations have been made for the same four cases as in previous work, but using the experimental conditions of Nein and Head. The results are presented in Table 8.

TABLE 8

NUMERICAL CALCULATION OF DIFFUSION RATES FOR NEIN AND HEAD EXPERIMENTAL CONDITIONS (GHe/LN_2, P = 50 psia, T_i = 460°R)

Case No.	y_{Ao}	$y_{A\infty}$	Φ	T_o, °R	T_{AVE}, °R	C_T $\frac{lb}{ft^3}$	D, $\frac{cm^2}{sec}$	$\dot{W}_A$ for θ = 30 sec
I and III	1.0	0	~3.3	161	236	0.0198	0.0513	25×10^{-4} $\frac{lb}{ft^2\text{-sec}}$
II	0.294	0	0.185	140	220	0.0212	0.0455	1.4×10^{-4}

Nein and Head report rates of evaporation in the range 25-35 x 10^{-4} lb/sec-ft^2 for the indicated conditions. This would seem to indicate that Cases I and III provide a fair model of the true situation, but that Case II is not very realistic.

Figure 11 may be used to estimate the penetration of the nitrogen into the ullage space. The value of $x_{Y_A=0.05}$ is the distance where $y_A - y_{A\infty}$ is only 5 percent of $(y_{Ao} - y_{A\infty})$; thus, this distance should be an excellent measure of the extent to which the vaporizing cryogen has penetrated the ullage space. Thus, the penetration distance for Y = 0.05 at 30 sec in Case I is given by:

$$x_{Y_A=0.05} \approx 3.5\sqrt{4\,(0.0513)\,(30)} = 8.7 \text{ cm} \quad 3.4 \text{ inches}$$

This result is compatible with the assumption that the penetration of the diffusing component is small compared to the dimensions of the ullage.

Similarly, Equation (42) may be used to estimate the rate of mass transfer at the surface of a helium-pressurized nitrogen tank due to the convective flow of gas over the surface. For the system of Nein and Head, Equation (42) predicts a convective mass transfer rate of 35 x 10^{-4} lb/sec-ft^2.

Mass transfer rates computed by this method are comparable to molecular diffusion rates for short time periods and, for the specific case of the Nein and Head test condition at 30 seconds, agreed fairly closely with both experimental data and molecular diffusion calculations. For longer time periods, mass transfer computed by the convective technique would be larger than that predicted by molecular diffusion.

Our conclusion from this investigation is that molecular diffusion is probably the predominant mode of the interfacial mass transfer. Even when using the most favorable assumptions, mass transfer due to convection does not appear to be substantially greater than that due to molecular diffusion.

F. INTERPRETATION OF RESULTS

Studies conducted in this section indicate that molecular diffusion appears to be a useful analytical tool for calculating interfacial mass transfer. Surface convective effects due to natural circulation of the ullage gas adjacent to the cold tank walls indicate that, as a maximum, the mass transfer by this mechanism will probably not be substantially above molecular diffusion and the fluids mechanics associated with this convection are really not well enough defined to permit a really quantitative evaluation of convective mass transfer. Unfortunately, we do not have sufficient experimental data to verify our estimates as to the relative importance of molecular diffusion and natural circulation. However, in one instance, experimental results were in approximate agreement with the diffusion quantity predicted either by molecular diffusion or by surface convection.

Convective effects due to diffuser jet impingements are strongly dependent on the particular diffuser flow rate and ullage geometry under consideration. However, for a "reasonably well-designed diffuser," fairly remote from the liquid surface, we should expect jet impingement effects to be unimportant. On the other hand, we would expect that when the diffuser is close to the surface, as is the case in initial pressurization, it would be difficult to avoid almost complete mixing of the ullage gas.

Based on our present knowledge, it appears that molecular diffusion offers the best method for calculating propellant evaporation for transfer and pressurized hold--i.e., cases in which the liquid is remote from the diffuser or the diffuser flow is either zero or very small. However, during initial pressurization, we would expect that molecular diffusion considerations are unimportant in that the ullage gas would be almost perfectly mixed by the eddies associated with the inflow pressurant gas.

Another significant facet of this work is that the propellant evaporation quantities are very small. Equivalent diffusion lengths, i.e., thicknesses of an equivalent layer of saturated vapor adjacent to the liquid surface, are generally of the order of a few inches. Therefore, in cases in which total tank height is of the order of 10 feet or more, the percentage of propellant present in the vapor will be very small.

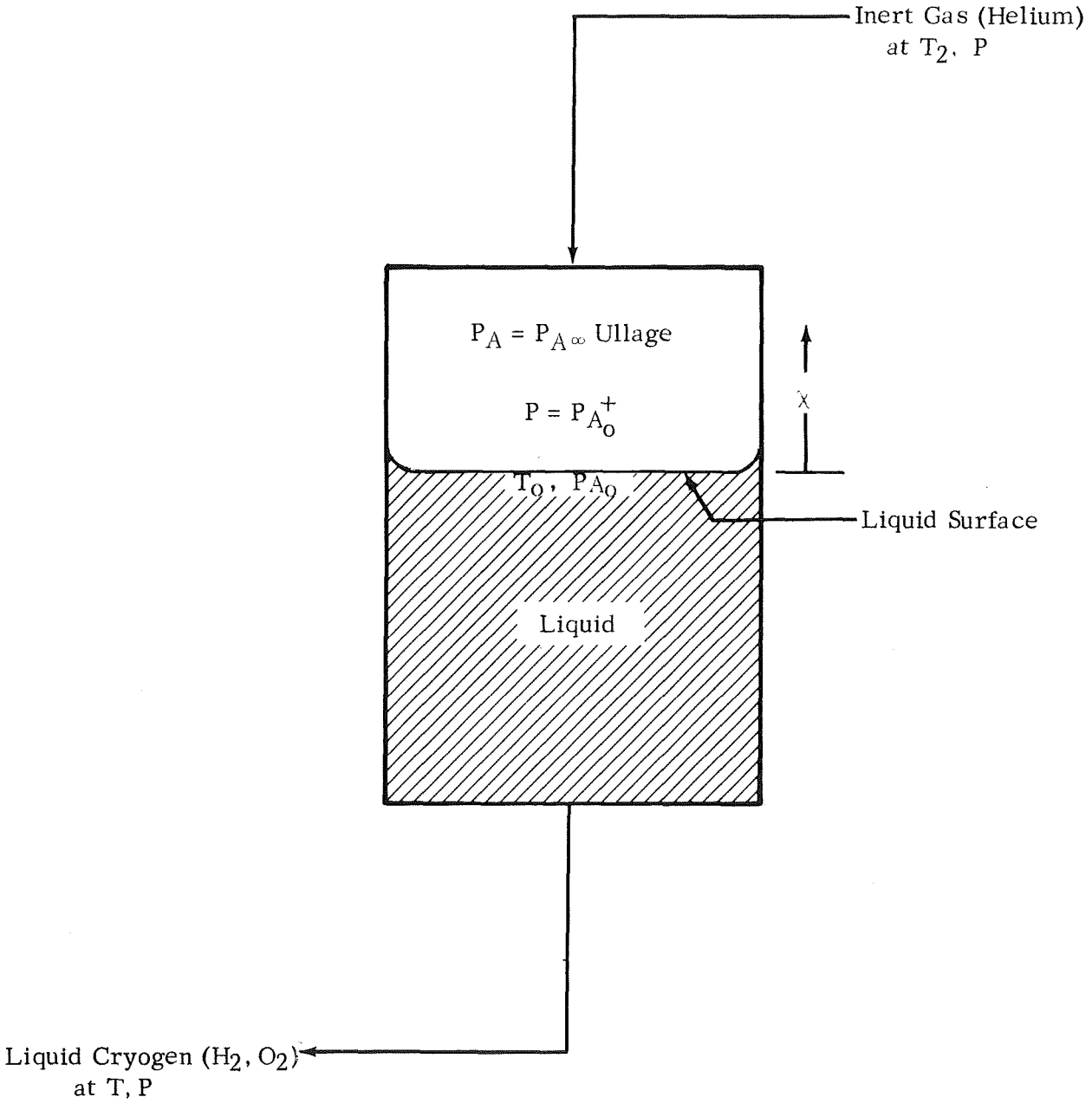

FIGURE 10 PROPELLANT TANK MODEL FOR MOLECULAR DIFFUSION ANALYSIS

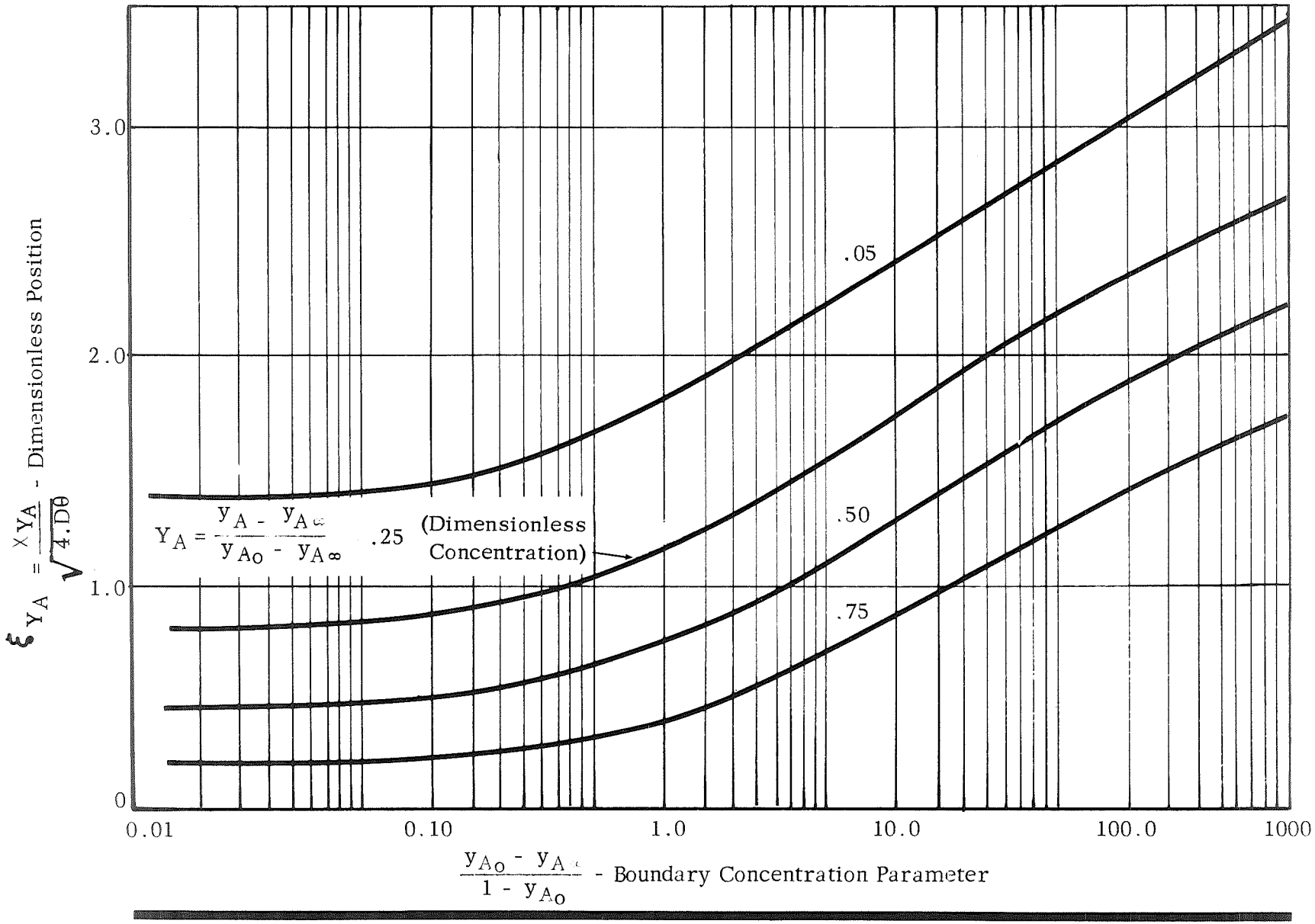

FIGURE 11 MOLECULAR DIFFUSION CONCENTRATION PROFILES

Note: $L_1\sqrt{D\theta} = \frac{W_A}{C_T M_A \sqrt{D\theta}} = 2\phi$

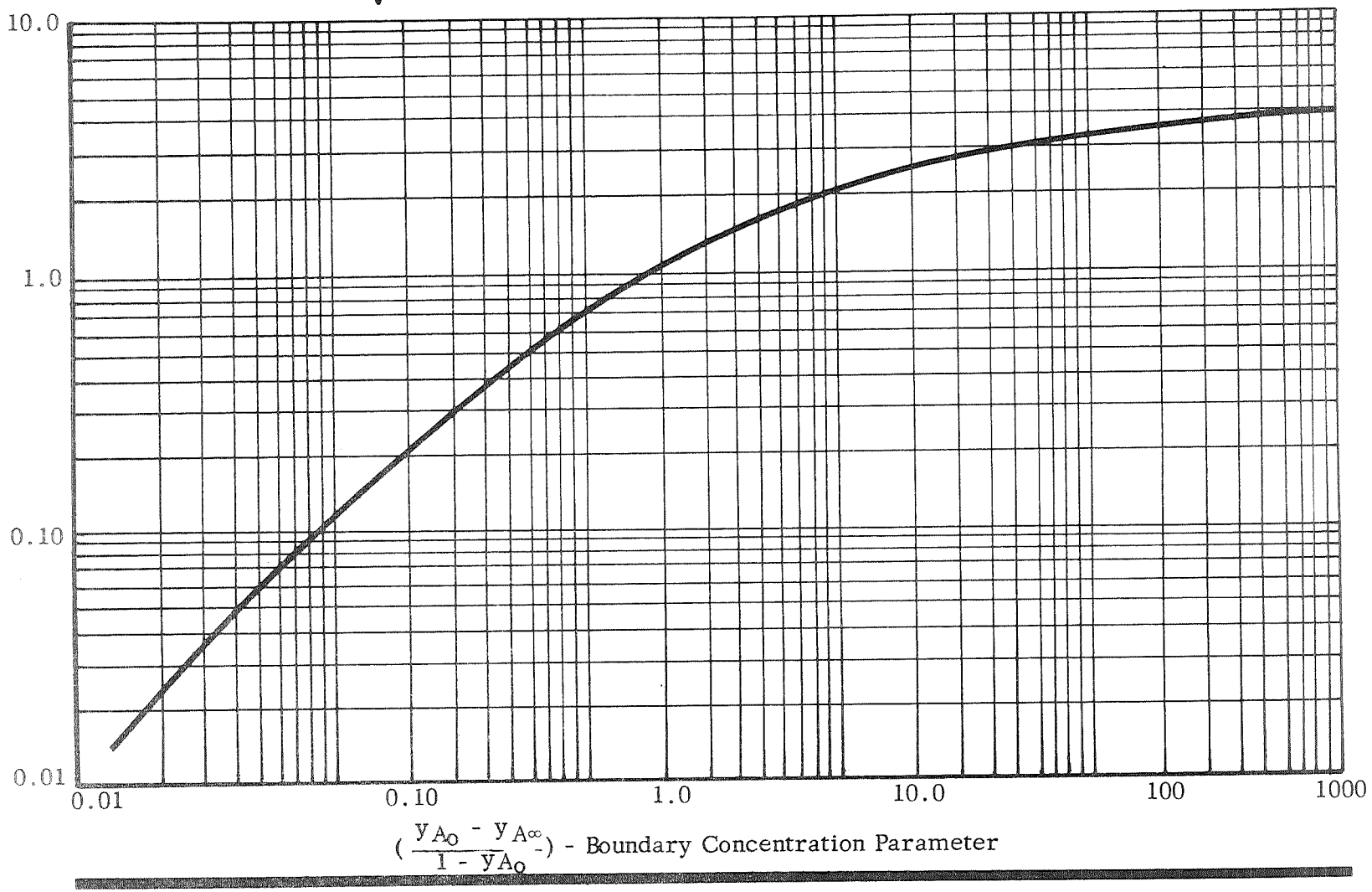

FIGURE 12 MOLECULAR DIFFUSION EVAPORATION QUANTITIES

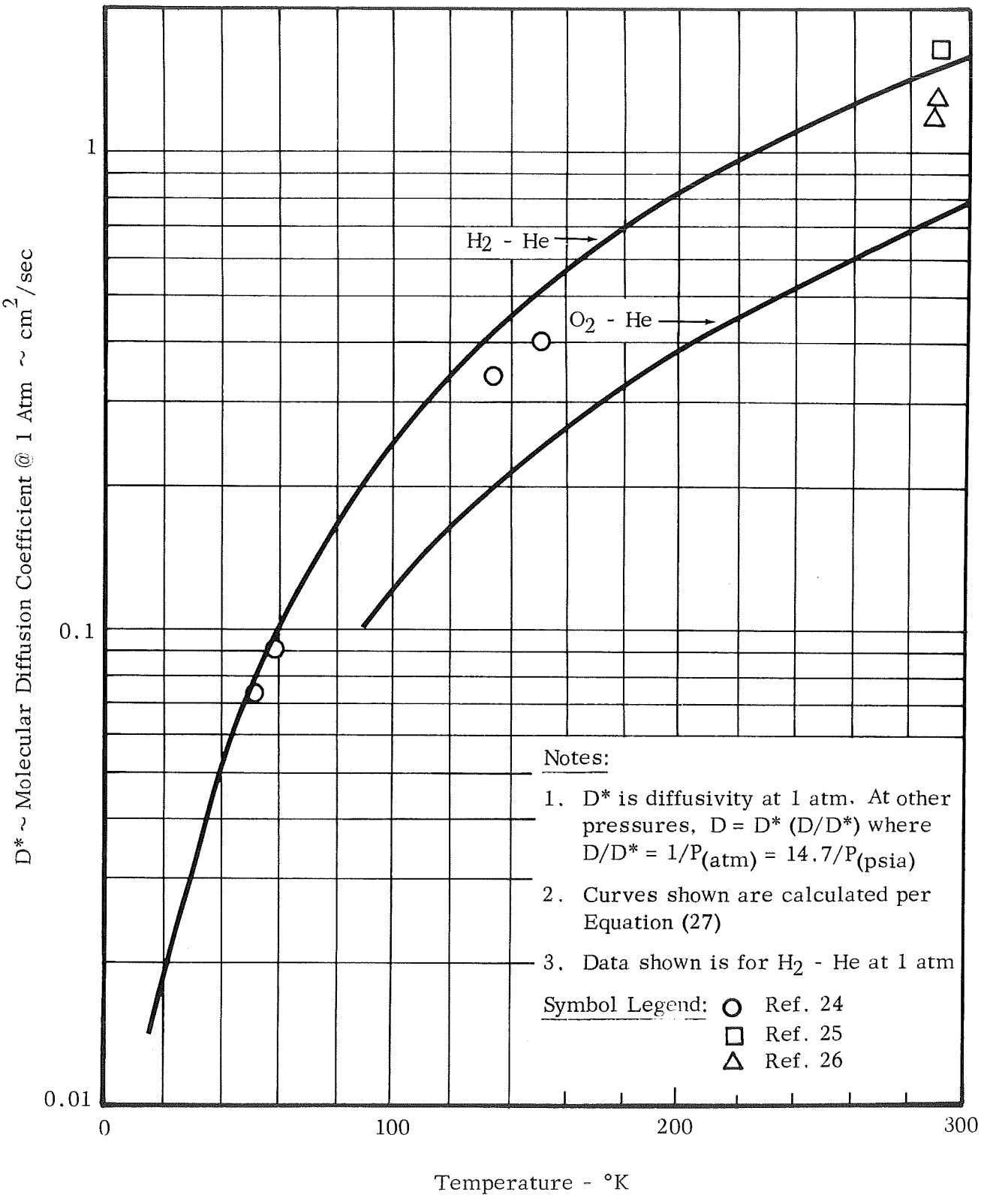

FIGURE 13 DIFFUSION COEFFICIENTS FOR HYDROGEN-HELIUM & OXYGEN-HELIUM SYSTEMS

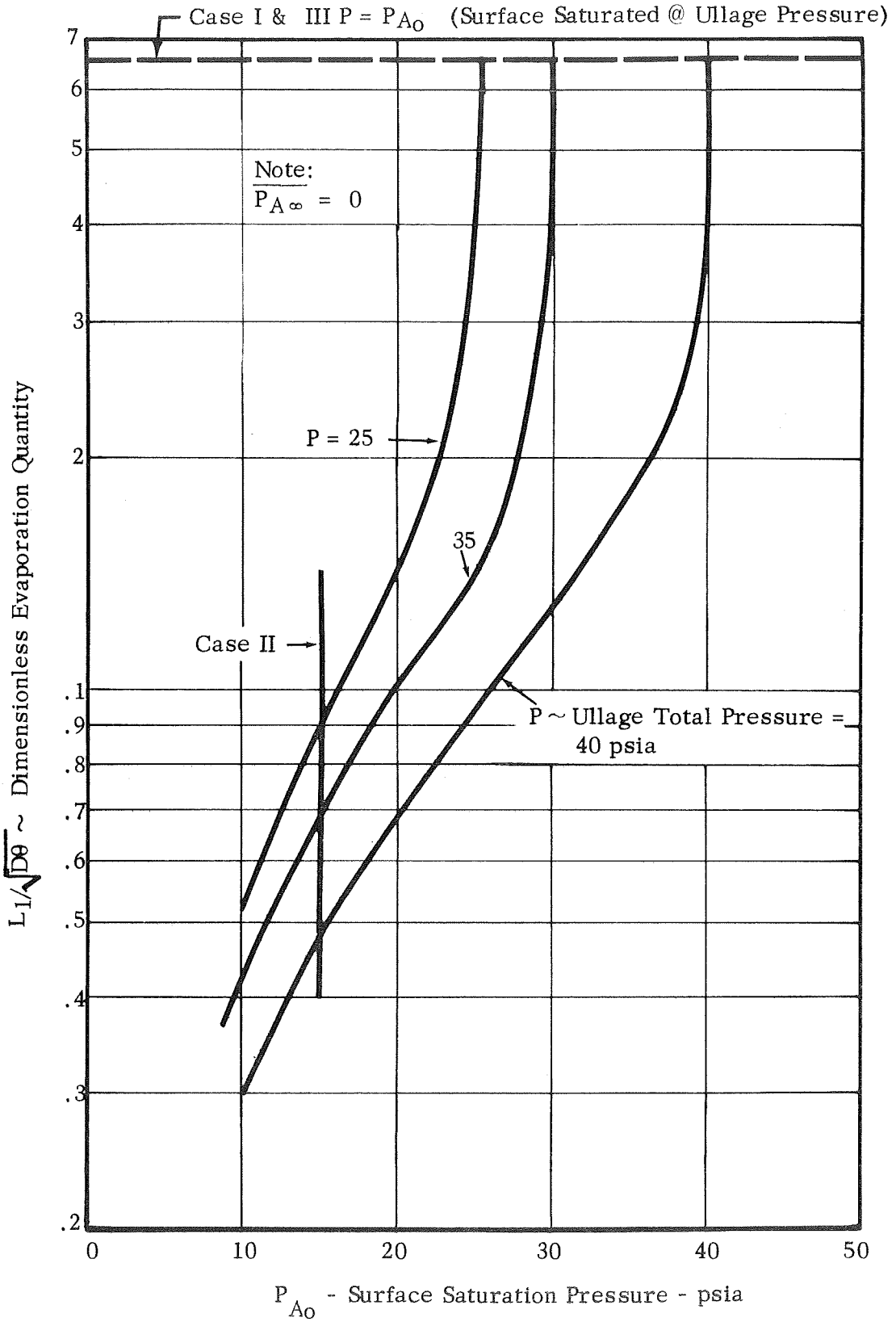

FIGURE 14 EFFECT OF LIQUID SURFACE SATURATION PRESSURE AND ULLAGE PRESSURE ON DIMENSIONLESS EVAPORATION QUANTITY

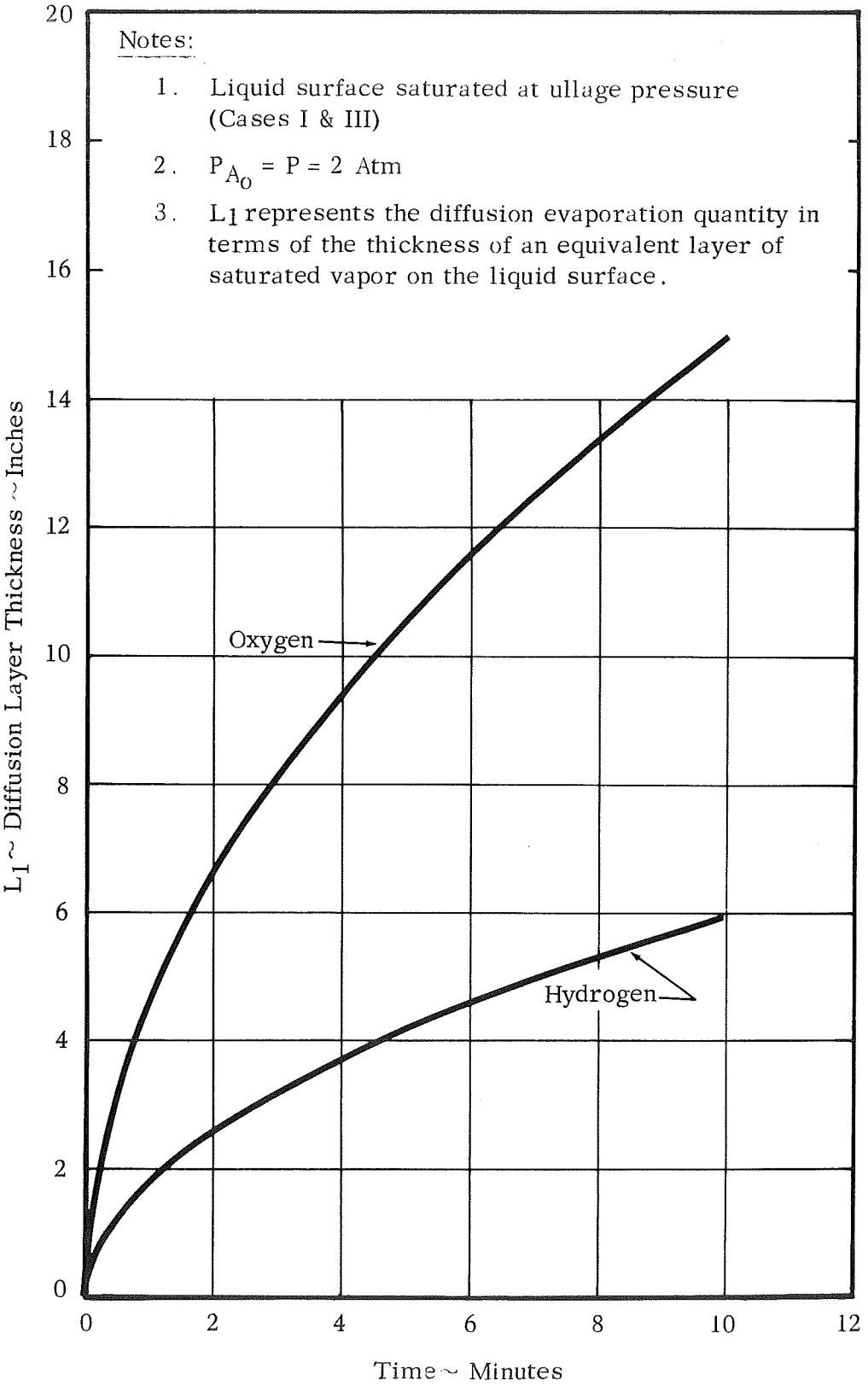

FIGURE 15 DIFFUSION LAYER THICKNESS FOR TYPICAL PROPELLANT SYSTEMS

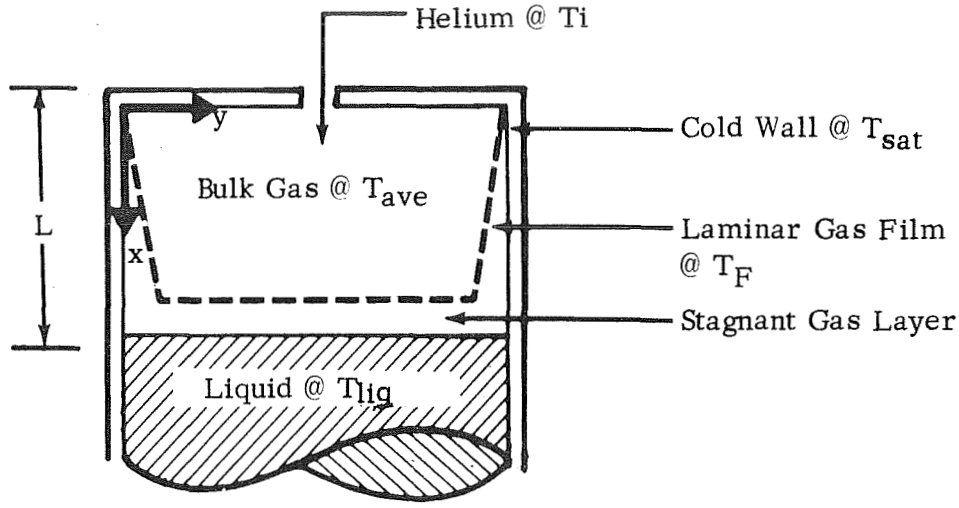

A. Basic Model Showing Downflow at Wall Resulting in Stagnant Surface Gas Layer

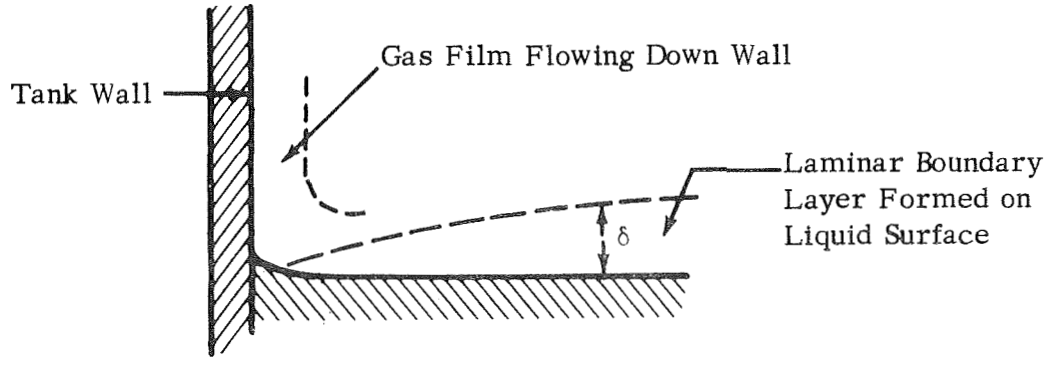

B. Alternate Model Illustrating Induced Flow Parallel to Surface

FIGURE 16 ULLAGE GAS FREE CONVECTION MODELS

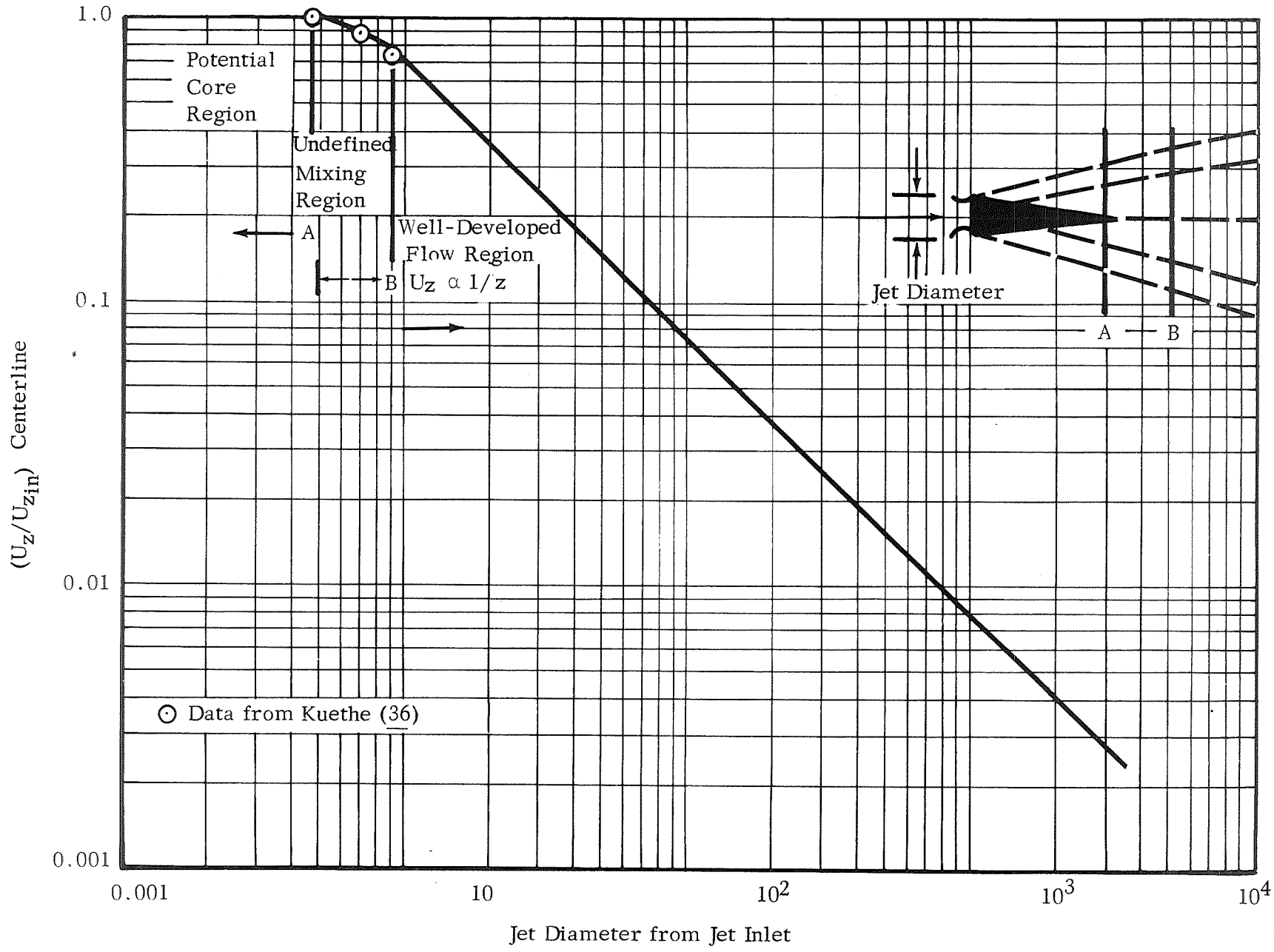

FIGURE 17 FRACTIONAL DECREASE IN JET CENTERLINE VELOCITY

VII. ESTIMATION OF LIQUID SURFACE TEMPERATURES AND FREE-BOILING EVAPORATION

A. GENERAL APPROACH

The molecular diffusion studies of the previous section have shown that liquid surface temperature is perhaps the major factor influencing the molecular diffusion process. In addition, the liquid surface temperatures and gradients in the vicinity of the surface may be extremely important in situations in which free-boiling is possible. In the general case liquid surface temperature will be the result of both the gas-liquid-surface interactions and the amount and distribution of external heat input to the liquid phase. We feel that in many cases the liquids surface temperature and gradients in the vicinity of the liquid surface can be calculated by methods which deal with the distribution of heat input to the liquid phase and which neglect the effects of gas-liquid interactions at the surface. Assuming that the surface temperature is controlled primarily by the liquid phase is a convenient viewpoint since it allows liquid surface temperatures to be calculated independent of gas-liquid interactions and also allows the use of techniques and experimental data from both self-pressurization and external pressurization tests. Therefore, we have devoted a large portion of our effort to analysis of the liquid phase. However, since there are undoubtedly some situations in which gas-liquid interactions will influence liquid surface temperature, we have devoted a portion of our analysis to a study of the liquid surface temperatures which would result from interaction between the pressure gas and the liquid.

The thermodynamic or limiting case analysis of Section V 5 examined the situation where arbitrary discrete factions of ullage gas and liquid were allowed to come into equilibrium. This analysis showed that the potential existed for the helium pressurant gas to evaporate a fairly sizable percentage of the helium propellant and to raise the liquid hydrogen surface temperature to near saturation. However, for the case of oxygen in which the volumetric specific heats and latent heats are much larger the percent of propellant evaporated was very small and the propellant liquid surface temperature did not rise substantially above saturation at one atmosphere. The thermodynamic analysis did not, of course, consider any limitation due to heat and mass transfer rates, other than that implied by the arbitrary factions of ullage gas and liquid which were assumed to come into equilibrium. In a section below we have re-examined the influence the gas-liquid interactions as limited by rates for a stagnant system in which heat transfer and mass transfer are by conduction and diffusion respectively.

A major effort has been devoted to a study of methods for predicting the effects of heat input to the liquid phase on surface temperature. These methods do not deal with gas-liquid reactions and may be considered to be most closely approximated experimentally by self-pressurizations or external pressurizations in which the ullage volume is extremely small. However, a successful solution of this type would, if necessary, be amenable to combination with gas-liquid surface effects. In addition, this type of solution is indispensable for indicating the onset in magnitude of free evaporation at the surface. In the development below we have attacked this problem by techniques primarily concerned with the boundary layer-flow at the wall of the tank and by a semi-empirical technique incorporating transient conduction analysis.

B. SURFACE TEMPERATURES RESULTING FROM GAS-LIQUID INTERACTION IN THE ABSENCE OF CONVECTION AND EXTERNAL HEAT TRANSFER

In well-insulated cryogenic tanks, ambient heat leak may be negligible both in terms of energy input to the contents and inducing natural convective mixing. Transfer by a warm, inert, pressurant gas could be accomplished without the injected gas producing appreciable convection in the ullage, if a highly effective diffuser were used. Under such conditions, since the system of a cold liquid topped by a warm gas is convectively stable, the heat and mass transfer at the liquid-gas interface would be controlled by conduction and molecular diffusion. An analysis of such processes, aimed at predicting surface temperatures, follows:

1. Analytical Model

We consider the one-dimensional, case of a semi-infinite cryogenic liquid, initially at a temperature $T_{L\infty}$, covered by an inert, warm, semi-infinite gas, initially at $T_{u\infty}$. At time zero, a separating partition at the interface is removed and transient heat transfer from the gas to the liquid and mass transfer (evaporation) from the liquid surface can commence. The situation is pictured in Figure 18.

To make the problem tractable we will make several simplifying assumptions. We will assume that all fluid properties are independent of temperature and that the liquid vapor diffusing upward from the interface does not affect the thermal properties of the gas. The vapor will absorb some sensible heat from the gas; this will be accounted for by considering that the enthalpy change to produce evaporation, is given by

$$\Delta H = \Delta H_{fg} + \frac{Cv}{2} (T_{u\infty} - T_s) \qquad (59)$$

i.e., on the average, evaporated liquid is heated to a temperature halfway between T_s and $T_{u\infty}$. When considering diffusion from the surface, we will assume the film temperature to be $T_s + T_{u\infty}/2$, and the partial pressure of fuel vapor far from the interface, $P_{v\infty}$, to be zero.

2. Analysis

A heat balance at the interface shows that

$$q_u - q_L = w \cdot \Delta H \tag{60}$$

The surface temperature, T_s, establishes the boundary condition for calculating q_u from the transient heat conduction equation for a semi-infinite slab of gas being cooled and q_L from the equation for a semi-infinite slab of liquid being warmed. Since T_s determines the fuel vapor pressure at the interface, p_g, it also establishes the boundary condition for calculation of w from the equation, for one-dimensional transient diffusion. Thus, T_s must vary in such a way that, as a boundary condition determining q_u, q_L and w, it produces a solution to equation 60. This, at first, seems to be an extremely complicated mathematical problem. Fortuitously, however, we find that the condition T_s = constant, i.e., invariant with time, produces relations for q_u, q_L and w which can satisfy (60) for a particular value of T_s. The relations for q_u, q_L and w for this condition are relatively simple, and when substituted into 60 produce an equation which can be conveniently used for estimating T_s. Thus, for T_s = constant, and considering the assumptions stated above,

$$q_u = \sqrt{\frac{\rho_u C_u k_u}{\pi \theta}} \, (T_{u\infty} - T_s) \tag{61}$$

and

$$q_L = \sqrt{\frac{\rho_L C_L k_L}{\pi \theta}} \, (T_s - T_{L\infty}) \tag{62}$$

$$w = \phi \cdot \frac{P}{R_v T} \sqrt{\frac{D}{\theta}} \tag{63}$$

where

$$\sqrt{\pi}\,(1 + \operatorname{erf}\phi)\;\phi \exp(\phi^2) = \frac{P_g - P_{v\infty}}{P - P_g} \tag{64}$$

*the derivation of equations (63) and (64) was presented in Section VI above.

and

$$P_g = f(T_s) \quad \text{(the vapor pressure relation)} \tag{65}$$

Substituting (61), (62), and (63) into (60) yields

$$\sqrt{\frac{q_u C_u k_u}{\pi \theta}}\,(T_{u\infty} - T_s) - \sqrt{\frac{q_L C_L k_L}{\pi \theta}}\,(T_s - T_{L\infty}) = \phi \cdot \frac{P}{R_v T} \sqrt{\frac{D}{\theta}} \left[H_{fg} + \frac{Cv}{2}(T_{u\infty} - T_s)\right] \tag{66}$$

The time, θ, cancels out of equation (66), showing that T would not vary with time and validating the use of relations (61), (62), and (63).

Making use of the relations

$$T = \frac{1}{2}(T_{u\infty} + T_s) \tag{67}$$

$$\rho_u = \frac{P}{R_u T_{u\infty}} \tag{68}$$

and

$$D = D_a \cdot \frac{P_a}{P} \tag{69}$$

equation (66) becomes

$$\sqrt{\frac{1}{P}\,\frac{p_L C_L k_L}{\pi D_a P_a}}\,(T_s - T_{L\infty}) + \frac{2\phi\left[H_{fg} + \frac{Cv}{2}(T_{u\infty} - T_s)\right]}{R_v (T_{u\infty} + T_s)} = \sqrt{\frac{C_u k_u}{R_u T_{u\infty} \pi D_a P_a}}\,(T_{u\infty} - T_s) \tag{70}$$

Now for given ullage pressure, p, liquid and gas properties, and specified $T_{u\infty}$ and $T_{L\infty}$, equations (64), (65), and (70) can be solved simultaneously to find T_s. We have carried out such solutions for gaseous helium

over liquid hydrogen and liquid oxygen. The liquids were assumed initially saturated at 15 psia; values for $T_{u\infty}$ = 530°R and 350°R have been considered. The results are shown in Figures 19 and 20 as plots of T_s versus ullage pressure.

3. Discussion of Results

With the analytical model considered, the surface temperature instantaneously assumes some value between $T_{u\infty}$ and $T_{L\infty}$, just after time zero, and remains steady at that value. Figure 19 shows that for liquid hydrogen, the surface temperature rises to near the saturation value corresponding to the ullage pressure. Figure 20 shows that for LO_2, the surface temperature stays considerably below saturation and, in fact, for low ullage pressures, T_s would drop below $T_{L\infty}$. (We have not done calculations for $T_s < T_{L\infty}$, but the trend is clear.) The latter behavior results from our assumption that $P_v = 0$ which apparently leads to evaporation rates large enough to depress the surface temperature. In a real transfer, where the ullage volume increases, the partial pressure of fuel vapor at some distance from the interface could be very low. Hence, with liquid oxygen, one might find cases where the surface temperature were lower than the bulk temperature.

The liquid hydrogen results imply that vapor-liquid interactions are important in determining surface temperature. This result might be anticipated from the low volumetric heat capacity and latent heat of hydrogen and is in accordance with the analysis of Section V which indicates that the helium pressurant gas had the potential for bringing the liquid hydrogen surface temperature to near saturation. Based on these results, we might assume that the liquid hydrogen surface temperature will always be near saturation -- and studies of the effects of ambient heat addition to the liquid will be primarily important for estimating free boiling evaporation. However, as will be discussed later, it is difficult to substantiate the conclusion from the limited amount of experimental data available.

The results for liquid oxygen indicate the surface temperature will be relatively unaffected by liquid-gas reactions. This result is also in accordance with the thermodynamic analysis of Section V. In liquid oxygen propellant tanks, we should expect the surface temperature to be primarily controlled by the amount and distribution of heat entering the liquid through the tank walls. This viewpoint allows the use of techniques of calculating liquid surface temperatures which are based on liquid convective and conduction effects and which do not deal with liquid-vapor interactions.

C. BOUNDARY LAYER CONSIDERATIONS

Fluid flow patterns in the liquid phase would be expected to have a strong effect on the distribution on ambient heat leak and the resulting temperature patterns in the liquid. In particular, the boundary layer flow along the tank walls which tends to deposit warm fluid at the liquid surface, might be expected to be a major factor in liquid temperature stratification. As an indication of the importance of this side wall boundary layer flow, we have computed the boundary layer flow rates and the volume of the surface thermal layer resulting from side wall boundary layer flow. In conjunction with this basic information, several techniques have been used to estimate liquid surface temperature.

1. Fluid Flow Patterns in the Liquid Phase

In a tank subjected to wall heating, an upward boundary layer flow exists along the tank walls as shown in Figure 21A. If we consider the tank liquid to be initially quiescent, i.e., no bulk convective patterns, we would expect all the heat input to the tank to be intercepted by the boundary layer and conveyed to the liquid surface. For this situation boundary layer theory specifically predicts that no heat passes through the boundary layer, and since the layer formed in the top of the tank is convectively stable, we should expect conduction and the gradual growth of the thermal layer to be the only means for conveying heat into the bulk of the liquid. Experiments conducted by NASA (38) tend to support the contention that, if the liquid is initially quiescent, boundary layer flow is confined to reach in close to the walls of the tank and does not mix with the bulk liquid. Small scale water experiments recently conducted at M.I.T. also indicate a nonmixing boundary layer.

Two factors which tend to modify the quiescent bulk liquid model mentioned above, are bottom heating and bulk convective currents resulting from free boiling at the liquid surface as indicated in Figure 22B and C. The NASA work reported in reference 38 indicates that bottom heating tends to cause a cellular column flow in the tank which effectively mixes the bulk liquid so that the bottom heat flux is uniformly distributed throughout the tank.

The role of bulk convective patterns caused by free boiling during prior tank venting is not well defined. However, it may be an important factor influencing formation of liquid temperature gradients. In a freely boiling vented tank the rising boundary layer fluid is cooled at the surface by evaporation. Cooled liquid rapidly sinks back into the bulk fluid resulting in a vigorous circulation pattern. Experience with such freely vented tanks has shown that a very prominent convection current exists. Under these conditions, it has been noted that a convectively unstable temperature pattern exists in which the temperature

increases with distance below the liquid surface. Since the free boiling convective loop and the associated reverse stratification pattern is essentially driven by the external heat input, we might expect the degree of "reverse stratification" to increase with increasing heat input and to approach saturation at local hydrostatic head as a limit. Some preliminary studies of test data obtained in prior programs, have indicated to us that such a relationship may be valid, although the data has not been complete enough to be conclusive. Since the viscosity of cryogenic liquids is extremely low, the circulation patterns set up during free boiling in a vented tank may persist for a substantial period after the vent is closed. Presumably this situation would be most acute in large tanks in which viscous damping due to wall shear would be a minimum. Unfortunately, the discussion of bulk circulation patterns set up during free boiling must remain qualitative in that we are unaware of any experimental evidence to define the magnitude of this effect.

In summary, the actual fluid mechanics in the liquid phase of a heated cryogenic tank are extremely complex. However, because of its relative simplicity, the simple boundary layer flow model which might be typical of wall heating in initially quiescent liquid, merits further consideration.

2. Calculation of Wall Bounday Layer Flow and Growth of Thermal Layer

As a first step in boundary layer analysis, it is necessary to ascertain if the boundary flow is primarily laminar or turbulent. The transition from laminar to turbulent flow in a convective boundary layer is generally found to occur when the Grashoef number exceeds 10^9. Base values of the Grashoef number applicable to heights of one foot and a wall liquid temperature differential of one degree Rankine are 2.5×10^{10} for oxygen saturated at one atmosphere; and 5.2×10^{10} for hydrogen saturated at one atmosphere. It should be noted that increased saturation pressure increases the base value of the Grashoef number. Secondly, to account for actual tank height and ΔT the base value shown should be multiplied by the factor $L^3 \Delta T$, where L represents the tank height in feet and ΔT is expressed in degrees Rankine. Therefore, the results indicate that for liquid oxygen and liquid hydrogen propellant tanks in which the height is substantially greater than one foot and in which, even for low heat leaks we should expect the wall liquid ΔT to be in order of one degree or greater, we should certainly expect a turbulent boundary layer. However, as a matter of interest, it might be noted that the base value of Grashoef number for water at 540 R is 3.5×10^7. Therefore, for small tank water tests with a low wall-liquid ΔT, a laminar boundary layer might be a possibility.

Boundary flow can be calculated from an energy balance on the boundary layer making use of empirical temperature and velocity profiles given in References (14) and (39). A convenient relationship for boundary flow which is developed in Reference (14) is the following:

$$Q = \frac{4hA}{\rho_L C_L} \tag{71}$$

Where

$Q \sim$ volumetric flow

$h \sim$ heat transfer coefficient

$A \sim$ tank area

$C_L \sim$ liquid specific heat

$\rho_L \sim$ liquid density

If we note that the tank area may be written in terms of tank volume (V) and tank diameter (d) as $A = 4V/d$, then equation (71) may be rewritten as:

$$Q = \frac{16\, h\, V}{C_L \rho_L d} \tag{72}$$

Equation (72) may be interpreted in two ways for computing boundary layer flow--and the integrated quantity of liquid passing thru the boundary layer. First, we consider Q to be the total boundary layer flow and consider that this flow is constant with time. This viewpoint assumes that the fluid flowing up the walls of the tank disperses and causes no inference with the wall boundary layer. In this case the volume V in equation (72) is interpreted as total tank volume.

Secondly, we may consider Q to represent the boundary layer flow feeding a stagnant thermal layer on top of the tank which has accumulated due to subsequent boundary layer flow. In this case, the volume V in equation (72) is total tank volume minus the integrated boundary layer flow -- and the boundary layer flow feeding the thermal layer densities as the tank volume (and area) below the thermal layer decreases. It should be noted that for either case the initial boundary layer flow is the same.

a. Constant Boundary Layer Flow

If we assume the boundary layer flow to be constant at its initial value

$$Q = Q_o = \frac{16hV_o}{C_L \rho_L d}$$

or
$$Q_o/V_o = \frac{16h}{C_L \rho_L d} \qquad (73)$$

The total integrated volume passing thru the boundary layer (V_T) is now merely equal to the product $Q_o\theta$, where θ is time. Or in ratio form:

$$V_T/V_o = \left(\frac{Q_o}{V_o}\right)\theta \qquad (74)$$

b. Time Dependent Boundary Layer Flow

If we interpret Q to be the boundary layer flow feeding a thermal layer on the surface of volume V_H which has resulted from subsequent boundary layer flow, then, noting from equations (71) and (72) that Q is proportional to area and volume below the thermal layer:

$$\frac{Q}{V_o} = \frac{Q_o}{V_o}\left(1 - V_H/V_o\right) \qquad (73a)$$

Noting that $Q = dV_H/d\theta$, equation (73a) may be integrated to determine the volume of the thermal layer

$$V_H/V_o = 1 - e^{-(Q_o/V_o)\theta} \qquad (74a)$$

It is evident from the above equations that $Q_o/V_o = \frac{16h}{C_L \rho_L d}$ is a time constant which determines the rate of tank volume "turnover" thru the boundary layer. If we assume constant boundary layer flow, the turnover volume is directly proportional to time--and the ratio V_T/V_o is numerically equal to $Q_o/V_o\theta$ as shown in Equation (74). However, if we consider that the boundary layer feeds a thermal layer on the surface whose growth reduces the subsequent boundary layer flow, the turnover volume ratio V_H/V_o is related to $(Q_o/V_o)\theta$ by the exponential relationship of equation (74-A). For small values of $(Q_o/V_o)\theta$, the two results are similar since in either case, the turnover volume ratio is small and boundary layer flow is essentially equal to the initial flow. However, as $(Q_o/V_o)\theta$ approaches and exceeds unity, the solutions diverge, since, the the thermal layer concept, V_H/V_o can only approach unity as asymptote. Typical results are illustrated in Table 9 and Figure 22.

TABLE 9

BOUNDARY LAYER TURNOVER VOLUME RATIO

$\frac{Q_o}{V_o}\theta$	Turnover Volume Ratio $\frac{V_T/V_o}{(Q=Q_o)}$	Turnover Volume Ratio $\frac{V_H/V_o}{Q=Q_o(1-V_H/V_o)}$
0	0	0
.2	.2	.182
.5	.5	.394
1.0	1.0	.632
2.0	2.0	.865
5.0	5.0	.993

A word of discussion should be devoted to the wall heat transfer mechanism. The development of reference (14) is specifically derived free convection temperature velocity profiles. For this case, free convective heat transfer correlations such as that suggested in references (14) and (40) are valid. If the heat flux is high enough to cause boiling, we should expect some variations in velocity profile. However, lacking any simple alternative we have assumed that the general methods are adequate if we use the heat transfer coefficients applicable to boiling. Typical heat transfer coefficients for hydrogen and oxygen are tabulated in Table 10 below.

TABLE 10

WALL HEAT TRANSFER COEFFICIENTS FOR FREE CONVECTION AND NUCLEATE BOILING WALL HEAT TRANSFER COEFFICIENTS
(Btu/hr ft^2 °F)

Heat Flux (Btu/hr ft^2)	Hydrogen		Oxygen	
	Conv.	Boiling	Conv.	Boiling
100	48.2	--		
500	72.1	77	82.8	--
1000	85.6	147	98.5	--
5000	--	--	147.3	195

In Table 10, free convection coefficients were calculated from relationship in references (14) and (40) . Nucleate boiling was assumed to occur when the wall temperature indicated by natural convection exceeded saturation temperature. In computing wall temperatures with natural convection heat transfer coefficients, it was assumed that the bulk liquid temperature was equal to saturation at 1 atmosphere. The mean liquid saturation temperature was taken to be saturation at an ullage pressure of 35 psia plus a hydrostatic head of 20' of liquid. In the nucleate boiling regime, the correlations of reference (41) were used to determine the temperature difference between wall and saturation as a function of q/A. Next a heat transfer coefficient applicable to nucleate boiling could be computed as q/A divided by the temperature difference between wall and bulk liquid.

The heat transfer coefficient data of Table 10, together with fluid properties and tank diameter allow for the calculation of the value turnover time constant Q_o/V_o . Typical results for the time constant Q_o/V_o are presented below for oxygen and hydrogen for a tank diameter of 20'. In these calculations, for generality, we have free convective coefficients. The use of nucleate boiling would increase volumetric turnover values shown.

TABLE 11

EFFECT OF HEAT FLUX ON INITIAL VOLUMETRIC TURNOVER DUE TO BOUNDARY LAYER FLOW

$\frac{q/A}{(Btu/hr\ ft^2)}$	$Q_o/V_o \sim \frac{\text{Initial Boundary Layer Flow}}{\text{Total Tank Volume}} - \frac{1}{min}$	
	Hydrogen	Oxygen
100	.0635	--
500	.0955	.0381
1000	.103	.0453
5000	--	.0687

The results of Table 11 and Figure 22 indicate that for heat flux ratios of interest, and a time of say 10 minutes, we would expect that, for constant boundary layer flow, we would expect turnover ratios of 60% to 100% for hydrogen and 40% to 70% for oxygen. Alternately, if we assume a time variant boundary layer flow in accordance with the thermal layer concept, the data of Table 9 and Figure 22 would indicate the thermal layer volume ratios to be in

the range of 40% to 60% for hydrogen and 25% to 50% for oxygen. In any event, the turnover volume appears to be a substantial portion of tank volume.

3. Calculation of Liquid Surface Temperature from Boundary Layer Considerations

The basic information on boundary flow and thermal layer volume can be used in a variety of ways, employing different physical models for calculating liquid surface temperature.

a. The Martin Thermal Layer Concept

The Martin thermal layer concept described in reference (14) assumes that all heat addition is absorbed by the thermal layer of volume (V_H) on the surface of the tank. Therefore, the rise in surface temperature ΔT_s can be determined by a simple energy balance on the thermal layer.

$$\Delta T_s = \frac{q\theta}{V_H \rho_L C_L} = \frac{q\theta}{V_o \rho_L C_L (V_H/V_o)} \tag{75}$$

Noting that $\frac{q\theta}{\rho_L C_L V_o}$ represents the rise in bulk temperature (Δ TB) which would result if the liquid were completely mixed, equation (75) can be rewritten as

$$\Delta T_s = \frac{\Delta T_B}{V_H/V_o} \tag{76}$$

The above equation merely states that the rise in surface temperature is in excess of the rise of bulk temperature by the fact that the thermal layer volume is less than the total tank volume. Initially, when V_H/V_o is much less than 1.0, the surface temperature rise is much greater than the bulk temperature rise. However, at long times, as V_H/V_o approaches 1, the bulk temperature tends to catch up with the surface temperature. It is interesting to examine the rise in surface temperature in the region of small times, when V_H/V_o is much less than 1. For this purpose equation (75) is somewhat more convenient than equation (76). For small values of time, and small values of V_H/V_o, we note, as as illustrated in Table 9 that $V_H/V_o \approx Vt/Vo \approx Q_o/V_o\theta$. Therefore, equation (75) may be rewritten as

$$\Delta T_s \quad \theta \longrightarrow o = \frac{q}{Q_o \rho_L C_L} \tag{77}$$

It may be noted from a steady flow energy balance on the boundary layer that the right hand side of equation (77) may be interpreted as the average temperature rise of fluid flowing thru the boundary layer. Therefore, the thermal layer concept predicts a finite surface temperature rise at zero time which corresponds to the steady state average temperature rise of liquid flowing thru the boundary layer. This surface temperature rise initially has only a very minor time dependence since, referring to equation (75), the factor $\frac{\theta}{V_H/V_o}$ is almost constant at small values of time. However, as V_H/V_o approaches unity, the rate of surface temperature rise increases and tends to fair into the bulk liquid temperature rise as an asymptote.

b. Alternate Approaches

An alternate technique in calculating surface temperature rise is to assume that the boundary layer is constantly re-mixed with the bulk liquid, and that liquid surface temperature is controlled by a thin layer of hot boundary fluid flowing across the surface. By this hypothesis, the surface temperature rise (ΔT_s) is the sum of the bulk liquid temperature rise (ΔT_B) and the temperature rise of the fluid flowing thru the boundary layer (ΔT_{BL}).

$$\Delta T_s = \Delta T_B + \Delta T_{BL} \tag{78}$$

(1) If we take the boundary layer temperature rise to be the average temperature rise of the fluid flowing thru the boundary layer

$$\Delta \overline{T_{BL}} = \frac{q}{Q_o \rho_L C_L} \tag{79}$$

and noting that $\Delta T_B = q_o/V_o p_L C_L$, equations (78) and (79) can be combined to form:

$$\Delta T_s = \Delta T_B \left[1 + \frac{1}{\left(\frac{Q_o}{V_o}\right)\theta} \right] = \Delta T_B \left[1 + \frac{1}{V_T/V_o} \right] \tag{80}$$

We may note that at zero time, $\Delta T_B = 0$. and from equations (79) and (75) it is apparent that the surface temperature predicted by this approach is the same as that predicted by the Martin model. Also, for large values of dimensionless time ($Q_o/V_o)\theta > 1$) the result appears to be asymptotic to the bulk temperature rise as is the case for the Martin model. However, in the initial time range, it predicts somewhat higher temperature rises.

(2) We might also assume that the maximum boundary layer temperature is the factor of interest in controlling surface temperature. The dimensionless temperature profiles for a turbulent boundary layer indicate that $\Delta T_{BLMAX} = 4 \Delta \bar{T}_{BL}$. Therefore, following a development similar to that above, equation 80 may be rewritten as:

$$\Delta T_s = \Delta T_B \left[1 + \frac{4}{V_T/V_o} \right] \tag{81}$$

This solution has somewhat the same characteristics as that discussed in (1) above except the initial surface temperature rise is high by a factor of 4.

Comparison of these solutions with experimental data and on the transient conduction model which is discussed below is presented in Section F.

D. TRANSIENT CONDUCTION MODEL FOR COMPUTING LIQUID TEMPERATURE GRADIENTS

Liquid temperature gradients result from the distribution of heat flux entering the liquid as accomplished by the fluid-flow patterns and conduction heat transfer in the propellant tank. In the previous section, methods of computing liquid surface temperature based on boundary layer flow considerations were outlined. In the development to follow, conduction heat transfer is taken to be the primary analytical tool for computing liquid temperature gradients. In this approach, the liquid temperature gradients due to stratification are described in terms of transient conduction solution and an empirically determined heat flux ratio.

1. Analytical Model

The analytical model of heat flux distribution which is used for the analysis of stratification is shown in Figure 23. In this model, the total heat flux entering the container (q_a) is divided into two parts.

a. One portion of the heat flux, designated q_s, is assumed to enter the bulk liquid by means of conduction downward from the liquid surface.

b. The other portion of the ambient heat flux (q_b) is assumed to be uniformly distributed heat transfer to the liquid.

Although the paths of q_s and q_b are different, the total of both is assumed to be absorbed by the bulk liquid, as an increase in internal energy.

$$q_s + q_b = q_a = (d\bar{T}_L/d\theta) M_L C_L \tag{82}$$

The proposed model is exactly analogous to the case of a thin rod subject to constant uniform heating (q_b) along its cylindrical surface plus a constant heat source (q_s) at one end. In the case of a cryogenic container q_s may be thought of as the sum of the heat which reaches the surface due to direct heat transfer from the ullage space and heat which is conveyed to the surface by natural convection boundary layer flow along the tank walls. The uniformly distributed heating (q_b) may be thought of as the sum of bottom heating plus that fraction of the side wall heating which is uniformly distributed within the bulk liquid by convective currents. It is assumed that the total heat leak (q_a) and its components q_s and q_b are constants for a particular cryogenic container and do not vary with time.

By assuming that q_s is constant with time, it is possible to employ transient conduction analysis to compute the time-dependent variation of the excess surface temperature ($T_s - \overline{T}_L$). For this analysis, we consider the container and contents (including inner vessel walls and any other equilibrating members) to be equivalent to a finite slab having similar average properties. A discussion of the method of analysis and the numerical evaluation of the resulting expression for temperature gradients is given in Appendix B. The results are plotted in Figure 24. This plot presents nondimensional temperature $\frac{T - \overline{T}_L}{q_s/E}$ as a function of nondimensional time ($\alpha\theta/L^2$) and nondimensional position (x/L). The symbols used in these terms are as follows:

T_s - surface temperature - °R

$\overline{T}_L$ - integrated mean liquid temperature - °R

q_s - surface heat flux - Btu/hr ft^2

E - equilibrating potential - $\frac{kA}{L}$ Btu/hr - °R

α - thermal diffusivity - $\frac{k_L}{\rho_L c_L}$ ft^2/hr

θ - time hr

x - position below surface - ft

L - liquid height ft

In applying this analysis to a composite system consisting of liquid, container walls and equilibrating members, the equilibrating potential and thermal diffusivity are computed as follows:

The total equilibrating potential (E) is taken as the sum of equilibrating potential of the various components. For example, for a cylindrical container

of depth L and diameter d containing a liquid of thermal conductivity kL, and having walls of thickness t and conductivity k_W, the equilibrating potential would be:

$$E = E_L + E_W = \frac{k_L A_L}{L} + \frac{k_W A_W}{L} \qquad (83)$$

where A_L and A_W are the cross-section areas available for heat conduction for the liquid and tank walls, respectively. ($A_L = \pi/4d^2$; $A_W = \pi dt$). The addition of an equilibrator having a cross-sectional area A_e and conductivity k_e would increase the equilibrating potential by $E_e = k_e A_e/L$.

The net thermal diffusivity is computed by summing up thermal conductivities and heat capacitances with respect to area. In most cases of practical interest, the influence of the walls and other equilibrating members is felt only as an increase in effective thermal conductivity. That is, the areas and heat capacitances of the walls and other equilibrating members are small in comparison with that of the liquid. Therefore, the effective thermal diffusivity can generally be written as:

$$\bar{\alpha} = \alpha_L \frac{E_{total}}{E_L} \qquad (84)$$

It should be noted that the analytical results are strictly applicable only to one dimensional heat transfer in a continuous medium. This restriction first of all limits the application to those containers geometric such as a vertical cylinder which are consistent with one dimensional heat flow. Secondly, any equilibrating members are assured to have sufficient contact with the liquid to minimize temperature differences between the equilibrating and the adjacent liquid.

All terms required for the calculation of liquid temperature gradients using Figure 24 can be obtained from known propellant tank geometry and operating conditions except for the surface heat flux (q_s). The method of determining the surface heat flux will now be discussed.

2. Determination of Heat Flux Ratio from Correlation of Experimental Data

Experimental data obtained in self-pressurizing tests has been used to check the basic time-wise trend in surface temperature indicated by the transient conduction analysis and to determine experimental values of heat flux

ratio. Data used in this correlation included tests on tanks containing oxygen, nitrogen, hydrogen, and helium for fairly wide range of heat leak. The detailed discussion is presented in Appendix C. The pertinent results are summarized below.

The first step in determining empirical heat flux ratios was to calculate the term $\frac{T_s - \overline{T}_L}{q_a/E}$ as a function of dimensionless time from experimental data. It may be noted that this term is similar in form to the dimensionless temperature shown on Figure 24 except that the surface heat flux (q_s) is replaced by the total heat flux (q_a) and may be referred to as the experimental excess surface temperature. Next, the experimental dimensionless excess surface temperatures were divided by the dimensionless excess surface temperatures taken from Figure 24 for comparable values of nondimensional time. Therefore, for each test we obtain a series of values of q_s/q_a representing various nondimensionless times at which the test data was obtained. The results of this work show that the ratio q_s/q_a was essentially constant with time for a particular test, although q_s/q_a for different tests at different heat inputs varied widely. The fact that q_s/q_a was constant with time for a given test tends to verify the analytical model which assumes that a constant surface heat flux generates the temperature gradients in the liquid.

Experimental values of the heat flux ratio for various tests are plotted in Figure 25 as a function of heat flux per unit side wall area. This plot indicates that the heat flux ratios from the various tests fall reasonably close to a single correlation line. This correlation line appears to approach an asymptote of 1.0 at very low values of heat flux per unit area where all the warm liquid may be assumed to be conveyed to the surface and remain there since the convective mixing currents are relatively small. However, at higher heat fluxes the surface heat flux becomes a very small portion of the total heat flux. We may rationalize this behavior on the basis that the convective currents in the tank may be quite high and much of the liquid flowing through the surface through the boundary layer may be mixed in the bulk liquid by convective currents.

One major weakness of the transient conduction model is that it depends on an empirical correlation of surface heat flux data and we have been unable to reproduce this correlation or even fully defend the concept of a constant surface heat flux from analytical reasoning. We have, however, been able to justify in part the variation of heat flux ratio with heat flow per unit area. By assuming that the surface heat flux is proportional to the flow rate in the boundary layer around the tank wall, it is possible to derive a proportionality relating heat flux ratio (q_s/q_a) to total heat flux per unit area ($q_a/\pi dL$). This proportionality, which is discussed in more detail in Appendix C predicts a slope which

is in excellent agreement with the experimental correlation of heat flux ratios, at all except the lowest heat fluxes ($q_a/\pi dL < 5$ Btu/hr ft^2). This circumstance suggests that the correlation of heat flux ratios which at present is purely empirical might ultimately be justified from boundary layer considerations.

E. RESULTS AND COMPARISONS OF METHODS FOR PREDICTING LIQUID TEMPERATURES

In Section C and D above we have presented two basic methods for computing liquid temperatures. In Section C a basic boundary layer analytical procedure with several variations for computing surface temperature was developed. In Section D a technique based on transient conduction which computes liquid temperature gradients as well as surface temperatures was presented. At this point, it is necessary to evaluate these methods by comparison with experimental data and select a single technique for subsequent work.

Figure 26 presents a typical application of the various methods as compared with experimental data. In this instance the experimental data was obtained from self-pressurization data on a liquid hydrogen tank reported in Reference (10). Shown on this plot are curves of surface temperature rise versus time obtained from experimental data, the ADL transient conduction model, and various modifications of the boundary layer approach for calculating liquid surface temperature. These versions include the basic concept proposed by Martin in which all the ambient heat input is assumed to be absorbed by a well-mixed thermal layer at the top of the tank; an alternate concept in which the surface temperature is taken to be the arithmetic sum of the bulk liquid temperature and the average temperature rise of fluid flowing through the boundary layer; and a second modification in which the surface temperature is taken to be the arithmetic sum of the bulk liquid temperature plus the maximum temperature rise of fluid flowing through the boundary layer. The surface temperatures predicted by the modified approach using the average temperature rise in the boundary layer differ very little from those predicted by the basic Martin model. On the other hand, the surface temperatures predicted by the modified approach using the maximum temperature rise in the boundary layer are considerably greater than that predicted by the basic Martin thermal layer concept. All of the boundary layer approaches, however, have the inherent characteristic of predicting a step rise in temperature at zero time which is essentially the temperature rise of fluid flowing through the boundary layer in a rather gradual increase in surface temperature as time increases. Both the experimental data and the ADL transient conduction model show a more or less continuous increase in surface temperature with time, although the increase is more rapid near the beginning of the self-pressurization. The trend of surface temperature rise

predicted by the ADL transient conduction model is in very good agreement with the experimental data. However, in this instance the absolute values are about 50% less than those indicated by experimental data. It may be noted that this difference in absolute value results from the fact that the correlation plot was used for establishing the heat flux ratio whereas, as shown in Figure 25, the actual data point corresponding to this test was approximately 50% above the correlation plot.

In Figures 27 and 28 we have compared with ADL transient conduction model and the Martin boundary layer model for a range of heat fluxes for hydrogen and oxygen tanks. For clarity, we have plotted only the Martin boundary layer solution; however, as noted above, the modified Martin boundary layer solution assuming an average temperature rise through the boundary layer did not differ from the Martin approach substantially and referring to Figure 26 we may note that the modified boundary layer solution incorporating the maximum temperature rise in the boundary layer predicts a temperature rise about four times higher than the basic Martin solution at zero time and tends to be roughly parallel to the Martin solution thereafter.

In general, the ADL transient conduction model predicts higher surface temperature than does the Martin boundary layer model except in the region of zero time. The cross-over point beyond which the ADL solution predicts higher temperatures varies with fluid and heat leak. It appears to be of the order of 1 minute or less for liquid hydrogen; the liquid oxygen "cross-over point" appears at larger values of time and appears to be dependent upon ambient heat leak. The range is from about 2 minutes of low values of heat leak to about 7 minutes at high values of heat leak. As previously noted, the transient conduction model predicts a continuous increase in surface temperature with time whereas the boundary layer approach indicates a sudden step increase at times zero with a rather weak time dependence thereafter. In general, we feel that the shape of the transient conduction temperature versus time curve is much more representative of experimental data than that predicted by the boundary layer approach. The similarity in the temperature versus time profiles between the transient conduction model and experimental data is illustrated in Figure 26 and is also implied by the plots of q_s/q_a as a function of nondimensional time presented in Appendix C. In addition, this correspondence has been noted in many other comparisons not specifically detailed in this report. On the other hand, the boundary layer approach has been applied with some success to data obtained by Martin in reference (14). This situation has not been fully resolved. However, there is evidence to suggest that the difference may lie in the test conditions. It is our understanding that the Martin tests were initiated by simultaneous application of the pressurant gas and initiation of heating. However, in most of the other situations the tank was freely boiling, at design heat flux, prior to the initiation of the test. It is felt that in the former case, the liquid

may have been initially quiescent, in that, prior to zero time, the heat input may have been too small to set up substantial convective currents. However, in the latter case in which the tanks were freely boiling at the design heat flux, substantial convective flow may have existed; moreover, it is felt that, because of the low viscosity of cryogenic liquids, an initial convective flow pattern of this type may persist for a substantial period of time. It is our opinion that the freely venting situation at design heat flux is more representative of flight vehicle conditions than the initial quiescent liquid situation.

Figures 27 and 28 also may be used as an indication of the rate at which the liquid surface temperature achieves saturation. Temperature rises corresponding to a saturation pressure of two atmospheres are indicated on these figures. Using the ADL transient conduction model as an indication of actual temperature rise, we see that the liquid oxygen surface temperature does not approach saturation until over ten minutes even at the highest heat leak (5000 Btu/hr ft^2). Again, applying the transient conduction model to the case of liquid hydrogen indicates that the saturation is achieved in little over 2 minutes with the higher ambient heat flux and within about 8 minutes for the lower heat fluxes. Generalizing rather broadly, it appears that the liquid hydrogen surface temperature is more apt to be elevated to saturation by liquid stratification than is the case for liquid oxygen. The single most important factor, here, is that saturation pressure is a much stronger function of temperature for liquid hydrogen than for liquid oxygen.

In Figure 29 the temperature gradients predicted with the transient conduction model are compared with typical experimental data for nitrogen and hydrogen for various heat leaks and times. In general, the results are fairly encouraging in that the transient conduction model tends to predict the gradient in the immediate vicinity of the surface quite well. It should be noted that the difference in absolute values of temperature can be related to the fact that the correlation plot of Figure 25 has a tolerance of the order of $\pm 30\%$ associated with it. For most of the tests, the transient conduction model does not do very well in predicting the gradient in the bulk liquid, i.e., the liquid remote from the surface. In general, the transient conduction model indicates a much more nearly constant temperature than in fact exists. In the instance of the hydrogen data at low heat leak, the agreement between experimental and analytical gradients is striking. However, since the heat leak is much lower than our range of interest we cannot, for our present purposes, consider it to be a very significant verification of our analysis.

Based on the comparisons presented above, we feel that the ADL transient conduction model is perhaps the most useful tool, presently at our disposal, for calculating liquid temperature gradients resulting from liquid stratification. This model appears to represent the time-wise variation in

surface temperature very well and shows good agreement with the shape of the liquid temperature gradient in the immediate vicinity of the surface. On the other hand, the transient conduction model leaves something to be desired in predicting the absolute value of surface temperature (a tolerance on the excess surface temperature of ±30% is generally anticipated) and the gradients predicted in the bulk liquid remote from the surface frequently are not in agreement with the experimental data. However, on an over-all basis we feel this model is useful for the purpose of estimating surface temperature and gradients in the vicinity of the liquid surface.

F. FREE BOILING EVAPORATION

If the liquid surface temperature tends to exceed saturation, free boiling at the surface may result. In certain cases of high heat leak to the tank, the free boiling process may result in a layer of pure vapor adjacent to the liquid surface. Hence, the free boiling mechanism might produce much more vapor than can migrate into the pressure gas by diffusion. On the other hand, in cases of low heat leak, the free boiling mechanism may be insignificant or not exist at all.

We plan to use the temperature profiles generated by the transient conduction solution as a tool for computing free boiling. The approach is as follows:

1. Compute temperature profiles as the function of time using the transient conduction model with no regard for whether or not surface temperature exceeds saturation temperature.

2. For those points at which the liquid surface temperature exceeds saturation, the integrated mean temperature of the hypothetical superheated liquid layer can be computed by constructing a plot of liquid temperature versus height in the vicinity of the surface.

3. We next recognize that the superheated layer cannot in fact exist and a portion of this layer must evaporate in order to reduce the temperature of the remainder of the layer to saturation. Therefore, an energy balance is applied to the superheated layer to determine the fraction evaporated and as a matter of interest, the remaining quantity of liquid which exists as a saturated layer on the liquid surface. The energy balance for computing the fraction of the superheated layer which evaporates is as follows:

$$\epsilon_{sh} = \frac{C_L (\bar{T}_{sh} - T_{sat})}{\lambda} \qquad (85)$$

where:

ϵ_{sh} = fraction of superheated layer evaporating

C_L = liquid specific heat

$\bar{T}_{sh}$ = integrated mean temperature of superheated layer

T_{sat} = saturation temperature corresponding to ullage pressure

λ = latent heat

It is felt this procedure can be best illustrated by simple example. This example we will consider a liquid hydrogen tank having a height of 40 feet and a diameter of 20 feet subjected to an ambient heat flux of 500 Btu/hr/ft^2 °F for ten minutes. We will consider a total ullage pressure of two atmospheres. As shown in Figure 28, the surface temperature as indicated by the transient conduction model exceeds saturation at approximately 220 seconds or 3.7 minutes. At ten minutes, the surface temperature has risen to 8.4° above its initial temperature, i.e., saturation at one atmosphere, whereas saturation at two atmospheres allows a temperature rise of 4.7°.

Using the transient conduction solution of Figure 24 and the heat flux correlation of Figure 25, it is possible to compute liquid temperature gradient as a function of the distance below the liquid surface. This gradient is illustrated in Figure 30. From this figure, it can be easily determined that the thickness of the saturated layer is .025 feet and the integrated mean temperature in the saturated layer is 6.6°R above saturation at one atmosphere. Using equation (85), the fraction of the superheated layer which vaporizes can be easily computed as

$$\epsilon_{sh} = \frac{(4.4)\,(6.6 - 4.7)}{194} = 2.3\%$$

This calculation shows that only about 2% of the superheated layer evaporates and the other 98% remains as a saturated liquid layer. It may be noted that the superheated layer itself is only .025 feet deep or .0625% of the total full tank liquid quantity. Therefore, the mass fraction evaporated expressed as a percentage of total liquid quantity is only 2.3% of .0625% or .0014%.

For better physical interpretation of free boiling evaporation, it may be useful to compare it with the amount evaporated due to molecular diffusion. For this purpose, it is useful to compute free boiling evaporation in quantity in terms of the thickness of a saturated vapor layer on the liquid surface.

First of all, the percent of total tank volume occupied by the saturated vapor layer is merely the mass fraction evaporated multiplied by the ratio of liquid density divided by vapor density. In this case, the volume fraction is merely equal to .0014 (4.4/.148) or .0415%. The volume fraction for cylindrical tank is, of course, equivalent to a height fraction; therefore, the thickness of the vapor layer is .0415% of 40 feet or .2 inches. In this case, the estimated free boiling evaporation quantity is much less than what we might anticipate due to molecular diffusion. Typical results in Figure 15 indicate that we might expect equivalent thicknesses on the order of several inches for molecular diffusion. Therefore, the free boiling quantity of .2 inches is, in fact, within the accuracy limits that we might expect for the molecular diffusion calculation.

G. INTERPRETATION OF RESULTS

Our comparisons of various techniques for predicting liquid temperature gradients indicate that a transient conduction technique utilizing an empirically determined heat flux correlation is reasonably accurate for predicting surface temperature and temperature gradients in the vicinity of the surface. We currently believe that this is the most practical approach for calculating liquid surface temperatures and gradients in the vicinity of the surface which are needed for free boiling calculations.

Analysis of the adiabatic, nonconvective liquid-ullage gas system indicates that with a liquid hydrogen propellant we would expect surface temperature to be elevated to near saturation by gas liquid interactions. On the other hand, for liquid oxygen, we would expect gas liquid interactions to have virtually no effect on liquid surface temperature, and in the absence of external heat leak, we would expect the liquid oxygen surface temperature to be saturated at 1 atmosphere. Calculation of surface temperature rise due to ambient heat leak using the transient conduction model indicates that for liquid hydrogen we might expect ambient heat leak to raise surface temperature to near saturation even at lower values of heat leak within a few minutes. Therefore, for liquid hydrogen, we might generally expect the liquid surface temperature to be near saturation, and at higher heat leaks we might expect free boiling. For liquid oxygen, on the other hand, fairly substantial heat leaks and long times are required to bring the surface temperature up near saturation. Therefore, in general, we would expect the liquid oxygen surface temperature to be below saturation and that free boiling would be a factor only at the high end of the ambient heat leak range. Free boiling calculations performed for liquid hydrogen indicate that although free boiling may theoretically occur quite early in the process, the liquid temperature gradients are so steep in the immediate vicinity of the surface that the free boiling evaporation quantity is very small and is, in fact, much less than the molecular diffusion quantity for a saturated liquid surface.

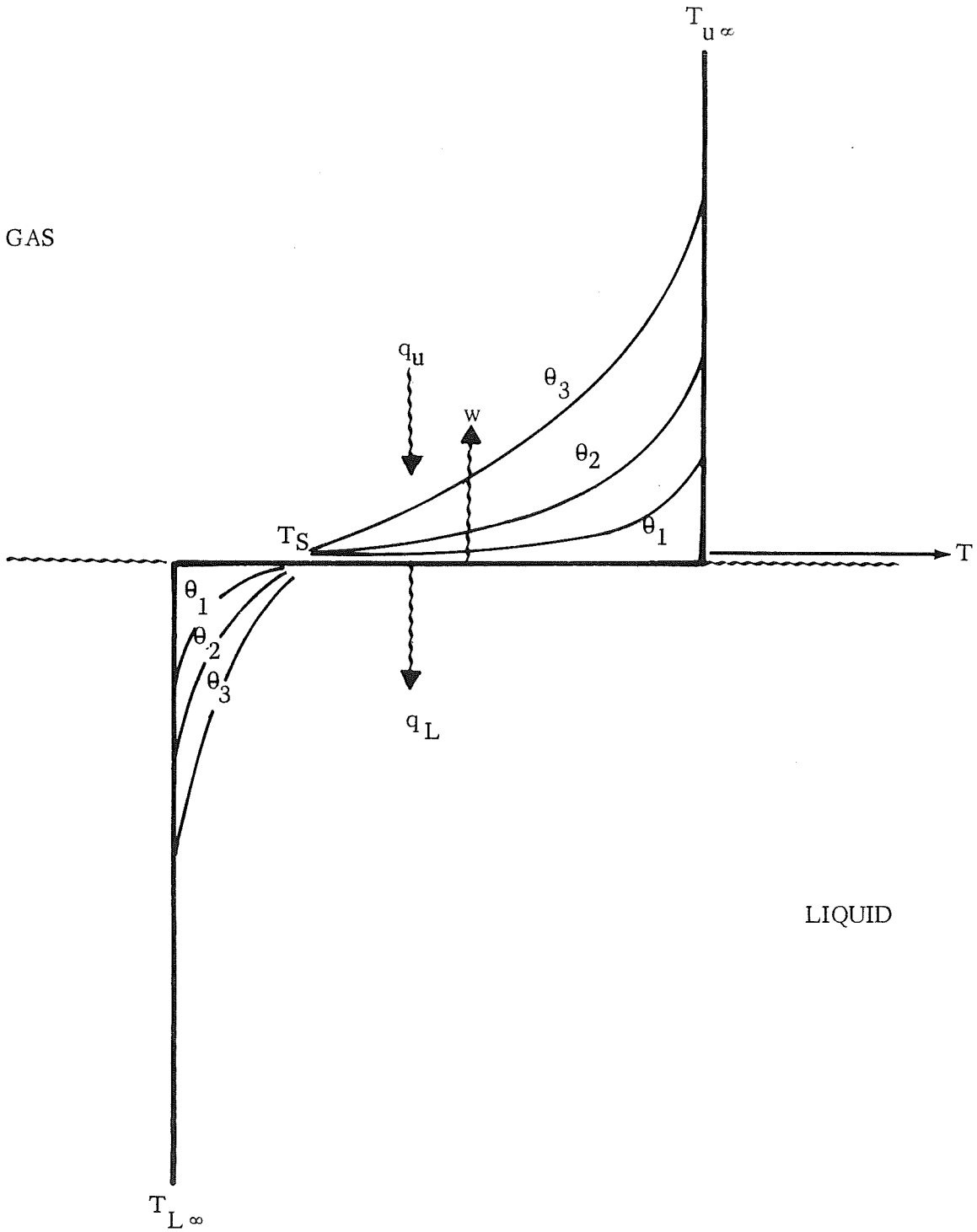

FIGURE 18 ONE-DIMENSIONAL MODEL OF STAGNANT GAS-LIQUID INTERFACE

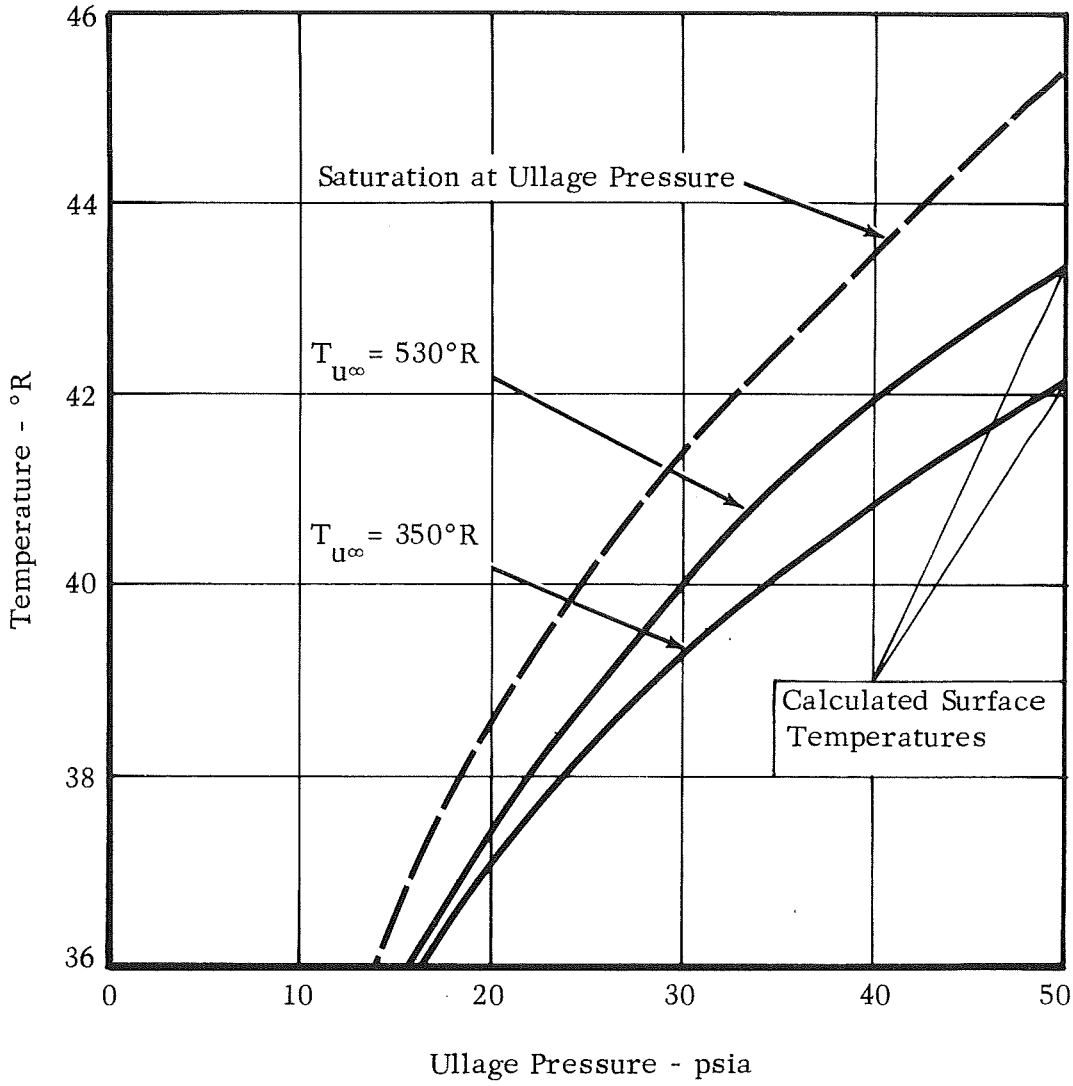

FIGURE 19 LIQUID SURFACE TEMPERATURES - GASEOUS HELIUM PRESSURIZED TRANSFER OF LIQUID HYDROGEN ONE-DIMENSIONAL MODEL, NO CONVECTION

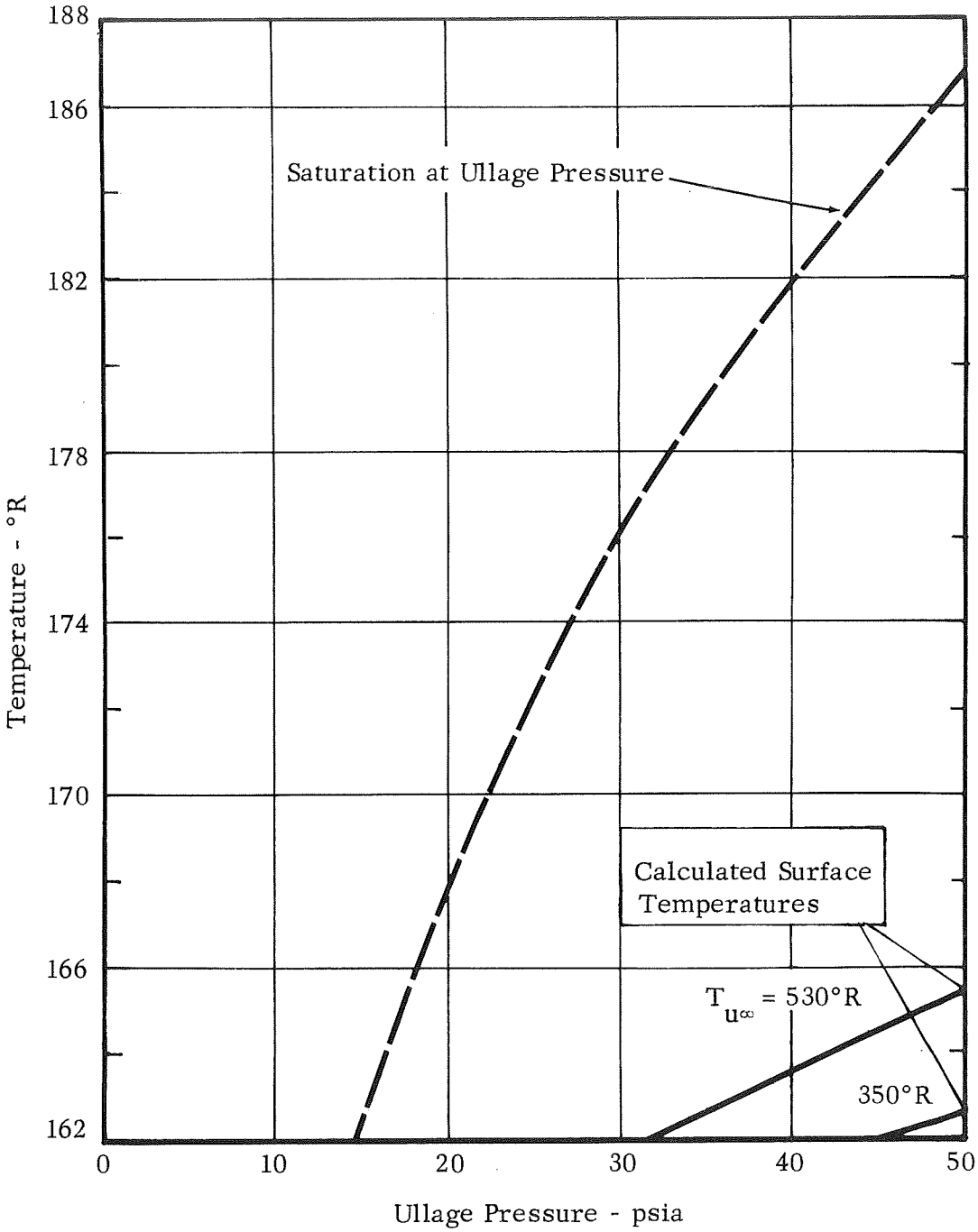

FIGURE 20 LIQUID SURFACE TEMPERATURES - GASEOUS HELIUM PRESSURIZED TRANSFER OF LIQUID OXYGEN ONE-DIMENSIONAL MODEL, NO CONVECTION

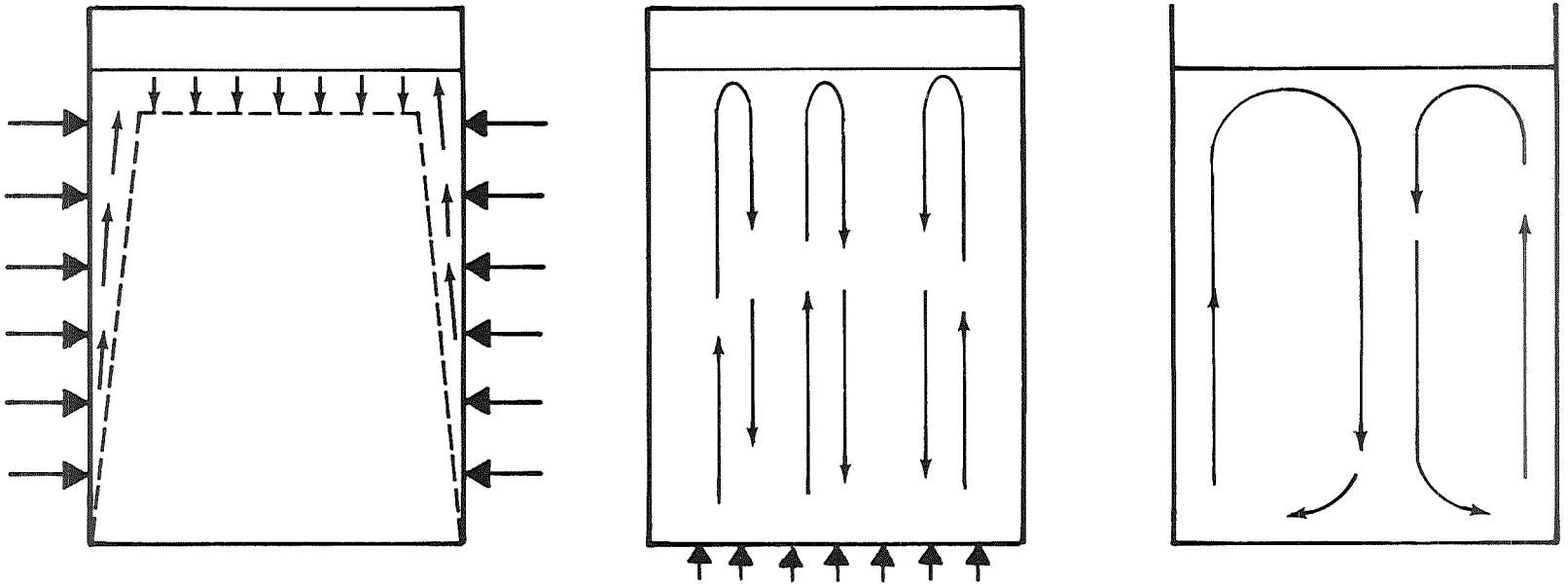

A. Wall Heating of Quiescent Liquid

B. Bottom Heating

C. Bulk Convective Flow Induced by Free Venting

FIGURE 21 LIQUID FLOW PATTERNS IN PROPELLANT TANKS

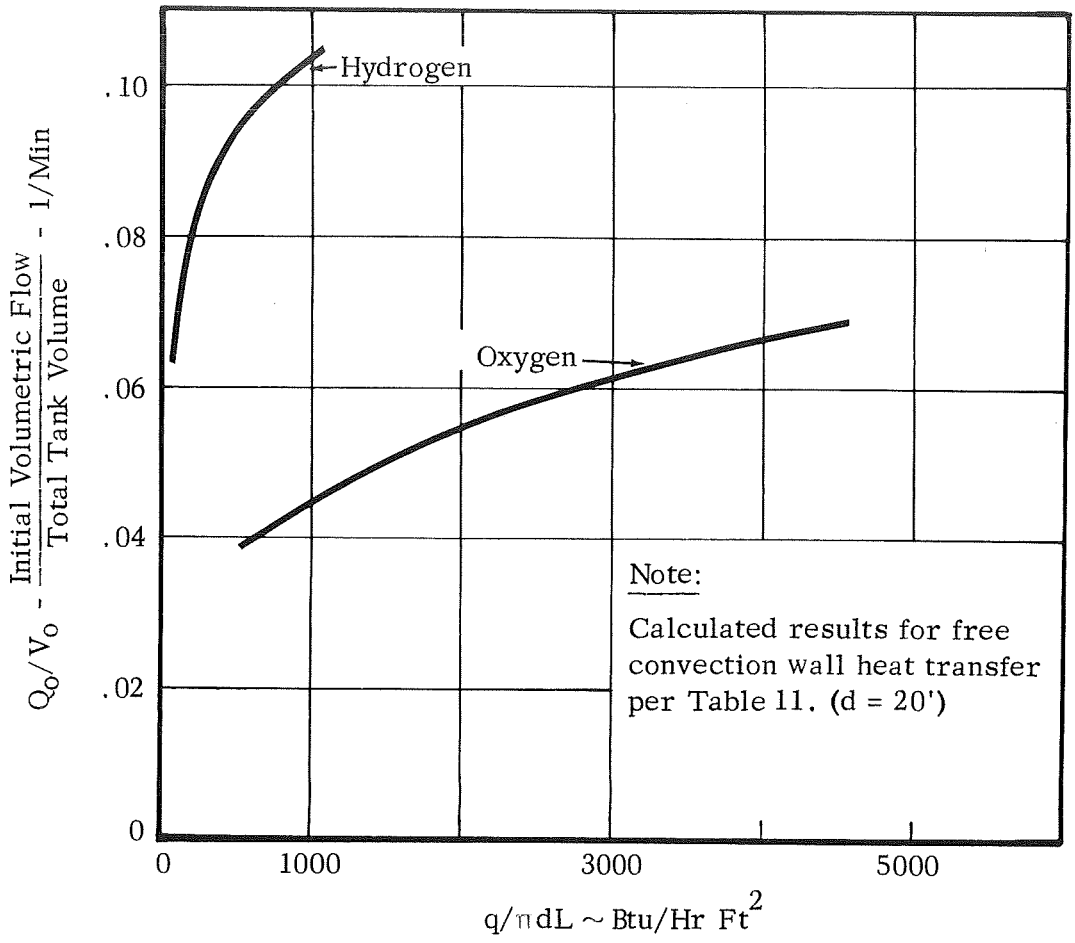

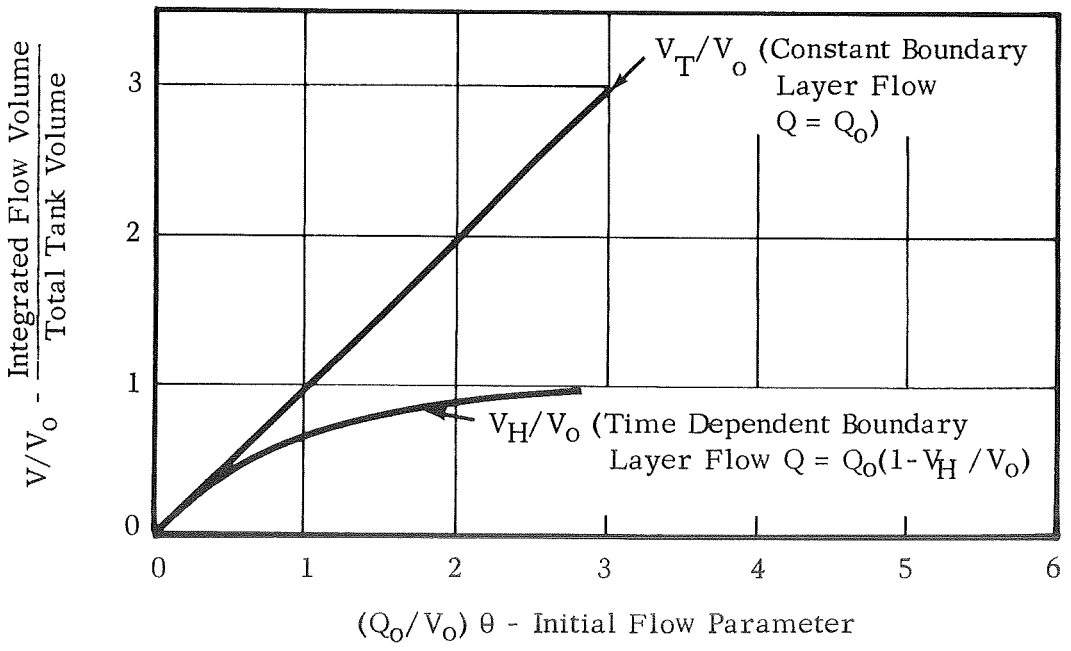

FIGURE 22 BOUNDARY LAYER FLOW RATE AND INTEGRATED FLOW VOLUME

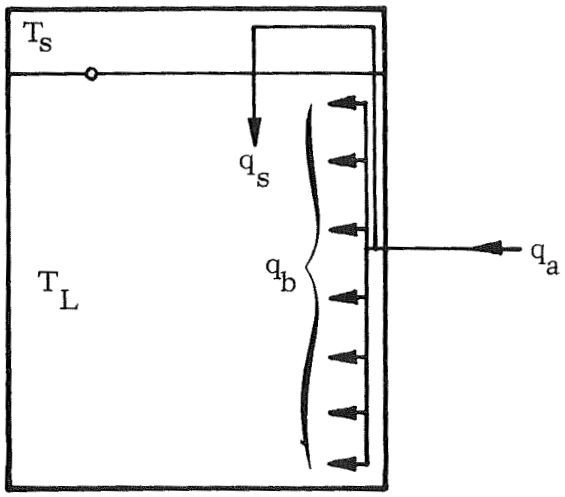

FIGURE 23 TRANSIENT CONDUCTION MODEL OF PROPELLANT TANK LIQUID

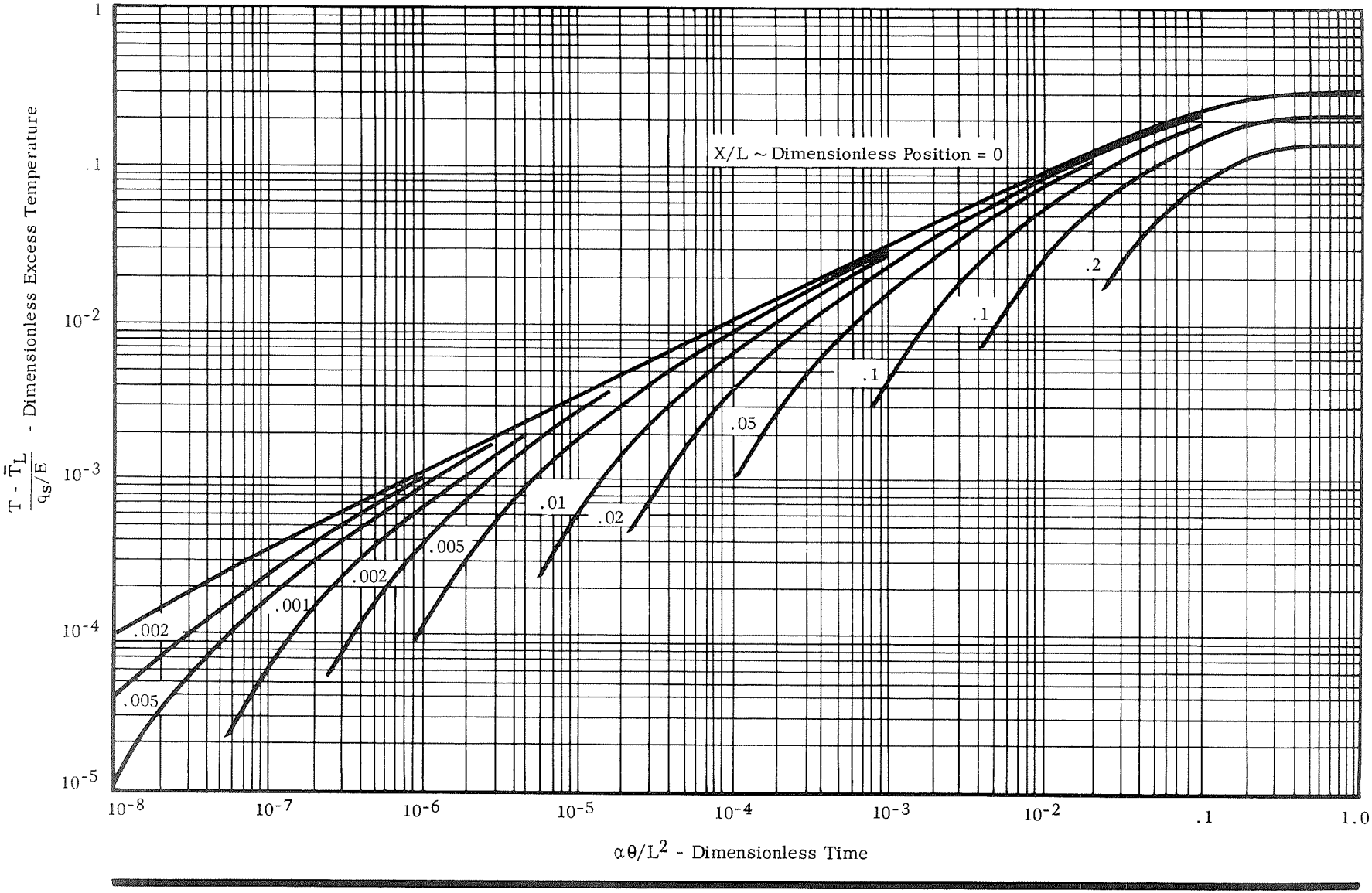

FIGURE 24 TRANSIENT CONDUCTION TEMPERATURE PROFILES IN A FINITE SLAB WITH CONSTANT SURFACE HEATING (Significant Positive Values for $10^{-8} < \alpha\theta/L^2 < 1.0$)

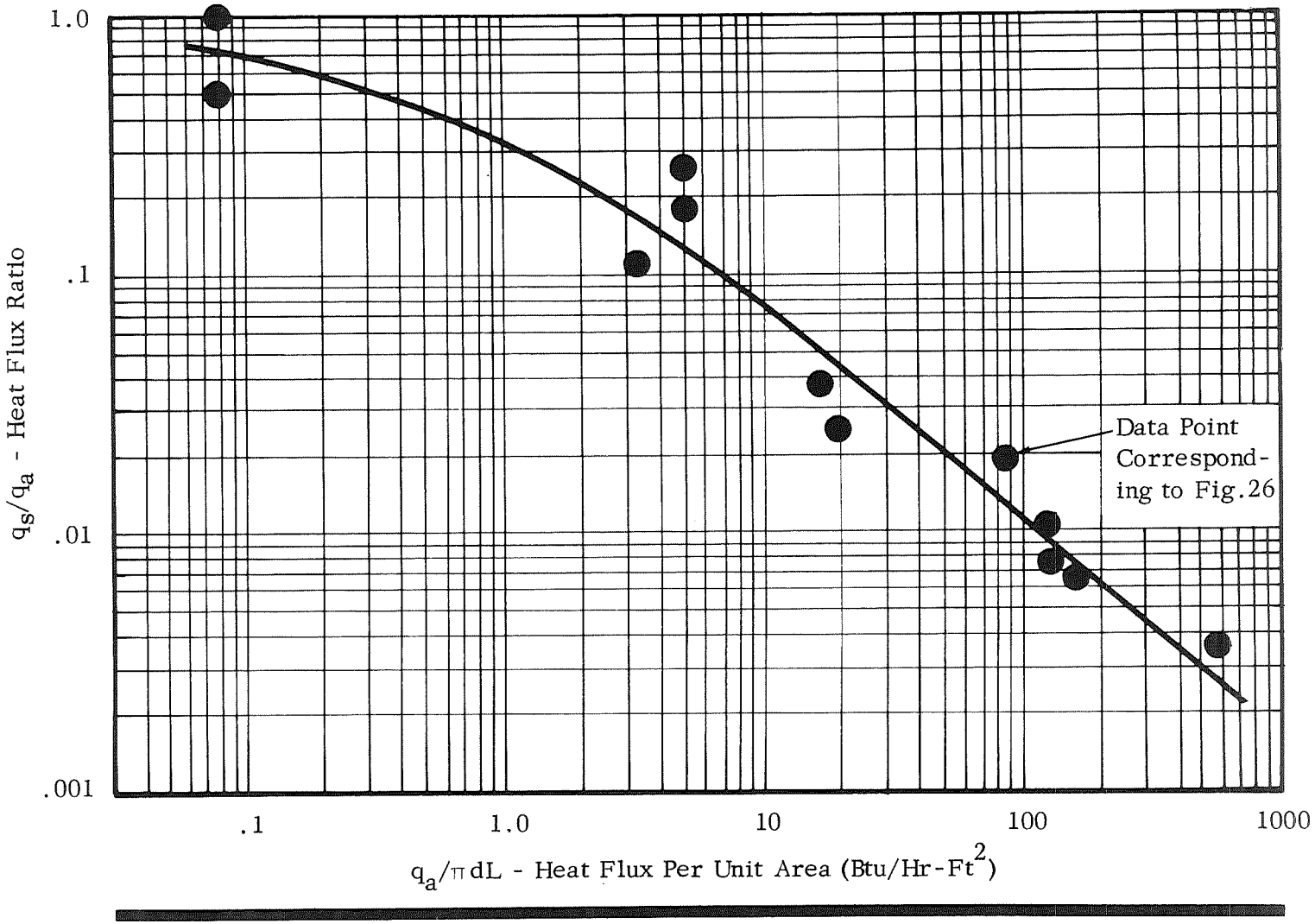

FIGURE 25 CORRELATION OF EXPERIMENTAL HEAT FLUX RATIOS

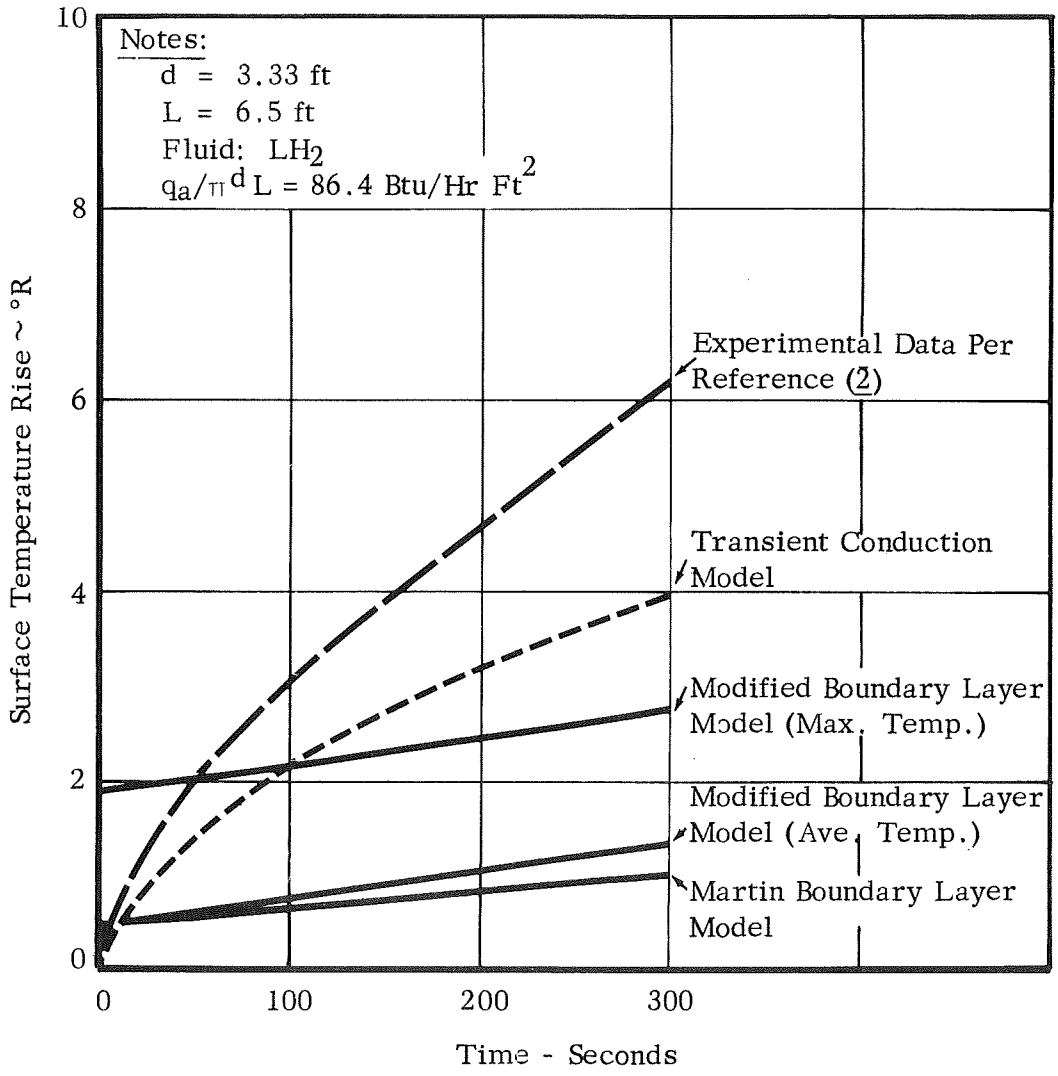

FIGURE 26 COMPARISON OF EXPERIMENTAL SURFACE TEMPERATURE INCREASE WITH ANALYTICAL RESULTS

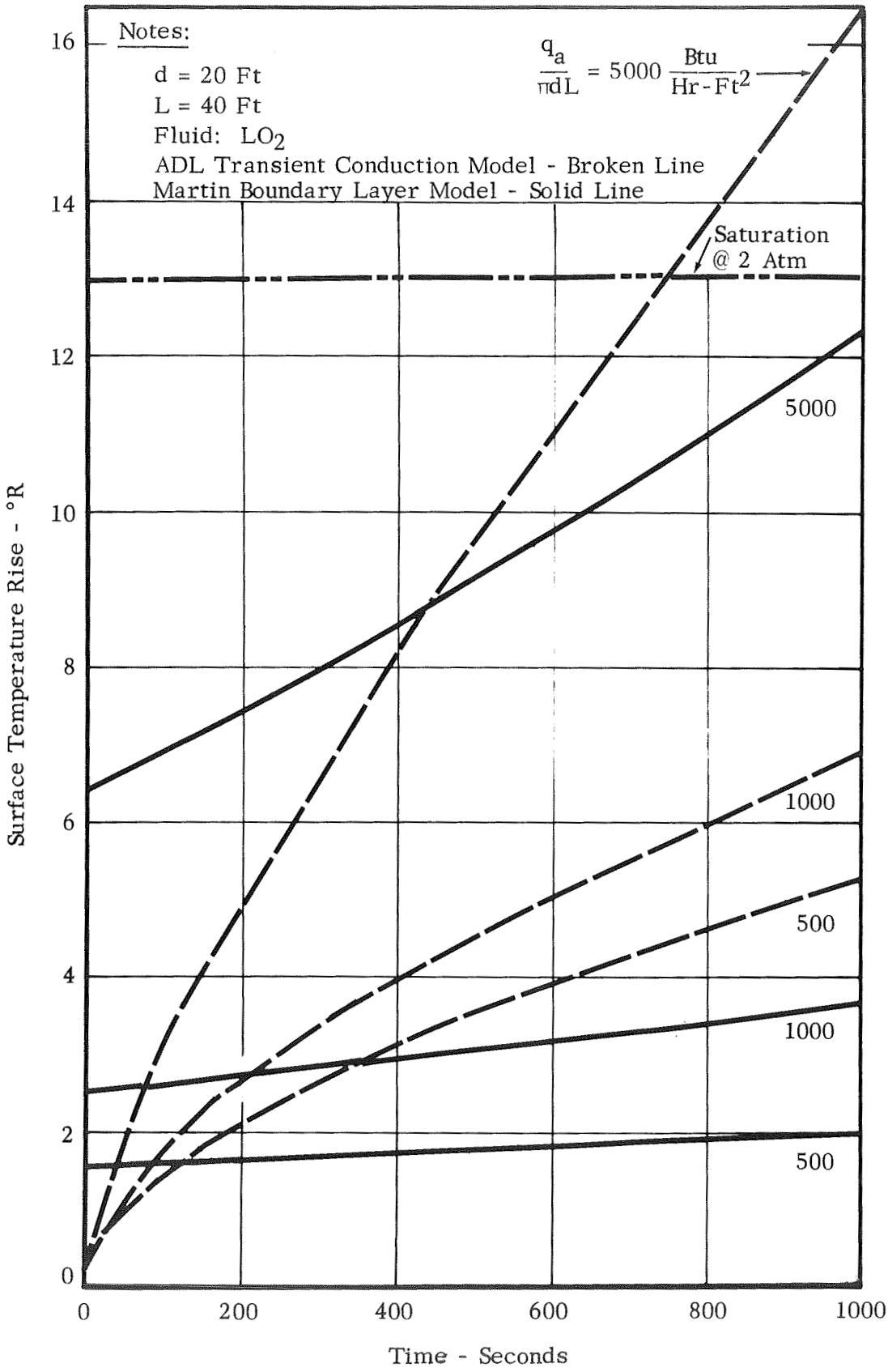

FIGURE 27 LIQUID OXYGEN SURFACE TEMPERATURE INCREASE PREDICTED BY ANALYTICAL MODEL

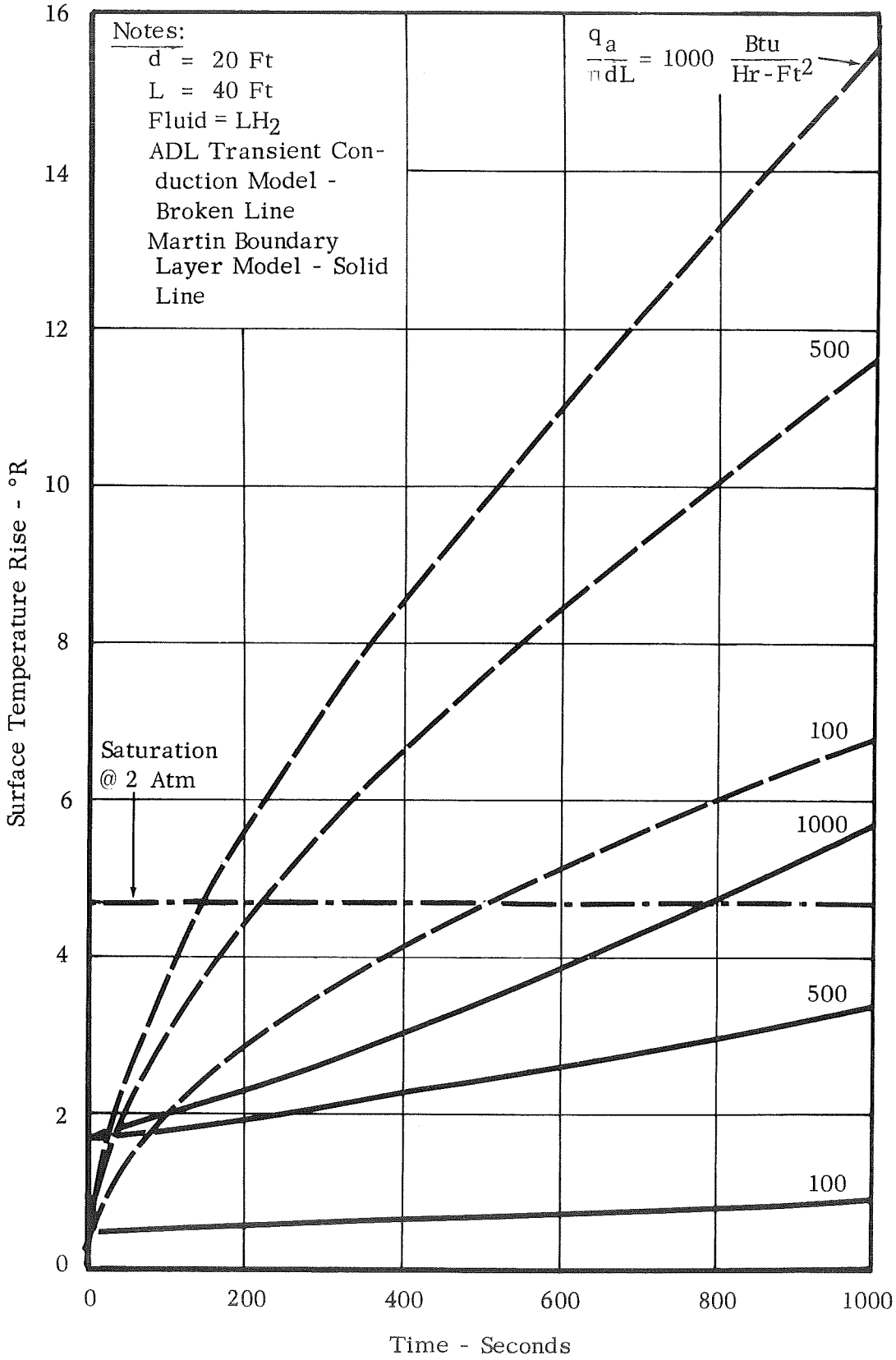

FIGURE 28 LIQUID HYDROGEN SURFACE TEMPERATURE INCREASE PREDICTED BY ANALYTICAL MODELS

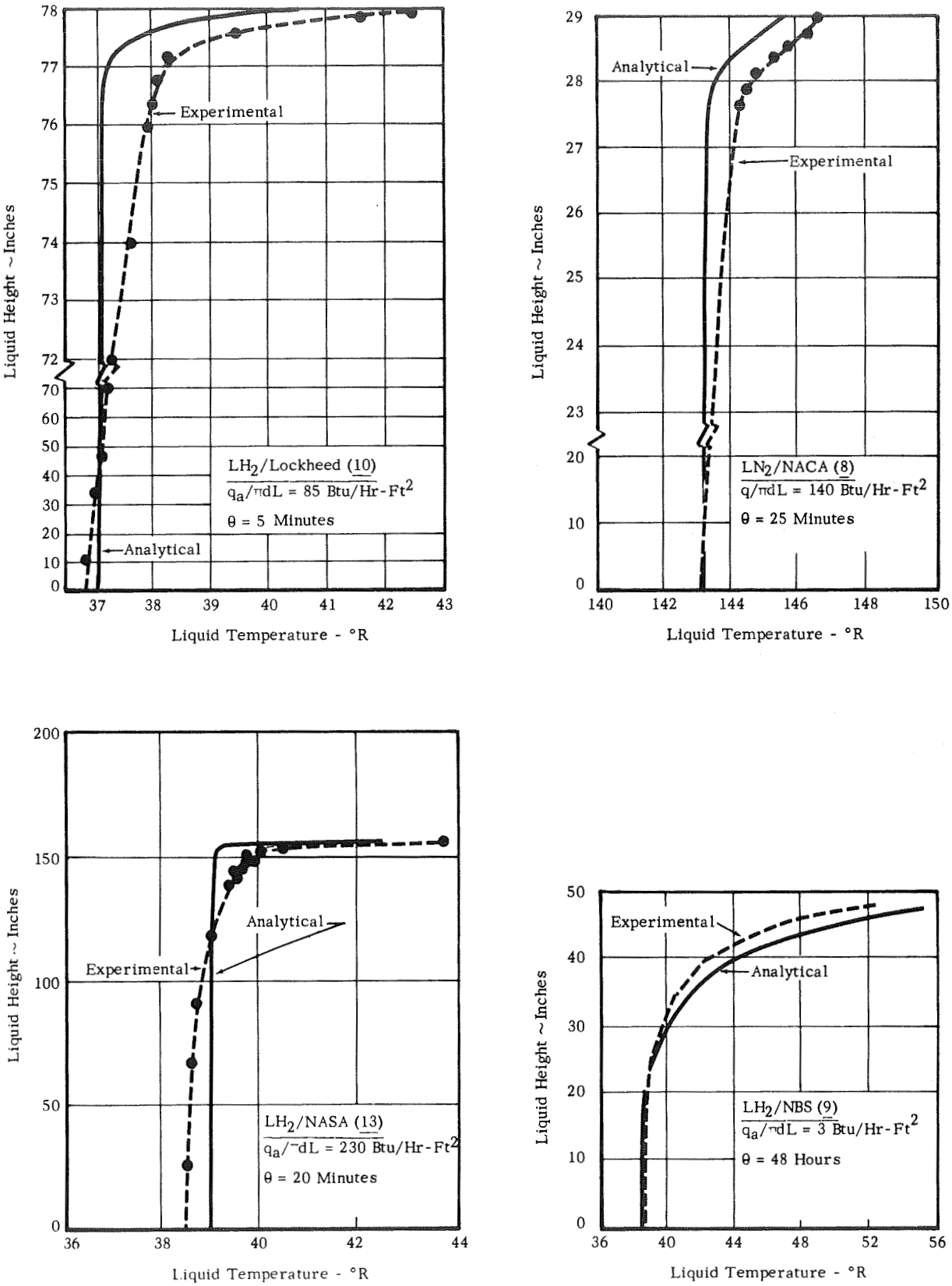

FIGURE 29 COMPARISON OF TEMPERATURE PROFILES PREDICTED BY TRANSIENT CONDUCTION MODEL WITH EXPERIMENTAL RESULTS

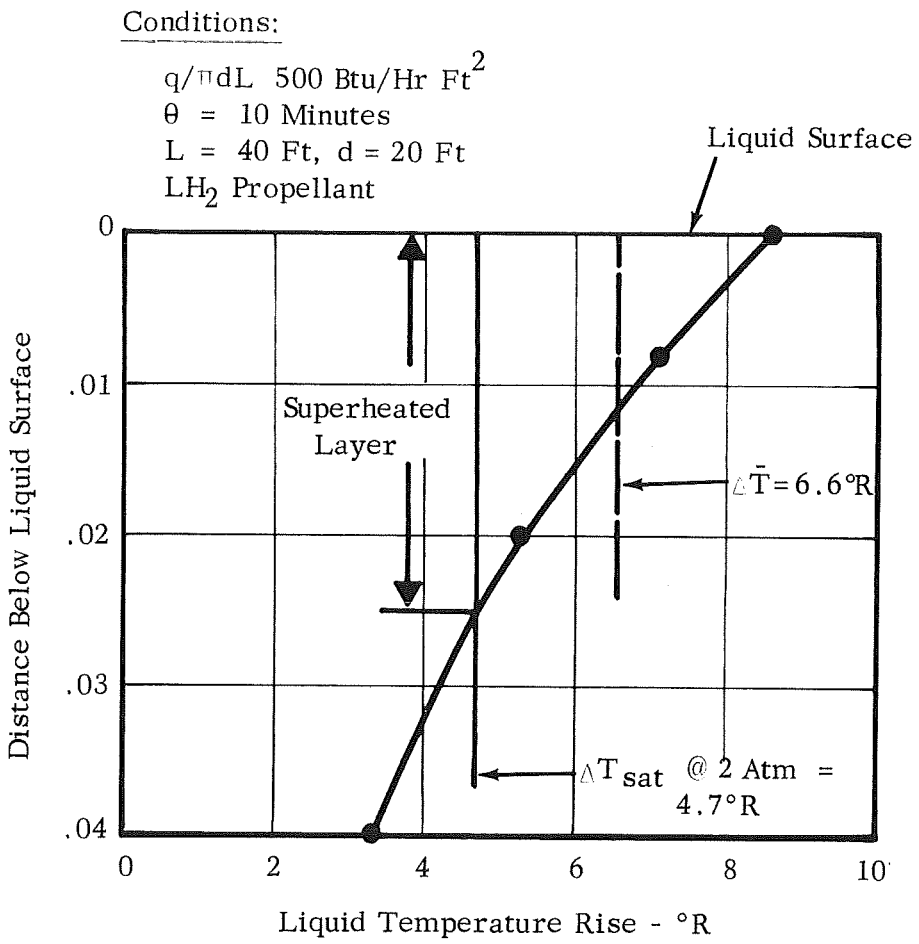

Portion of Superheated Layer Evaporating

$$\frac{C_L\,(\Delta\bar{T} - \Delta T_{sat})}{\lambda} = \frac{4.4\,(6.6 - 4.7)}{194} = 2.3\%$$

FIGURE 30 USE OF TRANSIENT CONDUCTION ANALYSIS TO ESTIMATE FREE BOILING EVAPORATION

VIII. PROPELLANT EVAPORATION DUE TO LIQUID FILM ON TANK WALLS

When liquids are drained from tanks, a thin liquid film adheres to the wall. If there is heating of these exposed walls it is possible that the film may be vaporized and contaminate the ullage pressurizing gas.

The general theory of draining films is examined and it is shown that the average film thickness, $\bar{t}$, neglecting surface tension, depends upon the rate of draining (v), the liquid density, ρ_L, the liquid viscosity, μ, and the gravitational acceleration, g. Specifically,

$$\bar{t} = (2/3) \left[(\mu/\rho) \ (v/g) \right]^{\frac{1}{2}} \tag{86}$$

If the surface tension is taken into consideration, there is no adequate theoretical relation but the available experimental data are correlated with two dimensionless groups,

$$Y = \bar{t} \left[(\rho/\mu) \ (g/v) \right]^{\frac{1}{2}}$$

$$X = \sigma/\mu v \quad (\sigma \text{ is the surface tension})$$

and $$\log_{10} X = (0.151) / (\log_{10} 1.5\,Y) + 1.44 - 5.45 \log_{10} (1.5\,Y) \tag{87}$$

Equation (87) reduces to Equation (86) in the limit where the surface tension (and thus X) approaches zero. Equation (87) is shown plotted in Figure 29. Over wide variations in X the value of Y changes only slightly and approaches > 0.6 as $X \to 0$. Figure 31 is discussed in detail by Van Rossum[42] The theory behind Equations (86) and (87) is discussed in detail in Appendix D.

Equation (87) is useful to estimate film thicknesses for hydrogen, oxygen, and nitrogen films for various draining rates. For all three materials, the average thicknesses are about the same for equal drain rates, i.e., if $\bar{t}$ is expressed in thousands of inches, for v = 0.1, 1, and 10 ft/sec then $\bar{t}$ = 0.2, 1.0 and 4.6.

Assuming the film thickness will evaporate completely, the contamination in the ullage from the evaporation may be calculated. In Appendix D, this contamination has been computed in terms of the thickness of a saturated vapor layer above the liquid surface. This method of presentation is chosen so that the evaporated film results can be easily compared with the molecular diffusion results. Pertinent results are summarized in Table 12 below for a tank L/d of 2.0, and a pressure of 2 atmospheres.

TABLE 12

ULLAGE CONTAMINATION DUE TO EVAPORATION OF LIQUID FILM ON TANK WALLS

Drain Rate (ft/sec)	Average Film Thickness (in.)	Thickness of Equivalent Saturated Vapor Layer on Liquid Surface (in.)	
		Hydrogen	Oxygen
.1	.0002	.063	.206
1.0	.001	.286	.85

Comparing the above results with the molecular diffusion results of Figure 15 indicates that evaporation of the liquid film on the tank walls is considerably less than the diffusion anticipated from a saturated liquid surface.

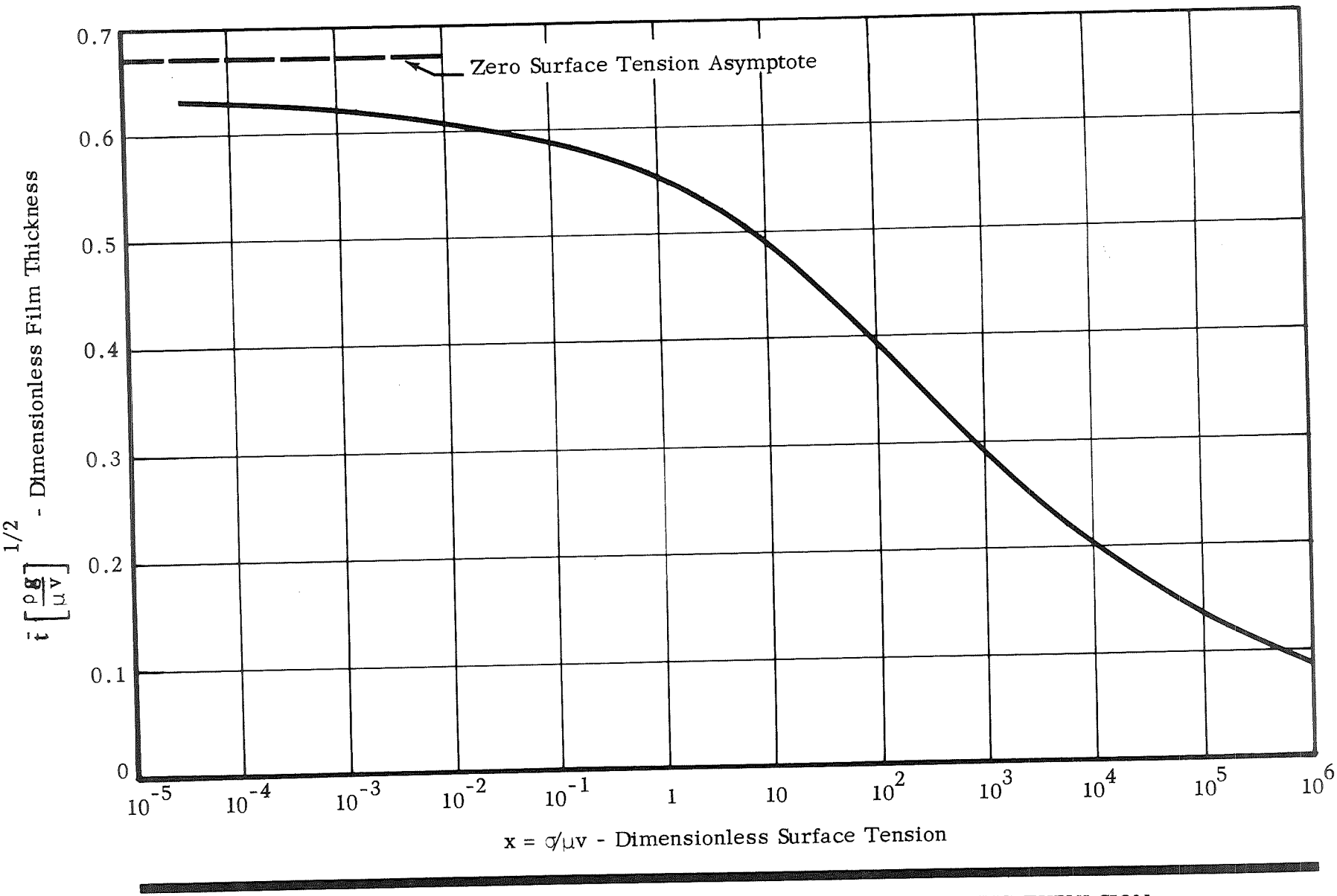

FIGURE 31 LIQUID FILM THICKNESS ON TANK WALL DURING EXPULSION

IX. FORMULATION OF ANALYTICAL MODEL FOR CALCULATING PROPELLANT VAPOR EVAPORATION

Based on the various analytical studies presented in the preceding sections, we may present a tentative model for calculating propellant evaporation under typical flight conditions. It should be emphasized, however, that this model is derived completely from analytical considerations and as such contains certain key assumptions and reasoning which cannot have a high level of confidence prior to experimental verifications. It would be highly desirable that the assumptions of the analysis be verified experimentally before the tentative methods outlined here are actually employed for quantitative design analysis.

A. BRIEF STATEMENT OF PERTINENT ANALYTICAL RESULTS

(1) The preceding analytical work has indicated that molecular diffusion is probably the most reasonable analytical technique for calculating propellant evaporation. Certain qualifications and exceptions which should be noted, are as follows: Analytical results of a rather first-order nature indicate that ullage natural convection circulation does not generally produce mass transfer coefficients in excess of that indicated by molecular diffusion. Since such natural circulation convective effects are not easily calculated, it has been convenient to neglect this mode of interfacial mass transfer. However, we have not been able to prove from any experimental data that the natural circulation effect on surface interfacial mass transfer is as weak as indicated by our analysis.

(2) For reasonably well-designed diffusers, remote from the liquid surface, we feel can neglect convective effects associated with pressurant gas jet impingement. However, the analysis of diffuser induced circulation currents is sufficiently complex to make it difficult to define the restrictions of "well-defined diffusers remote from the liquid surface" very exactly.

(3) For the specific case of initial pressurization of a small volume ullage, we would expect the circulation currents associated with the pressurant gas inlet flow to result in a high degree of mixing of the ullage gas and completely overwhelm any mass transfer effects due to molecular diffusion.

The transient conduction model previously described appears useful for computing liquid temperature resulting from external heat leak to the liquid phase. For liquid oxygen, in which the influence of gas liquid interaction on surface temperature, appears to be small, we would expect liquid surface temperature and liquid temperature gradients to be governed entirely by external heat leak. However, for liquid hydrogen, gas liquid interactions are much more important and determination of liquid surface temperature must involve consideration of both the contribution of external heat leak and the cooldown of the helium pressure gas.

B. APPLICATION OF ANALYTICAL RESULTS TO VARIOUS PHASES OF PROPELLANT TANK PRESSURIZATION AND EXPULSION

In this section we will consider the approaches to be followed in a typical flight sequence. Discussion will be divided into the processes of interest, namely, initial pressurization of a small volume ullage, pressurized hold, and expulsion.

1. Initial Pressurization

Initial pressurization is typically a rapid process (generally in the order of thirty seconds) and ullage volume involved is generally quite small (on the order of 1 percent). Initial pressurization generally follows a freely venting condition in which the tank ullage is filled with vapor saturated at one atmosphere.

Since the ullage volume is very small and the liquid surface quite close to the diffuser, we would expect that the pressurant gas becomes completely mixed with the gas initially in the ullage during initial pressurization. Definition of the quantity of propellant vapor present in the ullage after initial pressurization is somewhat difficult. We might adopt the viewpoint that the partial pressure of the propellant vapor is one atmosphere. This result would certainly seem reasonable since the ullage vapor is in very good contact with the liquid surface, which is essentially saturated at one atmosphere. In this case the quantity of propellant vapor actually present in the ullage would be dependent on ullage temperature. In order to avoid having the quantity of propellant vapor dependent on ullage temperature, it is useful to use a second assumption as to the quantity of vapor present in the ullage. This assumption is merely that the vapor initially present in the ullage, prior to initial pressurization, remains in the vapor state and that no net evaporation or condensation on the surface occurs. According to this definition, the partial pressure and temperature for calculating propellant density is saturation at one atmosphere. The two assumptions discussed are, of course, equivalent for the case in which the final ullage temperature is close to saturation at one atmosphere, which in fact would be close to the truth in many situations.

2. Pressurized Hold

Propellant evaporation occurring during pressurized hold can be computed by molecular diffusion methods. Boundary conditions for molecular diffusion are initial propellant concentration in the ullage gas and the liquid surface concentrations. In accordance with our discussion of 1 above, we will assume that for the pressurized hold period, propellant vapor concentration in the ullage gas is one atmosphere. The partial pressure adjacent to the liquid surface is evaluated using the ADL transient conduction model in conjunction with the adiabatic stagnant gas analysis which predicts the effect that gas liquid interactions have on

liquid surface temperature. As previously discussed, we would expect gas liquid interaction to have no effect on liquid oxygen surface temperature. However, in the case of liquid hydrogen, gas liquid interaction generally brings the surface temperature up nearly to saturation. A specific procedure to follow depends to a large extent on the surface temperature rise indicated by transient conduction theory. A reasonable set of rules is as follows:

a. If the liquid surface temperature predicted by transient conduction theory does not rise substantially above the saturation of one atmosphere,

(1) For liquid oxygen, assume surface saturated at one atmosphere.

(2) For liquid hydrogen, use surface saturation indicated by stagnant gas analysis of Section VII-B.

b. If surface temperature rises to near, but slightly less than saturation at ullage pressure,

(1) For liquid oxygen, the appropriate surface temperature is that pre-predicted by the transient conduction method. However, the variation in surface temperature during the pressurized hold process predicted by this method, does cause some problems in that the molecular diffusion solution is specifically derived for a constant surface temperature condition. If the variation of surface temperature is such that the molecular diffusion rate increases rapidly during the hold period, perhaps the best procedure is to use a step-wise calculation in which the variable temperature process is simulated by a series of finite constant surface temperature steps. As a test as to the need of such complexity, we recommend the following. First, compute the diffusion quantity on the basis of the mean surface temperature. Second, compute the diffusion quantity based on the initial and final surface temperature and obtain the arithmetic mean of these results. If the difference between the "mean pressure" diffusion rate and the diffusion rate, which is the mean of the rates corresponding initial and final pressure, is small, either procedure can be used. If the difference is intolerable, then the step-wise calculation mentioned previously is indicated.

(2) For liquid hydrogen, take the surface temperature which is the maximum of either the stagnant gas result, or final surface temperature indicated by transient conduction theory.

c. If surface temperature tends to exceed saturation, use saturation for molecular diffusion calculations and in addition compute free boiling evaporation using the methods of Section VII-F.

3. Expulsion

During the expulsion process, interfacial mass transfer is again computed from molecular diffusion considerations. Techniques previously mentioned for pressurized hold, apply here with one exception. For the case of pressurized hold, the partial pressure of the propellant vapor in the ullage space was taken to be one atmosphere. However, during expulsion, the relatively small quantity of propellant vapor which can possibly be contained in the small initial ullage, is diluted greatly by the increase in ullage volume. Therefore, we feel for the expulsion process, it is reasonable to assume that the partial pressure of the propellant vapor in the ullage is essentially zero.

C. TYPICAL NUMERICAL EXAMPLES

The procedures mentioned above can be most easily illustrated with numerical examples. For calculation purposes, we will assume a vertical cylinder tank having a diameter of 20' and a total height of 40'. We will assume that during the initial pressurization process, the ullage volume is one percent and the tank is very quickly pressurized to two atmospheres. We will further assume a five minute pressurized hold period in which the ullage pressure is maintained at two atmospheres and a five minute expulsion period with the ullage pressure remaining constant at two atmospheres. During this total flight, we will consider the heat leak per unit side wall area is constant. We will take a value of 500 Btu/hr ft^2 as being typical for hydrogen and a value of 1000 Btu/hr ft^2 as being typical for liquid oxygen.

In the calculations to follow as a primary unit of measure, we will compute the thickness of a layer of saturated propellant vapor present above the liquid surface. This method of expressing the quantity vaporized is very convenient for molecular diffusion and can be readily converted to other parameters of interest such as the volumetric or mass percentage of propellant vapor in the ullage gas.

1. Initial Pressurization

In accordance with our previous discussion, we will assume propellant vapor is present in the initial ullage at a density corresponding to saturation at one atmosphere. Since the total ullage pressure is two atmospheres, the thickness of an equivalent layer of vapor saturated at two atmospheres would be approximately one half the height of the ullage. In this case, since the ullage volume is taken to be one percent and the tank height 40 feet, the height of the ullage is four-tenths of a foot and the thickness of the saturated layer of vapor is .2 feet or 2.4 inches. It is interesting to note that by our assumptions, the result for initial pressurization is dependent only on the ullage volume and is the same for both liquid hydrogen and liquid oxygen.

2. Pressurized Hold for Five Minutes

First of all, in accordance with our previous discussion, we will state that the partial pressure of the propellant vapor in the ullage is one atmosphere.

Application of transient conduction theory to predict surface temperature for these conditions is illustrated in Figures 27 and 28. Results indicate that the liquid oxygen surface temperature rises approximately 3.4 degrees, which is equivalent to a rise in saturation pressure of about 3.4 psi. For the case of liquid hydrogen, transient conduction indicates that the surface temperature rises to somewhat above saturation at two atmospheres. The stagnant gas analysis, whose results are presented in Figures 19 and 20 indicates that liquid oxygen surface temperature is essentially unaffected by gas liquid interactions. However, for a pressurant temperature of 530 degrees R we might expect the liquid hydrogen surface temperature to rise 4 degrees R or about 80 percent of the way to saturation.

Based on the above results, we will assume that for the purpose of molecular diffusion calculations, the hydrogen surface may be considered to be saturated at two atmospheres and the oxygen surface saturated at a mean pressure of 16 psia (in this case, the liquid oxygen surface pressure increase is so modest that we are merely taking the mean pressure and not investigating the diffusion quantity resulting from both the initial and final pressure).

For liquid hydrogen, since the surface is near saturation at ullage pressure, diffusion is limited by surface kinetics. In accordance with the studies of Section VI and Figure 12, the dimensionless diffusion thickness is equal to 6.6. Therefore, the thickness of the equivalent layer of saturated vapor for a 300 second pressurized hold is as follows:

$$L_1 = 6.6 \sqrt{D\theta} = 6.6 \sqrt{(.007)(300)} = 9.56 \text{ cm} = 3.75 \text{ in.}$$

For the case of liquid oxygen, the concentration driving force is calculated as follows:

$$\frac{y_A - y_{A_\infty}}{1 - y_{A_o}} = \frac{p_{A_o} - p_{A_\infty}}{p - p_{A_o}} = \frac{16 - 15}{30 - 16} = .0715$$

In this case the dimensionless diffusion length is far less than the maximum value tolerated by surface kinetics and is as shown in Figure 12, equal to .08. Therefore, the thickness of the equivalent layer of saturated vapor for liquid oxygen is as follows:

$$L_1 = .08 \sqrt{D\theta} = .08 \sqrt{(.05)(300)} = .31 \text{ cm} = .122 \text{ in.}$$

3. Expulsion

The calculation techniques for expulsion are very similar to those used above for pressurized hold except that the numerical results may differ due to the fact that the partial pressure of the propellant vapor in the ullage is now assumed to be zero rather than one atmosphere.

For the case of hydrogen, in which the liquid surface has been previously assumed to have attained saturation, the diffusional process is limited by surface kinetics and the reduction in ullage propellant vapor concentration does not influence the diffusion process. Therefore, we can compute the total amount diffused for the combined pressurized hold plus expulsion process by repeating the calculation performed for the pressurized hold and considering the time to be 600 seconds rather than 300 seconds. The result is that the total diffusion quantity is that computed for the pressurized hold multiplied by the square root of two. Therefore, the thickness of the equivalent layer of saturated vapor for the total pressurized hold plus expulsion process is 5.3 inches and the quantity which diffuses within the expulsion process itself is 5.3 minus 3.8 or 1.5.

Since the liquid hydrogen surface temperature as indicated by transient conduction theory tends to exceed saturation. it is necessary to investigate free boiling evaporation. This calculation has, in fact, been performed in Section VII-F and indicates that the thickness of the equivalent layer of saturated vapor resulting in free boiling evaporation is only .2 inches which in this case is nearly negligible with respect to the molecular diffusion quantity.

For the case of liquid oxygen, in which the liquid surface temperature is less than saturation, we must again examine surface temperature history indicated by transient conduction model. From the results of Figure 27, it is apparent that the surface temperature rise at the beginning of expulsion is 3.3 degrees R and the surface temperature rise at the end of expulsion is 5 degrees R. For liquid oxygen, we are not in substantial error if we consider the rise in saturation pressure to be numerically equal to the rise in saturation temperature in this region. Therefore, the initial saturation pressure will be approximately 18.3 psia and the final saturation pressure at the surface will be approximately 20 psia. We will use this calculation as an illustration of averaging procedure for calculating molecular diffusion. First, let us compute the diffusion quantities based on the initial and final saturation pressure and take the average of these quantities. For a surface saturation pressure of 18.3 psia:

$$\frac{y_{A_o} - y_{A_\infty}}{1 - y_{A_o}} = \frac{p_{A_o} - p_{A_\infty}}{p - p_{A_o}} = \frac{18.3 - 0}{30 - 18.3} = \frac{18.3}{11.7} = 1.56$$

and per Figure 12, $\frac{L_1}{\sqrt{D\theta}} = .94$

Applying a similar procedure for the case of a surface saturation pressure of 20 psia, results in L_1 divided by the square root of $D\theta = 1.08$. Therefore, the arithmetic average diffusion quantity is $(.94 + 1.08)/2 = 1.01$.

Secondly, let us compute the diffusion rate based on the arithmetic mean pressure of 19.1 psia. In this case, the dimensionless diffusion quantity is 1.00 which is almost precisely the same as the result obtained from the average of the initial and final diffusion quantities. Therefore, a value of 1.00 may be used for calculating the equivalent diffusion thickness and

$$L_1 = (1.0)\sqrt{(.05)(300)} = 3.86 \text{ cm} = 1.52 \text{ in.}$$

The results of these calculations are presented in Table 13 below.

TABLE 13

EQUIVALENT DIFFUSION LAYER THICKNESSES CALCULATED FOR TYPICAL FLIGHT PROFILE

(inches)

Regime	Hydrogen	Oxygen
Initial Pressurization	2.4	2.4
Pressurized Hold	3.8	.1
Expulsion	1.5	1.5
Total	7.7	4.0

It should be emphasized that the above results apply only to a specific case incorporating certain conditions of initial ullage volume and heat leaks. However, since these conditions are hopefully typical of flight operation, the numerical values may have some significance. First of all, it is interesting to note that the evaporation quantity connected with the initial pressurization is a fairly significant number, especially in the case of liquid oxygen. As calculated, this quantity is directly proportional to ullage volume and in the specific numerical example used, the ullage volume was assumed to be one percent of the total volume. Next, we might note that during pressurized hold and expulsion, the total diffusion quantity for hydrogen is substantially larger than that of oxygen. This result is due to the fact that for the specific heat leak conditions chosen, liquid hydrogen surface temperature attains saturation quickly, whereas, the liquid oxygen surface temperature did not rise substantially above saturation at one atmosphere.

The third point is that the total diffusion thickness is a very small percentage of total ullage volume and consequently, volumetric and mass percentages of propellant in the ullage space will be relatively small. It may be of interest at this point to express the diffusion quantity as a percentage of total ullage gas rather than as a saturated layer of thickness. First of all, in obtaining a volumetric percentage, we must realize that the saturated layer is at a temperature much lower than the mean ullage temperature and that if this layer were mixed with the ullage gas, its volume would be increased by a ratio of ullage temperature and saturation temperature. If we assume that the mean ullage temperature is the arithmetic mean of the pressurant inlet temperature plus the saturation temperature of the liquid, the ratio of Tullage over Tsaturation may be written as:

$$\frac{\overline{T}\ \text{ullage}}{T\ \text{sat}} = \frac{T\ \text{inlet} + T\ \text{sat}}{2\ T\ \text{sat}} = \frac{1}{2}\left[\frac{T\ \text{inlet}}{T\ \text{sat}} + 1\right]$$

If we assume a pressurant inlet temperature of 530 degrees R, the ratio of ullage temperature to saturation temperature for hydrogen is 7.85; and for oxygen, 215. At this point, the thickness of the equivalent saturated layer may be translated into the volumetric percent of vapor in the ullage, making use of the total tank height L and the ratio of mean ullage temperature to saturation temperature previously calculated, that is:

$$\%\ \text{volume} = 100\left(\frac{L_1}{L}\right)\left(\frac{T\ \text{ullage}}{\overline{T}\ \text{sat}}\right)$$

Using the above equation, the numerical value for the total volumetric percent of hydrogen in the ullage is 12.6 percent; for oxygen, 2.58 percent.

Because of the large difference in density between hydrogen and oxygen, a given volumetric percent results in a much larger weight percent for oxygen than is the case for hydrogen. A plot illustrating this effect is presented in Figure 32. Using the volumetric percentages calculated in the above paragraph, it is apparent that the total evaporation quantity for hydrogen is approximately 7 percent of the total ullage gas on a weight basis. For the case of oxygen, the evaporated propellant is approximately 18 percent of the total ullage gas on a weight basis.

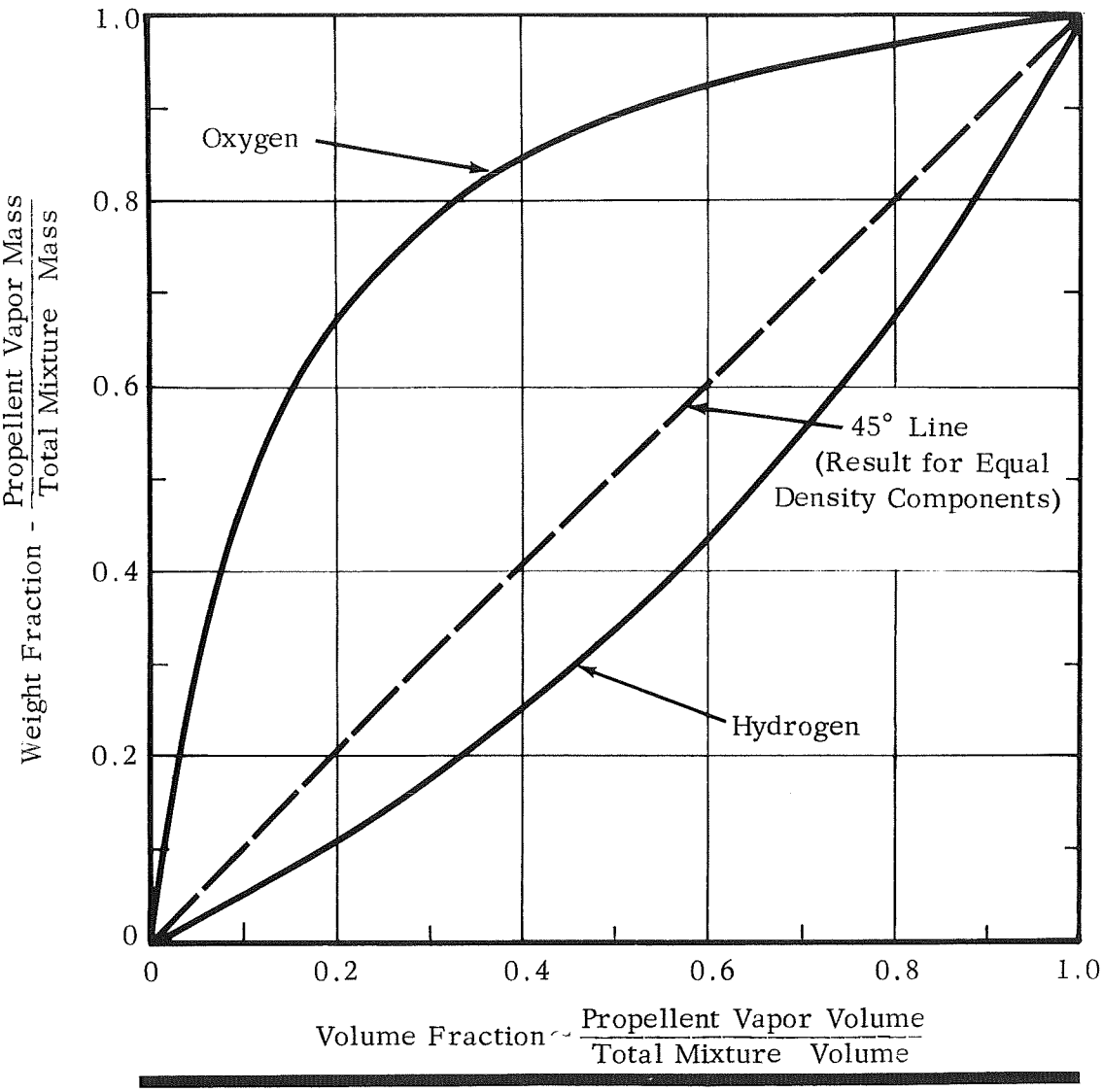

FIGURE 32 WEIGHT FRACTION VS VOLUME FRACTION FOR HYDROGEN-HELIUM AND OXYGEN-HELIUM MIXTURES

X. RECOMMENDATIONS FOR FUTURE WORK

In the course of our work we have analyzed many aspects of the propellant vapor diffusion problem and have become acquainted with much of the data on this subject available in the literature. Results of this work have indicated certain areas where analytical treatment has considerable promise and have also pointed up many areas where experimental data is required either to resolve specific points, to aid in understanding the physical mechanisms, or to serve as a basis for correlations.

A mathematical model for molecular diffusion has been developed which allows for the prediction of molecular diffusion rates and ullage gas concentration profiles if boundary conditions, in the form of the initial ullage concentration and the liquid surface temperature are known. This analysis would be expected to be reasonably accurate even for nominal convective effects at the liquid vapor surface. Preliminary calculations have indicated that convection currents due to the downflow of the ullage gas along the cold tank walls are probably not very important to the surface mass transfer. Studies of diffuser gas impingement, although also rather qualitative, indicated that for initial pressurization of a small ullage, when the diffuser is close to the liquid, we would expect near complete mixing of the ullage gas. However, during the expulsion process, when the liquid surface is remote from the diffuser, we should expect mixing due to diffuser velocities to be unimportant. Rather fragmentary pieces of data obtained in our literature search tend to indicate that interfacial mass transfer rates are roughly those predicted by molecular diffusion. However, in most cases the experimental mass transfer rates in question were so small as to be almost within the limits of measurement accuracy. Therefore, to date, we have not been able to achieve a satisfactory check of the molecular diffusion model for propellant vapor mass transfer. Further experimental work is required both to verify the basic molecular diffusion model and to check our assumptions with regard to ullage convective flow and diffuser impingement.

In the course of our work to date, we have devoted considerable effort to the study of liquid temperature gradients since these gradients, and in particular, the liquid surface temperature, are very important to the mass transfer at the liquid vapor surface. We have developed a model, based in part on transient conduction theory and incorporating an experimental correlation of surface heat flux ratio, which has shown some success in predicting liquid surface temperatures and gradients in the liquid. This model has been found to be quite good in predicting the trend of the time-wise variation of liquid surface temperature. Also, the model appears to approximate the slope of the temperature gradient in the immediate vicinity of the surface quite well. On the debit side, this model is not too accurate for predicting absolute values of surface temperature. Generally, the model predicts the difference between liquid surface temperature and integrated mean liquid

temperature to an accuracy of about ± 30%. Also, although the model appears to represent gradients in the immediate vicinity of the surface quite well, it tends to indicate a much steeper gradient in the bulk liquid than is generally measured experimentally. While we feel that this model is useful in at least approximating surface temperature, we feel that additional work in terms of improving this model or possibly adopting a more general approach, based on a more precise definition of the physical processes involved, may be in order. To this end, we feel that experimental studies of the nature of the flow patterns in a heated tank and correlation of these observations with the measured liquid temperature gradients will be invaluable.

It also should be noted that the present model implies that liquid temperature gradients are solely the result of the distribution of heat input in the liquid phase as effected by liquid boundary layer flow, bulk circulation, and transient conduction and are independent of vapor-liquid surface reactions. Strictly speaking, we would expect this model to be truly valid only for very small ullage self pressurizations. Other analyses which we have performed in the course of this program would indicate that at least for the case of liquid hydrogen, we would expect interaction between the ullage gas in liquid to have an influence on liquid surface temperature. We have not been able to satisfactorily resolve this point from the experimental data which we have been able to obtain in the literature and feel that additional testing to establish the effects of ullage volume and pressurant gas would be of great value.

Therefore, in summary, we feel that experimental work is indicated to verify, or possibly modify, certain assumptions in the analytical development. Specifically, we feel that experiments should be conducted in the following areas:

1. Adiabatic Helium Pressurization Studies

The objective of the work would be to answer the following questions:

a. For initial pressurization, are we correct in assuming that (near) complete mixing occurs?

b. During pressurized hold and expulsion, are evaporation quantities and concentration gradients compatible with molecular diffusion? -- or

c. Are ullage natural convection circulation and, in the case of expulsion diffuser, jet velocities responsible for significant surface convection?

d. Is surface temperature response to gas-liquid interaction in accordance with "stagnant fluid" analysis?

We would expect that static (i.e., constant ullage volume) tests would be useful for evaluating initial pressurization mixing, surface temperature response, and whether or not ullage free convection, cause diffusion rate to be in excess of molecular diffusion predictions. In these tests, measurements of temperatures and concentrations in the vicinity of the interface will be required.

Expulsion tests using two or three "representative" diffuser configurations appear to be the most practical means to investigate jet impingement convection during expulsion. The representative diffuser configuration would be chosen to simulate: (a) a theoretical ideal diffuser producing near uniform flow across tank area, (b) one or two typical flight type diffuser configurations.

2. Liquid Temperature Gradient Studies with External Heat Leak

The objectives of this work would be to:

a. Better define mechanism of thermal stratification

b. Improve prediction techniques

A transparent walled two dimensional non-cryogenic tank with capability for wall heating and measurement of liquid temperatures would be well suited to studying stratification mechanisms. Cryogenic self-pressurizing tests are a good source of surface temperature data and liquid temperature gradients for checking analytical prediction techniques.

3. Propellant Tank System Studies with Helium Pressurization and External Heat Leak

A limited number of tests in which external heat leak is combined with helium pressurization would be valuable to verify analytical techniques under simulated flight vehicle conditions.

REFERENCES

1. "Main Propellant Tank Pressurization System Study and Test Program," Lockheed Aircraft Corporation, Marietta, Georgia, report to the U. S. Air Force Systems Command, USAF SSD TR-61-21, Vol. I (Confidential), Vol. II, and Vol. III, December 1961.

2. Coxe, E.F., and Tatom, J.W., Lockheed-Marietta, "Analysis of the Pressurizing Gas Requirements for an Evaporated Propellant Pressurization System," Advances in Cryogenic Engineering, Vol. 7, 1962, p. 234.

3. Gluck, D.F., and Kline, J.F., NASA-Lewis Research Center, "Gas Requirement in Pressurized Transfer of Liquid Hydrogen," Advances in Cryogenic Engineering, Vol. 7, 1962, p. 219.

4. Nein, M.E., and Head, R.R., NASA-Huntsville, "Experiences with Pressurized Discharge of Liquid Oxygen from Large Flight Vehicle Propellant Tanks," Advances in Cryogenic Engineering, Vol. 7, 1962, p. 244.

5. Private Communication, C.C. Wood, M. Nein, J.R. Moses, NASA-Marshall Space Flight Center, 6 November 1962.

6. Private Communication, P. Hacker, J. Kline, D. Nored, NASA-Lewis Research Center, 13, 14 November 1962.

7. Private Communication, J. Tatom, Lockheed-Georgia Company, October 26 and November 6, 1962.

8. Huntley, S.C., "Temperature-Pressure Time Relationships in a Closed Cryogenic Container," NACA TN 4259, February 1958.

9. Schmidt, A.F. et al., "An Experimental Study Concerning the Pressurization and Stratification of Liquid Hydrogen," Proceedings of the 1959 Cryogenic Engineering Conference.

10. Tatom, J.W. et al., "Analysis of Thermal Stratification of Liquid Hydrogen in Rocket Propellant Tanks," Lockheed-Georgia Company, 1963.

11. Scott, L.E. et al., "Temperature Stratification in a Non-Venting Liquid Helium Dewar," Journal of the Research of the National Bureau of Standards, January-March, 1960.

12. Mair, C.E., "Preliminary Investigation of Thermal Conditions Inside Large Liquid Oxygen Container Exposed to Climatic Heating," Army Ballistic Missile Agency, DSE, Technical Note No. G-024, August 24, 1956.

13. George C. Marshall Space Flight Center Memorandum, "LH_2 Stratification Test on the S-IV Facilities Vehicle," H.G. Paul, January 23, 1964.

14. Bailey, T., Vande Kappel, R., and Skartvedt, G., Martin Company, and T. Jefferson University of Arkansas, "Cryogenic Propellant Stratification Analysis and Test Data Correlation," ARS Journal, July 1963.

15. Burke, J.C., Goldstein, M.E., and Neal, R.W., "Stratification in Non-Vented Cryogenic Container," Unpublished A.D. Little Preliminary Manuscript, April 28, 1961.

16. Randall, I.E., "A Review of the Pressurized Transfer of Liquid Cryogen," A.D. Little, Inc., Presented at AICHE, Pittsburgh Meeting, May 20, 1964.

17. Thomas, P.D., and Morse, F.H., "Analytical Solution for the Phase Change in a Suddenly Pressurized Liquid-Vapor System," Lockheed Missiles and Space Company, Advances in Cryogenic Engineering, Vol. 8, 1963, p. 550.

18. Bowersock, D.C., Jr., Arthur D. Little, Inc., and Reid, R.C., M.I.T., "An Analytical Method for Estimating Gas Requirements in the Pressurization and Transfer of Cryogenic Fluids," Advances in Cryogenic Engineering, Vol. 6, 1961, p. 261.

19. Saturn S-II Cryogenic Consulting Service Final Report to NAA-S&ID by Arthur D. Little, Inc., 4 February 1963.

20. Moore, R.W., et al., "Gas Pressurized Transfer of Liquid Hydrogen," Advances in Cryogenic Engineering, Vol. 5, 1959, p. 450.

21. Arnold, J.H., Tran AICHE, 40, 361 (1944).

22. Bird, R.B., Adv. in Chem. Eng. I, Academic Press, N.Y. (1956).

23. Jeans, Kinetic Theory of Gases.

24. "Measurements on Thermal Diffusion Combined with Ordinary Diffusion in Gas Mixtures," A. van Itterbeek, Proc. Int. Sym. Transport Properties in Statistical Mechanics; I. Prigogine, Ed., Intersience, 1958. p. 387.

25. Heath, H.R., Iblis, T.L., and Weld, N.E., Proc. Roy. Soc. (London), A 178, 380 (1941).

26. Reid, R.C., and Sherwood, T.K., "Properties of Gases & Liquids," McGraw-Hill Book Co., 1958.

27. Hirschfelder, J.O., Curtiss, C.F., and Bird, R.B., "Molecular Theory of Gases & Liquids," Wiley, N.Y., 1954.

28. Bird, R.B., "Theory of Diffusion," Adv. in Chem. Eng., Vol. I, Academic Press, N.Y., 1956, p. 155.

29. Eckert, E.R.G., and Drake, R.M., Heat and Mass Transfer, McGraw-Hill, New York, 1959.

30. Reid, R.C., and Gruber, G., The Physical and Thermodynamic Properties of Helium.

31. Sherwood, T.K., and Pigford, R.L., Absorption and Extraction, McGraw-Hill, New York, 1952.

32. Jet Propulsion 26, No. 9, 760 (1956).

33. Proc. Camb. Phil. Soc. 34, 185 (1938).

34. "Boundary Layer Theory," H. Schlichting, Pergammon Press, New York, 1955.

35. Lert. fur angewandte Mathematik und Mechanik, 6, 468 (1926).

36. Kuethe, A.M., Trans. A.S.M.E. 57, A-88 (1935).

37. Personal Communication, Dr. H.A. Becker, M.I.T., Cambridge, Massachusetts.

38. Anderson, B.H., and Kahn, M.J., "Experimental Investigation of the Behavior of a Confined Fluid Subjected to a Non-Uniform Source and Wall Heating," NASA TN D-2079, November 1963.

39. Eckert, E.R.G., and Jackson, T.W., "Analysis of Turbulent Free Convection Boundary Layer on a Flat Plate," NACA Rpt. 1015, July 1950.

40. McAdams, W.H., Heat Transmission, 3rd Edition, p. 172, McGraw-Hill, New York, 1954.

41. Richards, R.J., Steward, W.G., and Jacobs, R.B., "A Survey of the Literature on Heat Transfer from Solid Surfaces to Cryogenic Fluids," NBS Technical Data No. 122, October 1971.

42. Van Rossum, J.J., App. Sci. Research 7, 121 (1958).

43. Jacob, M., Heat Transfer Volume I, pp. 254-258, John Wiley, New York, 1949.

NOMENCLATURE

A	Area
B	Constant in Eq. 43
a_o	Constant in Eq. 49
b	Proportionality constant relating ℓ^2 to z^2, Eq. 46
C	Concentration
C_L	Liquid specific heat
C_z	Non-dimensional constant, Eq. 54
d	Tank diameter
D	Diffusion coefficient
E	Equilibrating potential, $E \equiv kA/L$
E_1	Constant in Eq. 44
F	Volume fraction of mixed liquid that does not evaporate
g	Acceleration due to gravity
G_r	Grashoef Number $\equiv (g\beta\Delta Tx^3)/\nu^2$
H	Enthalpy per unit mass
h	Heat transfer coefficient
J	Energy constant (778 ft-lb/Btu)
k	Thermal conductivity
k_1	Boltzmann's constant
K_2	Profile shape factor in Eq. 52
kg	Mass transfer coefficient

ℓ	Prandtl mixing length
L	Tank height
L_1	Diffusion layer thickness for the evaporating component
L_2	Ullage height
m	Mass of a molecule
$\dot{m}$	Momentum flux
M	(1) Mass (Section V) (2) Molecular weight (Section VI)
M*	$(M_1 + M_2) / (M_1 M_2)$
N	Molal flux
N_D	Number of jet diameters
P	Total pressure; partial pressure when used with subscript
p	Partial pressure
p_{Hem}	Log mean value of the Helium partial pressure
P_r	Prandtl number $\equiv c\rho/k$
q	Heat flux
Q	Volumetric flow
R	Gas constant for a particular gas
$\bar{R}$	Universal gas constant
Re	Reynold's number $d\rho u/\mu$
r	Radial distance
r*	Radius in a jet where $u = \frac{1}{2} u_{\mathcal{L}}$

t	Thickness
T	Absolute temperature
T_B	Liquid bulk temperature
T_S	Liquid surface temperature
T_{12^*}	$12°/kT$
ΔT_{BL}	Temperature rise of fluid flowing through boundary layer
T_{ave}	$T_o + \frac{1}{4}(T_i - T_o)$
U	Internal energy per unit mass
u	Velocity
u_m	N_T/C_T
v	Specific volume
V	Volume
w	Mass of evaporated cryogen
$\dot{w}$	Rate of cryogen evaporation
X	Volume fraction of liquid initially in tank that mixes with ullage gas
x	(1) Vertical distance above a liquid cryogen surface (Section VI) (2) Vertical distance below a liquid cryogen surface (Section VII)
x'	$L_2 - x$
y	(1) Mole fraction in diffusion analysis (2) Horizontal distance from tank wall in convection analysis
Y	Volume fraction of tank finally filled with a mixture of pressurant and fuel vapor

Y_A	$(y_A - y_{A\infty}) / (y_{Ao} - y_{A\infty})$
z	Axial distance in jet diffusion analysis

Greek Symbols

Γ	Sticking coefficient of molecules at a liquid surface
β	Coefficient of volumetric expansion $= \frac{1}{V} \left(\frac{V}{T} \right)$
γ	$\Gamma (2\ MRT_o)^{-\frac{1}{2}}\ C_T\ (D/\theta)^{\frac{1}{2}}$
δ	Thickness of boundary layer
Δ	Thickness of gas layer building up on the cold liquid surface
ϵ	Fraction of fuel vaporized
$\Sigma 12_o$	Minimum interaction potential energy in Lennard-Jones model; see Table IA of Ref. (27) $\Sigma 12_o = \left[(\Sigma_{o_1}) (\Sigma_{o_2}) \right]^{\frac{1}{2}}$
η	r/z in diffusion analysis
λ	Latent heat
μ	Dynamic viscosity
γ	Kinematic viscosity
ξ	$x/(2\sqrt{D\theta})$
ρ	Density
σ_{12}	Intermolecular distance when potential energy of attraction is zero, see Table IA of Ref. (27) $\sigma_{12} = \frac{1}{2} (\sigma_1 + \sigma_2)$

$$\phi = u_m \sqrt{\theta/D} = \left[\frac{-1}{2(1 - y_{Ao})} \left(\frac{dy_A}{d\xi} \right)_{\xi=0} \right]$$

$\Omega^{(1,1)}(T_{12}^*)$ collision integral function of T_{12}^*; see Table IM of Ref. (27)

θ time

Subscripts

a, b, c Refer to tanks a, b, c (Figure 1)

A Refers to component A, either H_2 or O_2

$\mathfrak{L}$ Refers to conditions at the centerline of a jet

f (1) Refers to conditions in a gas film (Section VI)
(2) Refers to fuel (Section V)

H Refers to thermal layer (Section VII)

i Refers to the inlet conditions of helium

L Liquid

m (1) Refers to mixed pressurant gas (Section V)
(2) Mean value

max Maximum

p Refers to pressurant gas (i.e., He)

r Radial

T Total

u Refers to unmixed pressurant gas

v Vapor

w	Wall
z	Axial
o	(1) Refers to conditions at the liquid surface (2) Initial condition (Section VII)
1, 2	(1) Refer to times before and after transfer, respectively (Sec. V) (2) Refer to components 1 and 2 (Section VI)

Superscripts

–	Average value
.	Denotes differentiation with respect to time
+	Refers to conditions in the gas just above the liquid surface
'	Refers to conditions corresponding to a jet having a velocity u', independent of radius across the jet nozzle
o	Refers to conditions at the outer boundary of a jet where $u_z = 0$.

APPENDIX A

DERIVATION OF EQUATIONS FOR MOLECULAR DIFFUSION ANALYSIS

1. Justification for Equation (16)

If a differential material balance on the total material in the system is written at position x, there results:

$$-\frac{\partial N_T}{\partial x} = \frac{\partial C_T}{\partial \theta} \qquad \text{(A-1)}$$

Since it has been assumed that $C_T \neq f(\theta)$, it follows from Equation (13) that $N_T \neq f(x)$. Further, it was assumed that $C_T \neq f(x)$ and was stated in the nomenclature that $u_m \cong N_T/C_T$. Therefore $u_m \neq f(x)$, $\frac{\partial u_m}{\partial x} = 0$, and Equation (15) reduces to Equation (16).

2. Derivation of Equation (19)

As before $u_m = N_T/C_T$ where C_T is a constant. Since N_T is independent of x, it can be written that

$$N_T = N_{A_o} = -C_T D \left(\frac{\partial y_A}{\partial x}\right)_o + N_T y_{A_o} \qquad \text{(A-2)}$$

or

$$N_T = -\frac{C_T D}{1-y_{A_o}} \left(\frac{\partial y_A}{\partial x}\right)_o$$

and

$$u_m = -\frac{D}{1-y_{A_o}} \left(\frac{\partial y_A}{\partial x}\right)_o$$

$$\therefore \quad u_m = -\frac{D}{1-y_{A_o}} \frac{1}{\sqrt{4D\theta}} \left(\frac{dy_A}{d\xi}\right)_{\xi = x = 0}$$

And Equation (18) becomes

$$\frac{d^2 y_A}{d\xi^2} + 2\left(\xi - \left[\frac{-1}{2(1-y_{A_o})}\left(\frac{dy_A}{d\xi}\right)_{\xi=o}\right]\right)\frac{dy_A}{d\xi} = o \qquad (A\text{-}3)$$

By defining

$$\phi \equiv \left[\frac{-1}{2(1-y_{A_o})}\left(\frac{dy_A}{d\xi}\right)_{\xi=o}\right] = u_m(\theta/D)^{\frac{1}{2}}$$

Equation (20) follows directly.

3. Derivation of Equations (22) and (23)

From Equation (20), we have

$$\frac{d^2 y_A}{d\xi^2} + 2(\xi - \phi)\frac{dy_A}{d\xi} = o \qquad (A\text{-}4)$$

with boundary conditions

$$y_A = y_{A_\infty} \quad \text{for } \xi = \infty$$

$$y_A = y_{A_o} \quad \text{for } \xi = o$$

First define:

$$Y = \frac{(y_A - y_{A_\infty})}{(y_{A_o} - y_{A_\infty})}$$

and by dividing Equation (A-4) by $(y_{A_o} - y_{A_\infty})$, there results

$$\frac{d^2 Y}{d\xi^2} + 2(\xi - \phi)\frac{dY}{d\xi} = o \qquad (A\text{-}5)$$

where

$$\Upsilon = o \text{ for } \xi = \infty \tag{A-6}$$

$$\Upsilon = 1 \text{ for } \xi = o \tag{A-7}$$

Now let $p = d\Upsilon / d\xi$ and Equation (A-5) becomes

$$\frac{dp}{d\xi} + 2(\xi - \phi)p = o$$

$$\therefore p = \frac{d\Upsilon}{d\xi} = C_1 \exp(-\xi^2 + 2\phi\xi) \tag{A-8}$$

where C_1 is an arbitrary constant.

Now Equation (A-8) may also be written as

$$\frac{d\Upsilon}{d\xi} = C_1 \exp(-\xi^2 + 2\phi\xi - \phi^2 + \phi^2) \tag{A-9}$$

$$\frac{d\Upsilon}{d\xi} = C_1 \exp(-(\xi - \phi)^2) \exp(\phi^2) \tag{A-10}$$

Equation (A-10) may be integrated using Equation (A-7)

$$\int_{\Upsilon=1}^{\Upsilon=\Upsilon} d\Upsilon = C_1 \exp(\phi^2) \int_{\xi=o}^{\xi=\xi} \exp\left[-(\xi - \phi)^2\right] d\xi$$

$$\Upsilon = 1 + \frac{C_1\sqrt{\pi}}{2} \exp(\phi^2) \left[\operatorname{erf}(\xi - \phi)\right]_{\xi=o}^{\xi=\xi} \tag{A-11}$$

$$\Upsilon = 1 + \frac{C_1\sqrt{\pi}}{2} \exp(\phi^2) \left[\operatorname{erf}(\xi - \phi) - \operatorname{erf}(-\phi)\right] \tag{A-12}$$

Now since $\text{erf } u = \frac{2}{\sqrt{\pi}} \int_o^u \exp(-u^2)\, du$

it follows that

$$\text{erf}(-u) = \frac{2}{\sqrt{\pi}} \int_o^u \exp\left(-[-u]^2\right)(-du)$$

or

$$\text{erf}(-u) = -\text{erf}(u)$$

Therefore

$$Y = 1.0 + \frac{C_1\sqrt{\pi}}{2} \exp(\phi^2)\left[\text{erf}(\xi - \phi) + \text{erf}(\phi)\right] \qquad \text{(A-13)}$$

Applying boundary condition, Equation (A-6)

$$0 = 1.0 + \frac{C_1\sqrt{\pi}}{2} \exp(\phi^2)\left[\text{erf}(\infty) + \text{erf}(\phi)\right]$$

$$\therefore C_1 = \frac{-2/\sqrt{\pi}}{1 + \text{erf}(\phi)} \qquad \text{(A-14)}$$

and

$$Y = \frac{1 - \text{erf}(\xi - \phi)}{1 + \text{erf}(\phi)} \qquad \text{(A-15)}$$

To obtain Equation (23), use is made of Equation (19):

$$\phi = -\frac{1}{2(1 - y_{A_o})}\left(\frac{dy_A}{d\xi}\right)_{\xi = o} \qquad \text{(A-16)}$$

and

$$\phi = -\frac{\left(y_{A_o} - y_{A_\infty}\right)}{2(1 - y_{A_o})}\left(\frac{dY}{d\xi}\right)_{\xi = o} \qquad \text{(A-17)}$$

Now if $u = \xi - \phi$, then

$$\text{erf}(u) = \frac{2}{\sqrt{\pi}} \int_0^u e^{-u^2} du$$

$$\frac{d}{d\xi}(\text{erf}(u)) = \frac{2}{\sqrt{\pi}} e^{-u^2} \qquad \text{(A-18)}$$

Combining Equations (A-15), (A-17), and (A-18),

$$\phi = \frac{-(y_{A_o} - y_{A_\infty})}{2(1 - y_{A_o})} \left(\frac{1}{1 + \text{erf}\,\phi}\right)\left(\frac{2}{\sqrt{\pi}} \exp\left[-(\xi - \phi)^2\right]\right)_{\xi=o} \qquad \text{(A-19)}$$

Finally, there follows Equation (23)

$$\left(\frac{y_{A_o} - y_{A_\infty}}{1 - y_{A_o}}\right) = \sqrt{\pi}\ (1 + \text{erf}\,\phi)\ \phi \exp(\phi^2) \qquad \text{(A-20)}$$

APPENDIX B

TRANSIENT CONDUCTION SOLUTION FOR LIQUID TEMPERATURE GRADIENTS

In the following discussion an expression for the excess surface temperature based on transient conduction theory is developed. For this analysis, we will consider the liquid to be similar to a finite slab having equivalent density, thermal conductivity and specific heat. As shown in the diagram below, we will assume that the upper surface of the slab (simulating the liquid free surface) is subjected to a constant heat flux (q_s), and that the bottom surface of the slab is insulated.

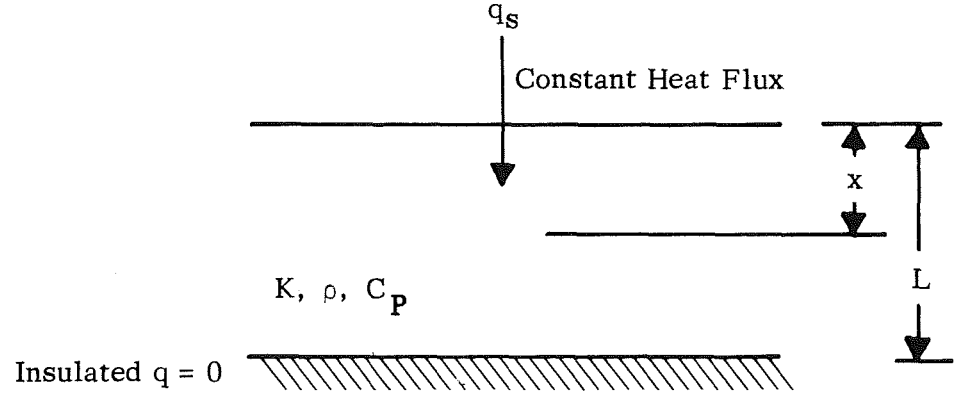

A. GENERAL EQUATIONS FOR A FINITE STATE

Since the heat flow for the above system is one-dimensional, it must satisfy Fourier's equation, or:

$$\frac{\partial t}{\partial \theta} = \alpha \frac{\partial^2 t}{\partial x^2} \qquad \text{(B-1)}$$

where: $$t = T - t_o \qquad \text{(B-2)}$$

We will choose a coordinate system such that at the gas liquid interface $x = 0$ and at the bottom of the tank $x = L$.

Since the heat input to the liquid is constant with time, therefore, $\partial t/\partial x \Big|_{x=0}$ must remain constant with time. Since no heat can leave through the bottom of the tank $\partial t/\partial x \Big|_{x=L} = 0$. Therefore, we have the following boundary conditions:

a) $\partial t/\partial x = -C \qquad x \to 0^{+} \qquad 0 < \theta$

b) $\partial t/\partial x = 0 \qquad x \to L^{-} \qquad 0 < \theta$

c) $t = 0 \qquad 0 < x < L \qquad \theta \to 0^{+}$

Let us introduce a new variable v such that:

$$v = C + \partial t/\partial x \quad . \tag{B-3}$$

substituting into Equation (B-2), we get:

$$\frac{\partial v}{\partial \theta} = \alpha \frac{\partial^2 v}{\partial x^2} \tag{B-4}$$

Rewriting the boundary conditions in terms of v:

a) $v \to 0 \qquad x \to 0 \qquad 0 < \theta$

b) $v \to C \qquad x \to L^{-} \qquad 0 < \theta$

c) $v \to C \qquad 0 < x < L \qquad \theta \to 0^{-}$

We again introduce a new variable, U, defined by:

$$v = C \frac{x}{L} + U \tag{B-5}$$

It can be seen from Equation (B-4) that U must satisfy the equation:

$$\frac{\partial U}{\partial \theta} = \alpha \frac{\partial^2 U}{\partial x^2} \tag{B-6}$$

We may now rewrite the last set of boundary conditions in terms of U as:

a) $U \rightarrow 0 \qquad x \rightarrow 0^{+} \qquad 0 < \theta$

b) $U \rightarrow 0 \qquad x \rightarrow L^{-} \qquad 0 < \theta$

c) $U \rightarrow C\left(1 - \frac{x}{L}\right) \qquad 0 < x < L \qquad \theta \rightarrow 0$

We may write down the solution to Equation (B-6) which satisifies the first two boundary conditions as:

$$U = \sum_{n=1}^{\infty} B_n \, e^{-(n\pi/L)^2 \alpha \theta} \sin\left(n \pi x/L\right) \qquad \text{(B-7)}$$

Substituting the above into Equation B-5 we get:

$$v = C\frac{x}{L} + \sum_{n=1}^{\infty} B_n \, e^{-(n\pi/L)^2 \alpha \theta} \sin\left(n \pi x / L\right) \qquad \text{(B-8)}$$

integrating Equation (B-3) we get:

$$\int v \, dx = cx + t + \delta + F(\theta)$$

Substituting in Equation (B-8) and performing the integration:

$$\frac{Cx^2}{2L} - Cx - \sum_{n=1}^{\infty} \frac{LB_n}{n\pi} \, e^{-(n\pi/L)^2 \theta \alpha} \cos\left(n \pi x/L\right) = t + \delta + F(\theta) \qquad \text{(B-9)}$$

where δ is a constant to be determined. Substituting (B-9) into Equation (B-2), we find:

$$F(\theta) = -\frac{\alpha C \theta}{L} + \lambda$$

where λ is an arbitrary constant.

Letting $\delta + \lambda = \eta$ and noting from condition c) in the first set of boundary conditions that as $\theta \rightarrow 0^+$ $\quad 0 < x < L \quad$ $t \rightarrow 0$, we may write (B-9) as:

$$\frac{Cx^2}{2L} - Cx - \sum_{n=1}^{\infty} \frac{LB_n}{n\pi} \cos(n\pi x/L) = \eta \qquad \text{(B-10)}$$

Since η is a constant, this equation can only be satisfied if:

$$\frac{LB_n}{n\pi} = \frac{2}{L} \int_0^L \left(\frac{x^2}{2L} - x\right) \cos(n\pi x/L)\, dx$$

and if:

$$\eta = -\frac{2}{L} \int_0^L \left(\frac{x^2}{2L} - x\right) dx$$

performing the above integrations and substituting the values for $\frac{LB_n}{n\pi}$ and η along with the value of $F(\theta)$ into Equation (B-9) we get:

$$t = \frac{Cx^2}{2L} + \frac{\alpha C\theta}{L} - Cx + \frac{CL}{3} - \frac{2LC}{\pi^2} \sum_{n-1}^{n=\infty} \frac{e^{-(n\pi/L)^2 \theta\alpha}}{n^2} \cos n\frac{\pi x}{L} \qquad \text{(B-10)}$$

The mass average mean liquid temperature $\bar{t}_L$ is given by:

$$\rho C_P \, LA \, \bar{t}_L = q_s = KAC\theta$$

$$\bar{t}_L = \frac{\alpha\theta C}{L} \qquad \text{(B-11)}$$

Making use of the boundary conditions, the definition of integrated mean temperature ($\bar{t}_L$), and the fact that $\bar{t} - t_L = T - \bar{T}_L$, Equation (B-10) may be rewritten as:

$$\frac{T - \bar{T}_L}{q_s/E} = \frac{1}{3} + \frac{1}{2}\left(\frac{x}{L}\right)^2 - \frac{x}{L} - \frac{2}{\pi^2} \sum_{n=1}^{n=\infty} \frac{e^{-n^2\pi^2 \frac{\alpha\theta}{L^2}}}{n^2} \cos n\pi\left(\frac{x}{L}\right) \qquad \text{(B-12)}$$

Evaluation of the series term included in the general equation above was sufficiently lengthy to justify machine computation of the dimensionless excess temperature. Therefore, general transient conduction equation was programmed for computation on an IBM 1401 located at Arthur D. Little, Inc. This machine

has a rather limited memory but is well adapted for relatively simple arithmetic problems. It was found that for values of dimensionless time ($\alpha\,\theta/L^2$) greater than 10^{-3}, the computer calculation of the dimensionless excess temperature was generally very expedient. However, for very small values of dimensionless time, the general equation was difficult to evaluate, even by machine computation, for two reasons:

1. The series converged very slowly since convergence was dependent to some degree on the value of the exponential factor -

$$e^{-n^2\pi^2(\alpha\theta/L^2)}$$

2. The non-dimensional excess temperature was obtained by subtraction of the series term from a grouping of other terms, all of which are relatively large numbers. Since the non-dimensional excess temperature becomes small as dimensionless times become very small, a very high degree of series convergence was required at small values of dimensionless time, in order that the resulting dimensionless excess temperature have numerical significance.

B. SEMI-INFINITE SLAB SOLUTION FOR SHORT HEATING TIMES

Rather fortuitously it was possible to use a semi-infinite slab approach for values of dimensionless time less than 10^{-2}. For relatively short heating periods, the semi-infinite slab approach is valid since the temperature gradients do not extend to the far end of the slab. Using the basic development presented in Jacob,[43] we expressed the dimensionless excess temperature for a semi-infinite slab subjected to constant surface heat input as follows:

$$\frac{T - \overline{T}_L}{q_s/E} = \frac{2}{\sqrt{\pi}}\sqrt{\frac{\alpha\theta}{L^2}}\;\psi(u) - \frac{\alpha\theta}{L^2} \qquad \text{(B-13)}$$

where

$$\psi(u) = e^{-u^2} - u\sqrt{\pi}\left[1 - f(u)\right]$$

$$f(u) = \frac{2}{\pi}\int_0^u e^{-u}\,du \text{ (tabulated error function)}$$

and

$$u = \frac{x/L}{2\sqrt{\alpha\theta/L^2}}$$

This equation was quite simple to evaluate by hand calculation and gave excellent agreement with the exact general solution discussed above in the region of dimensionless time from 10^{-3} to 10^{-2} where both solutions were employed to achieve an "overlap" of methods.

C. DISCUSSION OF RESULTS

Figure B-1 presents temperature profiles as a function of dimensionless time and dimensionless position. While a linear plot such as Figure B-1 is not very useful for calculation purposes, since a wide range of dimensionless times cannot be presented, it does give a good indication of the general shape of the curves.

First of all, it may be noted that for values of dimensionless time equal to or greater than 1, a stable gradient exists in the liquid. This stable gradient can be calculated simply by assuming equal rate of heat absorption at each plane in the slab. This reasoning results in the local heat flux or temperature gradient at any point x, being directly proportional to 1 - x/L. The resulting expression for the non-dimensional temperature excess can then be written:

$$\frac{T - T_L}{q_s/E} = \frac{(x/L)^2}{2} - x/L + 1/3$$

This result is, of course, exactly the same as general solution except that the series term is not present. For values of dimensionless time equal to, or in excess of, 1.0, the series term of the general equation approaches zero.

It may also be noted that the non-dimensional temperature excess has negative as well as positive values. A negative value means that the temperature at the point in question is less than the integrated mean temperature of the liquid. For points which have not been affected by the heat flux traveling from the surface it can be easily shown that dimensionless temperature excess is just equal to $-\alpha\theta/L^2$. The locus of these points determines a "no temperature rise" asymptote inclining downward at 45°. It may be further noted that temperature at the remote face of the slab, x/1 = 1, does not substantially depart from this "no temperature rise"asymptote until the dimensionless time is considerably greater than 10^{-2}.

Figure 24 in the main body of this report, presents significant positive values of non-dimensional excess temperature in a logarithmic plot. The term "significant," as used here, implies that the temperature excesses of interest are of the order of 1% or more of the surface temperature excess. This plot illustrates that for many of the conditions of practical interest (dimensionless times of the order of 10^{-6}) temperature gradients predicted by the transient conduction solution are essentially confined to a small fraction of one percent of the liquid depth below the surface.

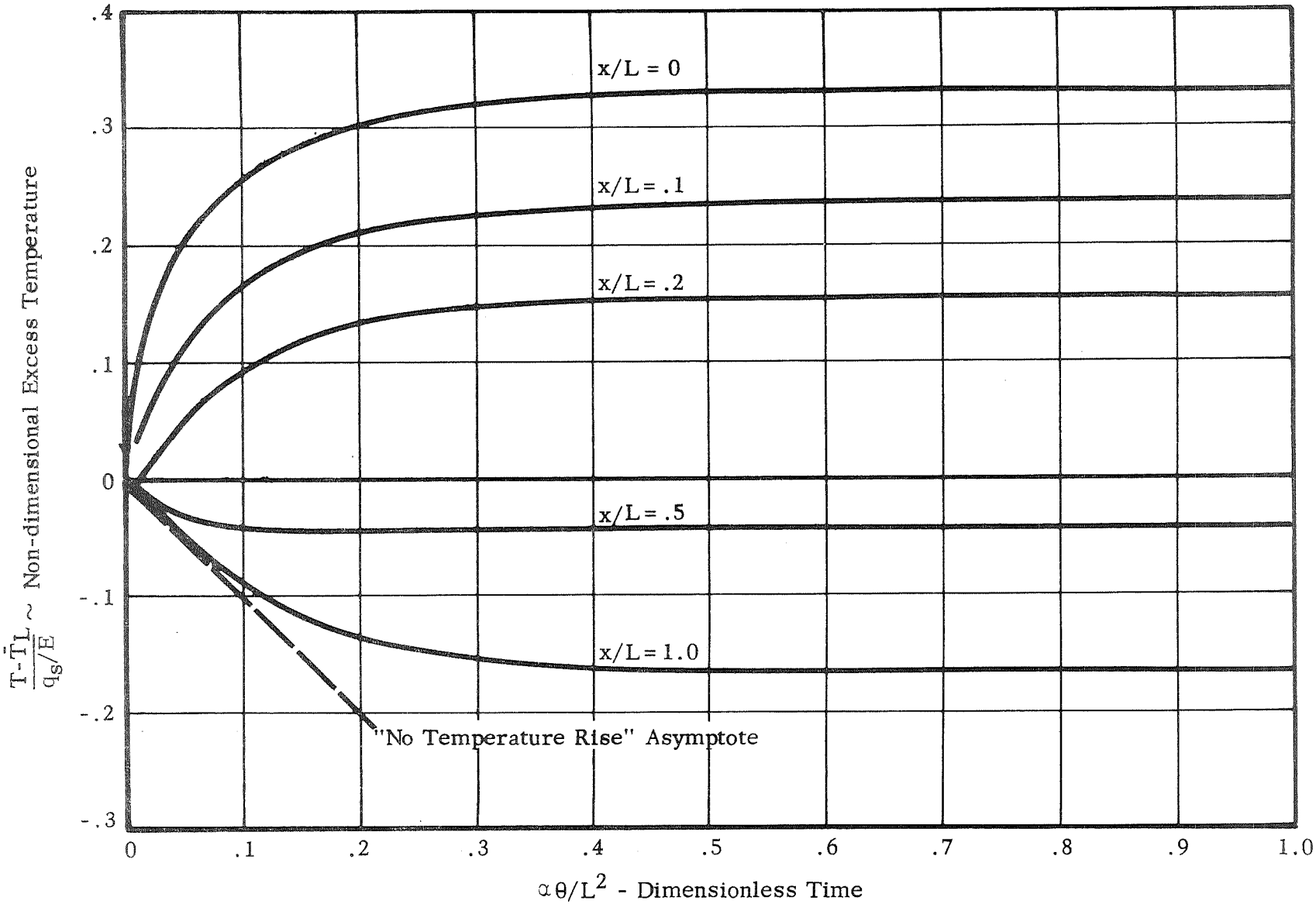

FIGURE B-1 TRANSIENT CONDUCTION TEMPERATURE PROFILES IN A FINITE SLAB WITH CONSTANT SURFACE HEATING (OVERALL LINEAR PLOT)

APPENDIX C

EXPERIMENTAL HEAT FLUX RATIO CORRELATION

In this Appendix, experimental data obtained from nonvented pressure build-up tests is used to check the surface temperature trends predicted by the transient conduction analysis and to establish a correlation for determining the empirical heat flux ratio q_s/q_a. Data from thirteen test runs with liquid oxygen, liquid nitrogen, liquid helium, and liquid hydrogen were used. A brief description of the test runs is given in Table C-1.

In Figure C-1, experimental values of excess surface temperature have been plotted as a function of nondimensional time for a few typical test runs. Also shown on this plot is the slope of the excess surface temperature curve which results from transient conduction analysis. This slope is obtained by arbitrarily assigning a value of 100°F to the factor q_s/E appearing in the nondimensional excess surface temperature plotted in Figure 24, in the main body of the report. The slopes of the experimental results are in general agreement with the slope of the transient conduction solution.

Figure C-2 shows the experimental heat flux ratios for a few typical tests runs as a function of nondimensional time. The experimental heat flux ratios were determined as follows:

$$(q_s/q_a)_{exp} = \frac{\left(\frac{T_s - \bar{T}_L}{q_a/E}\right)_{exp}}{\left(\frac{T_s - \bar{T}_L}{q_s/E}\right)_{cond.\ theory}}$$

This plot shows that although the heat flux ratios for the test runs vary widely, for a particular test run, q_s/q_a is essentially constant with time. The results for many tests, such as Run #5, Run #7 and Run #13 are in excellent agreement with the analytical model, i.e., the variation of q_s/q_a with time is very slight. For other tests, such as Run #3, q_s/q_a appears to "drift" with time. This "drift" may be due to extraneous transients such as the warm-up of cold vapor trapped in the vent line. However, in general, the agreement is good. From the above results, we conclude that the analytical model is adequate to describe the time-wise variation in excess surface temperature, except for the effects of extraneous transients which may influence the results at the beginning of the nonvented hold periods.

The second objective to be achieved is to establish a method of estimating the heat flux ratio applicable to any system. The heat flux ratio for a particular system is undoubtedly dependent, in part, on the distribution of ambient heat leak entering the container through the walls and piping. However, in most cases, convective currents within the container probably accomplish a major re-distribution of the heat entering the container. For containers of low ambient heat leak, we might expect that convective currents would primarily act to convey warm liquid to the surface with little mixing of the bulk fluid, resulting in a high value of q_s/q_a. On the other hand, in containers of high heat leak we might expect the convective currents to accomplish considerable mixing of the bulk fluid, thereby reducing q_s/q_a. Because of the number and complexity of the factors which go into establishing the heat flux ratio, it is doubtful that this problem would be amenable to any sort of rigorous analysis. However, for containers having similar geometry we might expect that ambient heat leak would be at least one of the more important factors in establishing the heat flux ratio q_s/q_a. Therefore, we have used the total ambient heat leak per unit side wall area as a correlating factor.

The experimental values of heat flux ratio are plotted as a function of heat leak per unit area in Figure C-3. In the case of the short test runs, in which q_s/q_a tended to drift with time, the final values of q_s/q_a were chosen as being less affected by initial transients and, therefore, more representative. This plot shows that experimental heat flux ratio drops off markedly with increasing heat flux per unit area. The various test runs all fall quite close to a single correlation line.

No theoretical basis has yet been found for the plot of Figure C-3. However, we have noted that for all, except very low heat leaks, ($q_a/\pi DL < 5$ Btu/hr-ft^2), the slope of the experimental plot may be closely matched by assuming that the surface heat flux (q_s) is proportional to the boundary layer volume flow.

If we assume that surface heat flux (q_s) is proportional to the volume rate of flow (Q) in the boundary along the tank; where from the Martin model*

$$Q = \frac{4\pi dLh}{\rho_L c_L}$$

and from natural convection heat transfer

* See Section VII-C.

$$h = .216 \left[\frac{\rho_L^2 \beta c_L k_L^2 q_a}{\mu_L \pi d L} \right]^{.25}$$

q_s = surface heat flux

q_a = total heat flux

d = tank diameter

L = tank length

Q = boundary layer flow

h = heat transfer coefficient (turbulent free convection)

ρ_L = liquid density

c_L = liquid specific heat

β = expansivity

k_L = liquid thermal conductivity

μ = viscosity

Then

$$\frac{q_s}{q_a} \alpha \frac{Q}{q_a} = \frac{4\pi d L h}{\rho_L c_L q_a}$$

$$= \frac{4\pi d L}{\rho_L c_L q_a} \times 0.216 \left[\frac{\rho_L^2 \beta c_L k_L^2 q_a}{\mu_L \pi d L} \right]^{0.25}$$

$$\frac{Q}{q_a} = .0864 \left[\frac{\beta k_L^2}{\mu_L \rho_L^2 c_L^3} \right]^{.25} \left[\frac{q_a}{\pi d L} \right]^{-0.75}$$

or

$$\frac{q_s}{q_a} = B \left[\frac{q_a}{\pi d L} \right]^{-0.75}$$

where B is determined by fluid properties.

A plot of experimental q_s/q_a versus $q_a/\pi d L$ is presented in Figure C-3. Also shown is the slope of that line predicted by the reasoning above. The agreement is very good and suggests that the surface heat flux used in the Arthur D. Little, Inc., transient conduction model is proportional to boundary layer flow.

TABLE C-1

EXPERIMENTAL DATA

Description	Test Runs 1	2	3	4	5	6	7	8	9	10	11	12	13
Fluid	N_2	N_2	N_2	N_2	N_2	N_2	N_2	H_2	H_2	H_e	H_e	O_2	H_2
Liquid Height (in.)	30	28.5	60.2	56.6	40	40	20	48	78	18	18	65	120
Vessel Inner Dia. (in.)	30	30	30	30	21.6	21.6	15	53.4	40	12	12	70	220
Heat Leak (Btu/hr)	329	2610	717	5860	69	71	742	184	5870	.341	.341	54800	174000
Total Test Time (hr)	2	.5	2	.5	8	8	1	72	.08	33	33	1	.33

NOTES:

1. All test containers were of vertical cyclinder construction with stainless steel inner vessels except for Run #12 which was aluminum.
2. All test containers except for Runs #7, 9 and 12 were vacuum insulated. The container for Run #7 was insulated with bulk insulation. The containers for Runs 9 and 12 were uninsulated.
3. In all runs, except Run #7, the vessel walls were too thin to provide a major source of equilibrator.
4. The container for Run #5 and 6 had a 1-inch aluminum bar equilibrator mounted on the side of the vessel extending down about 1/3 of the total height. Tests were performed with the vessel at a 30 degree inclination. In Run No. 5, the equilibrator was in vapor space. In Run #6, the equilibrator was submerged.

TABLE C-1 (Continued)

5. The container for Run #10 had four copper rod equilibrators with a total cross-sectional area of 0.258 sq. in. mounted vertically.

6. References:

Runs #1 - 4 Huntley, S.C., "Temperature-Pressure Time Relationships in a Closed Cryogenic Container," NACA TN 4259, February 1958.

Runs #5 - 7 Arthur D. Little, Inc., unpublished data. Burke, J.C., internal memos, April 22, 1960, and April 18, 1961.

Run #8 Schmidt, A.F. et al., "An Experimental Study Concerning the Pressurization and Stratification of Liquid Hydrogen," Proceedings of the 1959 Cryogenic Engineering Conference.

Run #9 Tatom, J.W. et al., "Analysis of Thermal Stratification of Liquid Hydrogen in Rocket Propellant Tanks," Lockheed-Georgia Company, 1963.

Runs #10-11 Scott, L.E. et al., "Temperature Stratification in a Nonventing Liquid Helium Dewar," Journal of the Research of the National Bureau of Standards, January - March 1960.

Run #12 Mair, C.E., "Preliminary Investigation of Thermal Conditions Inside Large Liquid Oxygen Container Exposed to Climatic Heating," Army Ballistic Missile Agency, DSE, Technical Note No. G-024, August 24, 1956.

Run #13 George C. Marshall Space Flight Center Memorandum "LN_2 Stratification Test on the SI-V Facilities Vehicle," H.G. Paul, January 23, 1964.

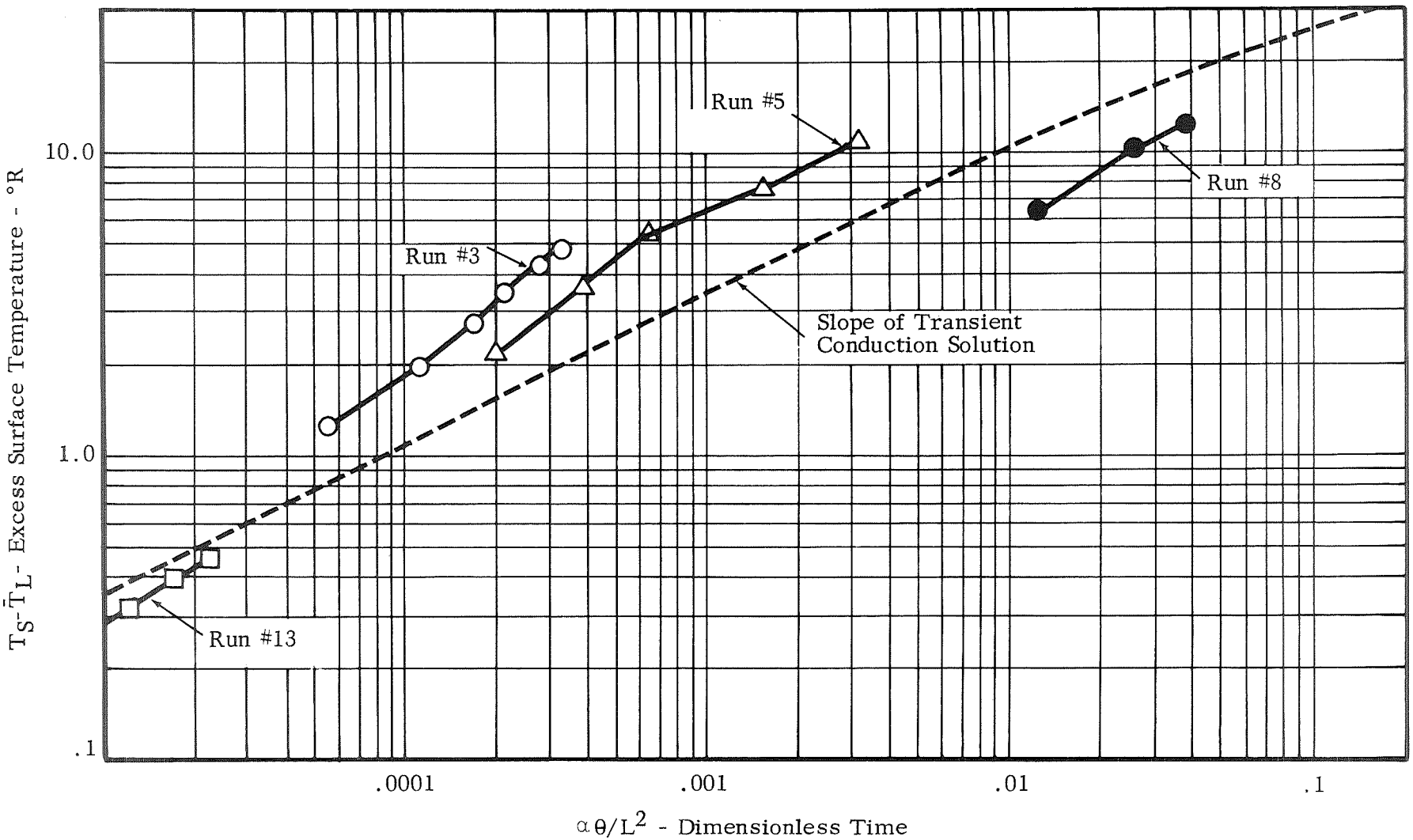

FIGURE C-1 EXPERIMENTAL VALUES OF EXCESS SURFACE TEMPERATURE

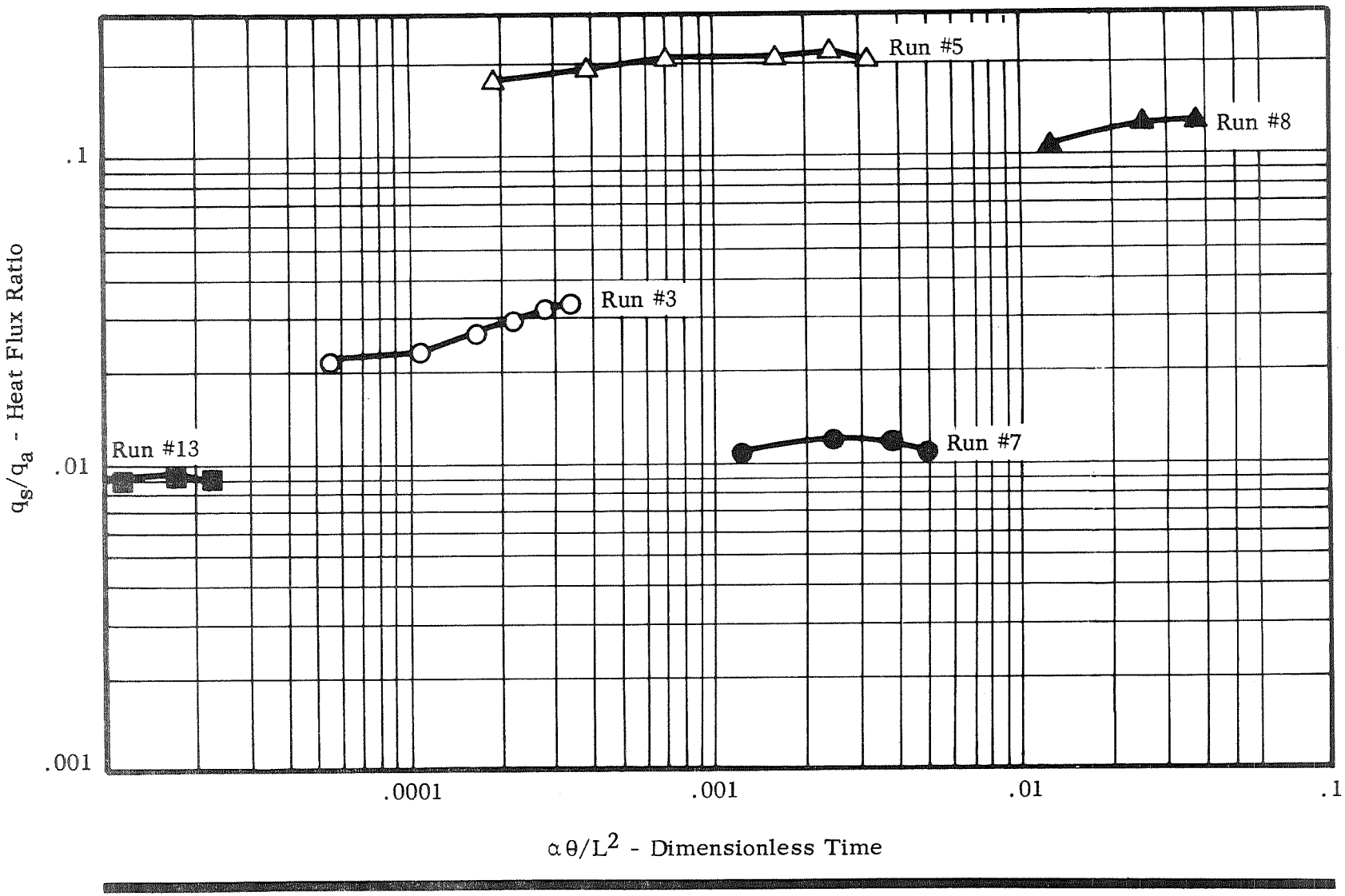

FIGURE C-2 EXPERIMENTAL HEAT FLUX RATIOS

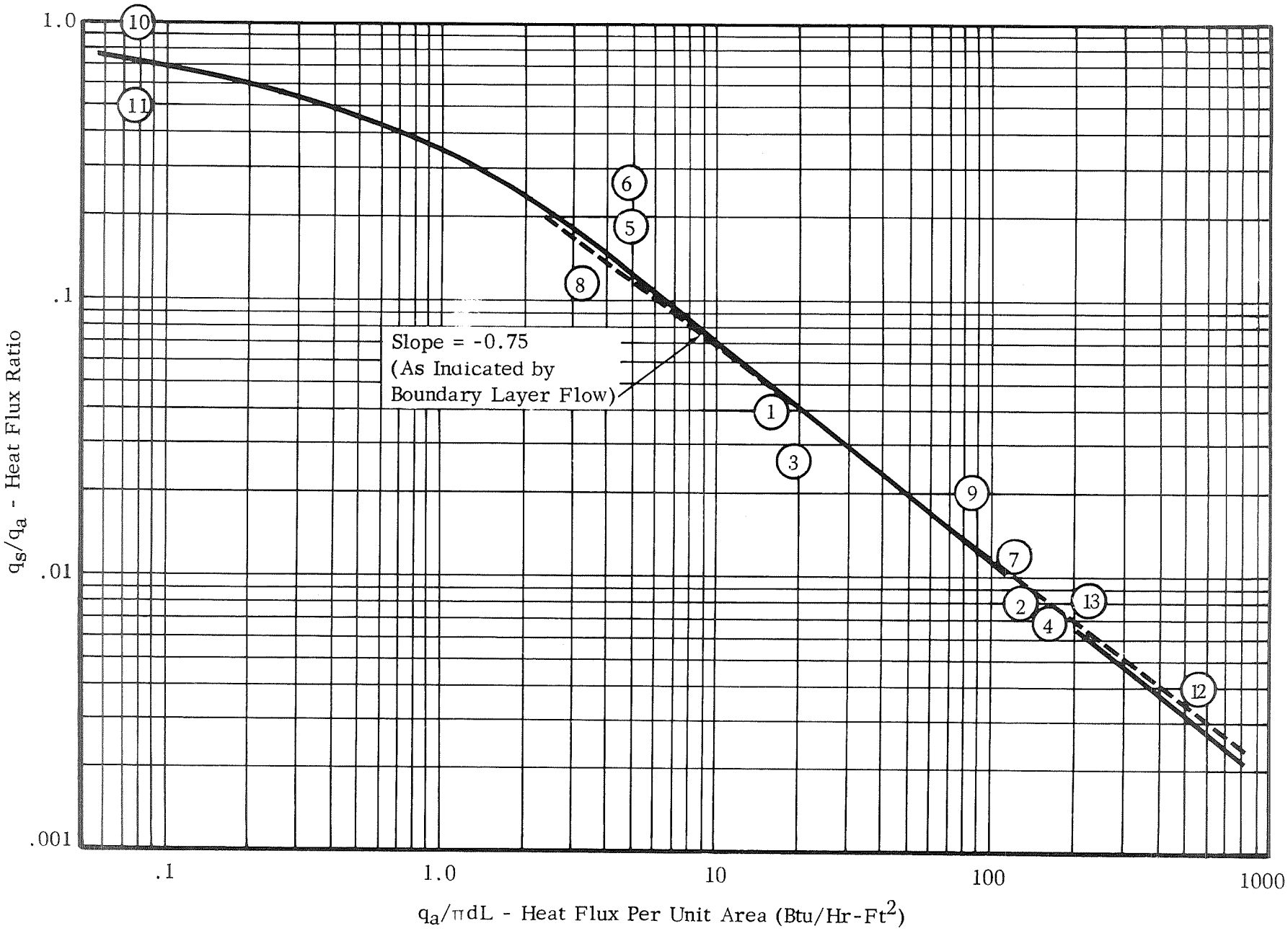

FIGURE C-3 CORRELATION OF EXPERIMENTAL HEAT FLUX RATIOS AND COMPARISON WITH SLOPE PREDICTED BY BOUNDARY LAYER THEORY

APPENDIX D

FILMS OF LIQUIDS ON VERTICAL WALLS

I. INTRODUCTION

Usually thin films of liquids on walls will, after a transient, flow down in a parabolic velocity profile. This is relatively easy to show by a momentum balance.

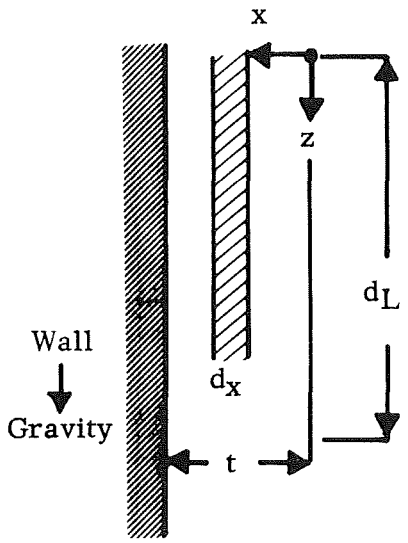

The film is examined over some short length dL. The thickness in this dL is t and we examine a small element dx within the film.

The width (i.e., in the y direction, perpendicular to the paper) is W.

The flow in at z = 0 is v_{z_o} and out at z = dL is $v_{z_{dL}}$.

Assume steady state so $v_{z_o} = v_{z_{dL}}$, i.e., the momentum flow into and out of the element Wdx balance each other. The shear stress is τ and varies wi with x.

Momentum flow in at x = $(dL)\, W \tau_x$

Momentum flow out at x + dx = $(dL)\, W \tau_{x+dx}$

Net momentum + body force = 0, i.e.,

$$(dL)\, W \tau_x - (dL)\, W \tau_{x+dx} + (dx)\,(dL)\,(W)\,(\rho\, g) = 0$$

dividing out the dL and W, then

$$\frac{d\tau}{dx} = \rho g$$

$$\therefore \tau = \rho g x + C_1$$

but $x = 0$, $\tau = 0$ (at gas interface),

$$\therefore C_1 = 0$$

$$\text{and } \tau = \rho g x \qquad \text{(D-1)}$$

at the wall $\tau = -\mu\, dv/dx$

$$= \rho g x$$

$$\therefore dv = -\frac{\rho g x}{\mu} dx$$

$$v = -\frac{\rho g x^2}{2\mu} + C_2$$

$$\text{at } x = t,\ v = 0,\ \therefore C_2 = \frac{\rho g t^2}{2\mu}$$

$$\text{and } v = \frac{\rho g t^2}{2\mu}\left[1 - \left(\frac{x}{t}\right)^2\right] \qquad \text{(D-2)}$$

Thus the velocity at any z is parabolic.

II. AVERAGE VELOCITY

The average velocity across the film is

$$\bar{v} = \int_{y=0}^{W}\int_{x=0}^{t} v\,dx\,dy \Big/ \int_{y=0}^{W}\int_{x=0}^{t} dx\,dy$$

$$\bar{v} = \frac{1}{t}\int_{x=0}^{t} v\,dx = \frac{1}{t}\int_{0}^{t} \frac{\rho g t^2}{2\mu}\left[1 - \left(\frac{x}{t}\right)^2\right]dx$$

$$= \frac{\rho g t^2}{3\mu} \qquad \text{(D-3)}$$

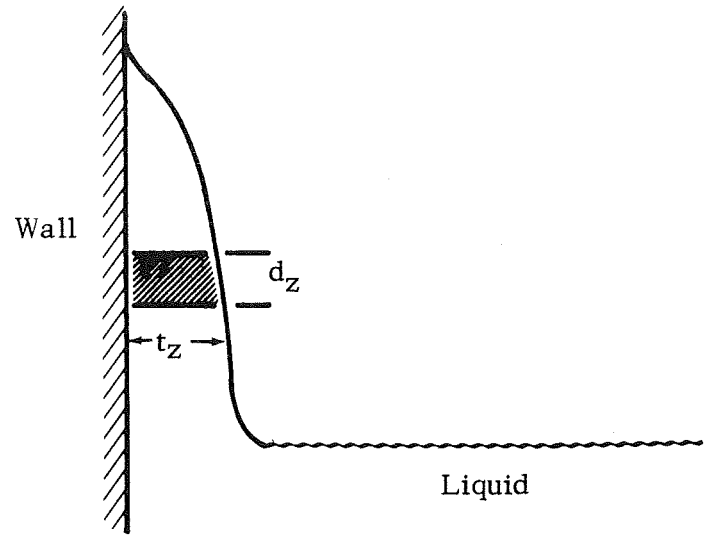

A material balance over z shows

$$\text{In} = (\bar{v}\,\rho)\,Wt$$

$$\text{Out} = (\bar{v}\,\rho)\,Wt_2 + \frac{\partial}{\partial z}\,(\bar{v}\,\rho\,Wt)\,dz$$

$$\text{Accumulation} = \frac{d}{d\theta}\,(\rho\,W\,dz\,t)$$

In - Out = Accumulation

$$-\frac{\partial}{\partial z}\,(\bar{v}\,\rho\,Wt)\,dz = Wdz\,\frac{\partial t}{\partial \theta}$$

$$\therefore \frac{\partial}{\partial z}\,(\bar{v}\,t) = -\frac{\partial t}{\partial \theta} \qquad \text{(D-4)}$$

Substituting (D-3) into (D-4)

$$\frac{\partial}{\partial z}\left[\frac{\rho g t^3}{3\mu}\right] = \frac{\partial t}{\partial \theta}$$

$$\frac{\rho g}{\mu}\,t^2\left(\frac{\partial t}{\partial z}\right)_\theta = -\left(\frac{\partial t}{\partial \theta}\right)_z$$

divide by $\left(\frac{\partial t}{\partial z}\right)_\theta$

$$\frac{\rho g t^2}{\mu} = -\left(\frac{\partial t}{\partial \theta}\right)_z \left(\frac{\partial z}{\partial t}\right)_\theta$$

but since $t = f(z, \theta)$, then

$$\left(\frac{\partial t}{\partial \theta}\right)_z \left(\frac{\partial z}{\partial t}\right)_\theta = -\left(\frac{\partial z}{\partial \theta}\right)_t$$

$$\therefore \frac{\rho g t^2}{\mu} = \left(\frac{\partial z}{\partial \theta}\right)_t$$

or $$z = \frac{\rho g t^2}{\mu} \theta + \phi(t)$$

where $z = 0$ at $\theta = 0$ (i.e., at the start of draining)

$$\therefore \phi(t) = 0$$

and $$z = \frac{\rho g t^2}{\mu} \theta$$

or $$t = \left(\frac{\mu}{\rho g} \frac{z}{\theta}\right)^{\frac{1}{2}} \qquad \text{(D-5)}$$

Equation (D-5) may be easily visualized as follows:

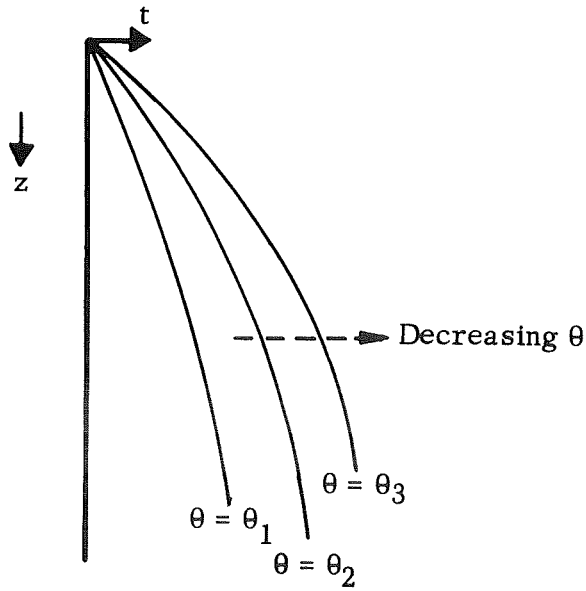

Here $z = v\theta$ (D-6)

When $z = L$, the total exposed film, then θ = the total time from start of draining θ, and

$$L = v\,\theta_T, \quad v = \text{velocity of drain.}$$

$$t_{z=L} = \left(\frac{\mu}{\rho g}\,\frac{L}{\theta}\right)^{\frac{1}{2}}$$

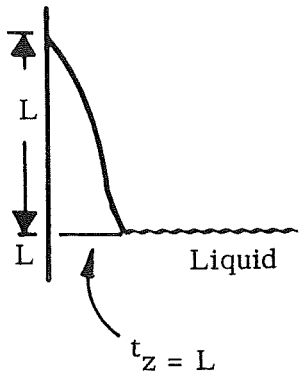

The average thickness of the film at this time θ is found by integration,

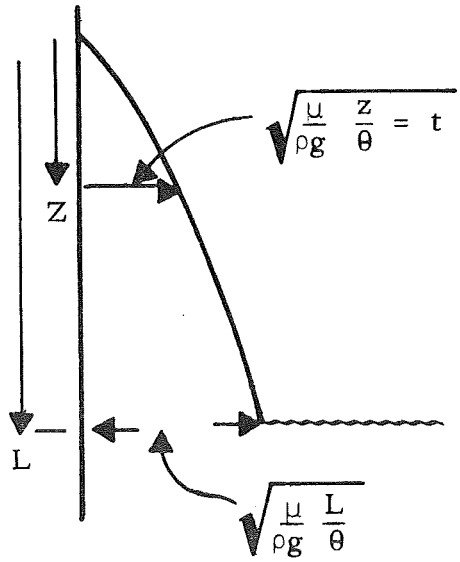

$$\bar{t} = \int_0^L \sqrt{\frac{\mu}{\rho g}\,\frac{z}{\theta}}\,dz \Big/ \int_0^L dz$$

$$= \frac{2}{3}\sqrt{\frac{\mu}{\rho g}\,\frac{L}{\theta}} = \frac{2}{3}\sqrt{\frac{\mu}{\rho g}\,v} \qquad \text{(D-7)}$$

where v is velocity (assumed constant) of drain.

V. MOVING FILMS WITH SURFACE TENSION

The formula of $\bar{t}$ derived for Equation (D-7) does not take into account interactions between the liquid film and the vapor, i.e., through surface tension forces.

There does not appear to be any theoretically satisfactory method to handle this problem. However, if the problem is stated that from the above considerations,

$$\bar{t} = f\ (\mu,\ g,\ \rho,\ v,\ \text{and}\ \sigma),$$

where σ is the surface tension, then it can be shown that from dimensional analysis that

$$\bar{t}\ \sqrt{\frac{\rho g}{\mu v}} = f\left[\frac{\sigma}{\mu v}\right] \qquad \text{(D-8)}$$

designating $$Y \equiv \bar{t}\ \sqrt{\frac{\rho g}{\mu v}}$$

$$X \equiv \frac{\sigma}{\mu v}$$

experimental data show that

$$\log_{10} X = \frac{0.151}{\log_{10}(1.5Y)} + 1.44 - 5.45 \log_{10}(1.5Y) \qquad \text{(D-9)}$$

This equation is plotted as Figure 31 in Section VIII of the main body of this report.

VI. APPLICATION TO THE DRAINING OF HYDROGEN/OXYGEN TANKS

A. Properties

1. Hydrogen

$T = 20.6°K$

$\rho = 4.42\ \text{lb/ft}^3$

$\sigma = 2.13\ \text{dynes/cm}$

$\mu = 0.014\ \text{cp} = 9.4 \times 10^{-6}\ \text{lb/ft sec}$

$v =$ velocity of draining, ft/sec

then

$$Y = \bar{t} \sqrt{\frac{(4.42)\,(32.2)}{9.4\times10^{-6}(v)}}$$

$$= \frac{\bar{t}}{\sqrt{v}}\ 3.9 \times 10^{3}\ \ (\bar{t} \text{ in ft, v in ft/sec})$$

$$X = \frac{\sigma}{\sqrt{v}} = \frac{2.13}{(9.4\times10^{-6})\,(454)\,v}$$

$$= \frac{500}{v}$$

2. Nitrogen

$T = 77.4°K$

$\rho = 50.4 \text{ lb/ft}^3$

$\sigma = 8.94 \text{ dynes/cm}$

$\mu = 0.158 \text{ cp} = 1.06 \times 10^{-4} \text{ lb/ft-sec}$

$$Y = \frac{t}{\sqrt{v}}\ (3.9 \times 10^{3})$$

$$X = \frac{\sigma}{\mu v} = \frac{186}{v}$$

3. Oxygen

$T = 90.2°K$

$\rho = 71.3 \text{ lb/ft}^3$

$\sigma = 13.2 \text{ dynes/cm}$

$\mu = 0.188 \text{ cp} = 1.26 \times 10^{-4} \text{ lb/ft-sec}$

$$Y = \bar{t}\ (4.27 \times 10^{3}) \,/\, \sqrt{v}$$

$$X = \frac{231}{v}$$

B. Film Thicknesses

v (ft/sec)	X	Y	$\bar{t}$, ft x 10^5	$\bar{t}$ (thousands of inches)
		Hydrogen		
0.1	5×10^3	0.22	1.9	0.2
1.0	5×10^2	0.32	8.2	1.0
10	5×10^1	0.43	37	4.4
		Nitrogen		
0.1	1.86×10^3	0.26	2.2	0.26
1.0	1.86×10^2	0.36	9.2	1.1
10	1.86×10^1	0.47	40	4.8
		Oxygen		
0.1	2.31×10^3	0.255	2.0	0.24
1.0	2.31×10^2	0.355	8.3	1.0
10	2.31×10^1	0.46	35	4.2

VII. ULLAGE CONTAMINATION

The liquid film evaporating into the ullage may be visualized as a ring of height L, thickness $\bar{t}$, and diameter d. The volume of this ring of liquid is $\pi \bar{t} L d$ and the mass is $\rho_L \pi \bar{t} L d$. If the liquid evaporates into the ullage, the fraction contamination of the ullage is

$$\frac{4 \rho_L}{\rho_g} \frac{\bar{t}}{d}$$

where ρ_g is the density of the ullage gas.

Assuming the ullage is an ideal gas at an average temperature T, this fraction becomes,

$$4 \rho_L \bar{t} \; RT/Pd.$$

Applied to the particular case of hydrogen and oxygen films evaporating into helium, ρ_L for both hydrogen and oxygen is about 2.2 lb moles/ft^3. Thus

$$\text{mole (or volume fraction contamination)} = 94 \bar{t} \; T/Pd$$

where $\bar{t}$ and d are in ft, P in psia, and T in °R.

Another way to visualize the contamination is to relate the evaporation of this draining film to the thickness of a layer of vapor on the liquid surface. The film is assumed to be at a temperature corresponding to saturation of propellant at the system pressure, T_s. This thickness is then,

$$4 \rho_L \bar{t} \; LRT_s / Pd$$

To illustrate typical thicknesses for oxygen and hydrogen into helium, with P = 50 psia, ρ_L = 2.20 lb-moles/ft^3, d = 20 ft, and T_s = 141°R (0_2). 46.4°R (H_2), then with draining rates of 0.1 and 1 ft/sec,

v (ft/sec)	$\bar{t}$, ftx10^5	L	Thickness of Layer At T_s and P, ftx10^3	Thickness of Layer (inches)
		Hydrogen		
0.1	1.9	2	0.166	0.0020
1.0	8.2		0.72	0.0086
0.1	1.9	10	0.83	0.010
1.0	8.2		3.6	0.043
0.1	1.9	20	1.6	0.019
1.0	8.2		7.2	0.086
		Oxygen		
0.1	2.0	2	0.52	0.0062
1.0	8.3		2.1	0.025
0.1	2.0	10	2.5	0.030
1.0	8.3		11.	0.13
0.1	2.0	20	5.2	0.062
1.0	8.3		22.	0.26

CAMBRIDGE • CHICAGO • NEW YORK • TORONTO
LONDON • WASHINGTON • ZURICH • EDINBURGH
SANTA MONICA • SAN FRANCISCO • MEXICO CITY